EXPERIMENTAL INVESTIGATIONS ON A STANDING-WAVE THERMOACOUSTIC ENGINE

By

Mahmoud Mohamed Emam

A Thesis Submitted to the Faculty of Engineering at Cairo University in Partial Fulfillment of the Requirements for the Degree of

MASTER OF SCIENCE

In

MECHANICAL POWER ENGINEERING

FACULTY OF ENGINEERING, CAIRO UNIVERSITY

GIZA, EGYPT

2013

EXPERIMENTAL INVESTIGATIONS ON A STANDING-WAVE THERMOACOUSTIC ENGINE

By

Mahmoud Mohamed Emam

A Thesis Submitted to the Faculty of Engineering at Cairo University in Partial Fulfillment of the Requirements for the Degree of MASTER OF SCIENCE

In

MECHANICAL POWER ENGINEERING

Under Supervision of

Prof. Dr. Mahmoud A. Foad

Professor of Mechanical Power
Mechanical Power Engineering Department,
Faculty of Engineering
Cairo University

Dr. Ehab Abdel-Rahman

Professor of Physics, Associate Dean for Graduate Studies and Research
School of Sciences and Engineering,
American University in Cairo

Dr. Abdelmaged H. Ibrahim Essawey

Assistant Professor, Mechanical Power Engineering Department, Faculty of Engineering, Cairo University

FACULTY OF ENGINEERING, CAIRO UNIVERSITY

GIZA, EGYPT

2013

Acknowledgements

So many people provided help and support throughout the course of this work. I am particularly grateful towards my advisors, Professor Dr. Mahmoud A. Fouad, Professor Dr. Ehab Abdul-Rahman, and Dr. Abdelmaged H. Ibrahim, for their continuous help, guidance, support, and understanding in every step of this work. I believe that their philosophy and friendship bring out the best in all of their students and make a deep and lasting impression on their lives. Their broad knowledge and constant encouragement are very much appreciated. The highly appreciated understanding and support by Prof. Dr. Fouad is critical for me, not only in this work, but along my entire academic life. The friendship of Dr. Abdelmaged Ibrahim towards me and my family is something for which I am especially grateful. I am very thankful to Professor Ehab Abdul-Rahman who has been a wonderful source of advice and encouragement throughout my graduate career. I acquired great knowledge from all the discussions I had with him. I am very thankful to his continuous support and encouragement. Special thanks to Professor Essam Khalil for his valuable help and discussions during the early stages in preparing this work. His support and encouragement are much appreciated. The support from my colleagues at the thermoacoustic lab in AUC was essential. I would specially like to thank the efforts of the engineers in the thermoacoustic research team in AUC. I have to thank the twin engineers Ahmed and Khaled El-Beltagy for their efforts to help in producing this work. Special thanks to engineers Micheal Rezk and Tarek Nigim for their continuous help during various parts of this work.

The experimental procedures of this work were done in the labs of the physics department in the American University in Cairo. The results were obtained using the experimental apparatus in the labs of Youssef Jameel Science and Technology Research Center. Special thanks to the thermoacoustic research team in the American University in Cairo for their help and support.

I am very thankful to my family members: My mother, my sisters, and my father for their love, support and prayers. The support and sacrifices made by my family before and during this work are priceless.

Table of Contents

List of Figures

List of Tables

Abstract

Thermoacoustic engine is one of the emerging technologies in the field of energy conversion. Thermoacoustic engines convert thermal energy, possibly at relatively low temperatures to mechanical energy in the form of acoustic oscillations of high amplitudes that can drive a thermoacoustic refrigerator or can be converted to electrical energy using a linear alternator. In this work, a prototype of a thermoacoustic engine was built, operated and tested. Sustainable operation of the engine is possible due to the relatively efficient hot and cold heat exchangers that were able to sustain the temperature gradient across the stack.

Both the transient and steady-state performance of the thermoacoustic engine are investigated using variable gas mixtures and using square-cell stacks of variable porosities. The engine performance is studied during full runs consisting of start-up, steady operation, and shutting-down. The steady-state engine performance and wave characteristics are investigated at different heat input values, different gas mixtures, and different stack porosities. Inserts with different patterns and open areas are used inside the resonator to investigate their effect on suppressing the high harmonics of the produced acoustic wave. A numerical model of the current prototype is built using the free simulation software DELTAEC. The model is validated using the experimental data and is then used to obtain more information about the engine performance.

Results show that the used gas mixture, the pressure ratio, and the stack cell dimensions significantly affect the engine power output, the wave dynamic pressure amplitude, and the harmonic content of the wave. Experimental data agrees with DELTAEC calculations in trend, but the values of acoustic power and dynamic pressure are significantly lower than the numerical model calculations. The values of the frequency are within 3% of the measured values.

The transient analysis shows that the dynamic pressure amplitude of the gas reaches a peak after onset and then decreases to a steady value during the run. The onset temperature of the engine is always higher than the temperature at which the system stops producing oscillations while shut-down. The hysteresis characteristics is significantly affected by the thermal conductivity of the gas mixture, the stack cell dimensions, the mean temperature at starting, and the time of the cycle. The heat exchange process at the cold side is enhanced by the existence of the wave.

In this work, several inserts of different thicknesses, open area, positions, and hole patterns are inserted into the resonator to suppress the harmonics. All inserts caused lower harmonic content with respect to the case with no inserts. Inserts of low open area cause the performance to degrade and produce low acoustic powers. Inserts with higher thickness gave better performance. Amongst all inserts used, the highest acoustic power is obtained using an insert with an open area of 50% of the resonator area, a pattern of several distributed holes, a thickness of 3 cm, and at a position of 0.33 of the fundamental wavelength measured from the cold-side blind flange.

1. Introduction

Thermoacoustics is a promising technology that has a rapidly growing field of applications. Thermoacoustic engines and refrigerators based on the interactions between temperature, density and pressure variations on the acoustic longitudinal wave are safe, reliable, durable and environmentally friendly. These applications have the advantages of using no adverse chemicals, containing no environmentally unsafe contents, having no or few moving parts. Thermoacoustic devices can readily be driven using solar energy or waste heat and they can be controlled using proportional control. They can use heat available at low temperatures which makes it ideal to regeneration using waste heat from engines, and suitable for solar energy applications. The components included in thermoacoustic engines are usually very simple compared to conventional engines. The device can easily be controlled and maintained.

1.1 Thermoacoustics

Thermoacoustics utilizes the rich interactions between thermodynamics and acoustics. In any sound wave, there exist coupled pressure, displacement, density, and temperature oscillations. The pressure oscillations induce temperature oscillations which in turn cause heat transfer to or from nearby solid surfaces. The combination of these oscillations and the placement of enough solid walls at the proper position in the acoustic wave, close enough to the heated or cooled areas in the gas, produce a rich variety of thermoacoustic effects.

Nikolaus Rott [(1)] gave a definition of thermoacoustics in his review article as "a subject dealing generally with effects in acoustics in which heat conduction and entropy variations of a medium play a role". Thermoacoustics in modern research has a more specific domain which includes the energy conversion processes dealing with acoustic and heat energies, namely thermoacoustic engines and thermoacoustic refrigerators. This type of energy conversion is a fast developing technology that contributes to the global trend towards the use of renewable energies.

Thermoacoustic engines are devices that use heat to produce mechanical work in the form of acoustic pressure oscillations. Thermoacoustic refrigerators and heat pumps are devices that use acoustic work to transfer heat against a temperature gradient to achieve refrigeration or heating effect. The two types of devices usually contain the same elements: a thermoacoustic element (a stack), surrounded by hot and cold heat exchangers. The system is housed inside a resonator. Acoustic drivers are used in refrigerators and heat pumps to drive the refrigeration effect, while linear alternators are used in engines to harvest the acoustic energy and convert it into electricity.

The stack is the element in which the main thermoacoustic phenomena take place to produce or consume acoustic work under a temperature gradient. The thermoacoustic cycle takes place in the working fluid near the walls of a solid substrate. The stack is an element with enough channels parallel to oscillation of the gas. The walls of the channel provide more contact area between the working fluid and the solid which is vital to achieve the correct phasing between the gas and the solid surface and to complete the thermoacoustic cycle. The performance of the thermoacoustic stack depends on its material, length, position in the wave, the geometry of its pores, and its porosity. The porosity is the ratio between the gas open area and the stack total area, which depends on the number of pores in the area unit and the wall and pore thicknesses.

The thermoacoustic effect inside the stack takes place mainly in the region that is close to the solid walls of the stack. The layers of gas too far away from the stack walls experience adiabatic oscillations in temperature that result in no heat transfer to or from the walls, which is undesirable. Therefore, an important characteristic for any thermoacoustic element is the value of the *thermal and viscous penetration depths*. The thermal penetration depth δ_k is the thickness of the layer of the gas where heat can diffuse through during half a cycle of oscillations. Viscous penetration depth δ_v is the thickness of the layer where viscosity effect is effective near the boundaries. The ratio of the thermal to viscous penetration depths is the square root of the Prandtl number. For pure gases at standard pressure and temperature, Prandtl number is about 0.7, while for mixtures of gases; lower values of Prandtl can be obtained.

The oscillations of the gas in a standing-wave thermoacoustic engine take the form of a part of a longitudinal standing-wave. The mode and the frequency of the wave are controlled by the boundary conditions of the resonator in which the wave is contained. The resonator is a path of certain geometry where the gas is allowed to oscillate according to the boundary conditions that control the pressure and particle velocity of the gas. A resonator with a perfectly closed end forces the oscillations in the velocity of the gas to be zero (a node in the wave) at the closed end, whereas a resonator with a perfectly open end forces the oscillations in the velocity of the gas to be maximum (a velocity antinode) at the open end. The oscillations in the pressure of the gas in a standing-wave with no energy transfer are different in phase with the oscillations in velocity with 90^o. That means that in a non-dissipating standing-wave, a node of velocity oscillations occurs in the same position with an antinode of pressure oscillations and vice versa.

Heat is added and removed from the thermoacoustic engines and refrigerators through heat exchangers. The heat is added or removed from the oscillating gas around the heat exchanger to ensure that the thermoacoustic stack is under a temperature gradient that allows the thermoacoustic effect to take place. In the case of oscillating gas, the particle of the gas will have a maximum displacement in the direction of the temperature gradient. A heat exchanger with fins longer than the value of this displacement does not make use of the additional fin space. This puts limitations on the design of the heat exchangers used in thermoacoustics.

In thermoacoustic refrigerators (TAR), acoustic energy is introduced into the system by acoustic drivers which are devices that convert electric power to acoustic power using a magnetically-oscillating electric coil. Improving the electro-acoustic conversion efficiency of these devices is critical to the improvement of the acoustically-driven thermoacoustic refrigerators. On the other hand, in thermoacoustic engines (TAE) electric power is produced from the acoustic wave by the movement of a piston in a linear alternator. Alternating current is produced by these devices at a frequency equal to the frequency of the oscillations.

In thermoacoustically-driven thermoacoustic-refrigerators (TADTAR), the acoustic power is introduced in the system through a thermoacoustic engine. This technology leads to the refrigeration with no moving parts. The moving element in this case is just the gas itself. This increases the reliability and durability of the device.

The first law conversion efficiency in TAE is defined as the ratio between the acoustic power produced and the heat input to the engine. The second-law efficiency describes the reversibility of the engine and is defined as the ratio between the first law efficiency and the Carnot cycle efficiency operating at the same temperature limits.

The performance of TAR is characterized by the coefficient of performance (COP) which is the ratio between the refrigeration of heat pumping heat and the input work to the system. The ratio of the COP to COP of a Carnot cycle operating at the same temperature limits is used as an indication of the reversibility of the TAR.

The process of designing a thermoacoustic device became easier using the design environment (Design environment for low-amplitude thermoacoustic energy converters, DELTAEC). This software solves the one-dimensional mono-frequency wave equation to predict the performance of any configuration of thermoacoustic elements. It is used widely in the design and performance analysis of thermoacoustic devices. The real and imaginary parts of the dynamic pressure and the volumetric efficiency are matched between at the start of every segment with the end of the previous segment so that continuity is conserved. DELTAEC, however, suffers from many drawbacks. It does not take the turbulent losses into account. It also doesn't account for minor losses, harmonic content, or streaming.

1.2 Historical review of thermoacoustics

As sound is one of the five senses of the human, acoustics was a field of observations and research since the early existence of the man on earth. In the 6^{th} century BC, the Greek philosopher Pythagoras investigated the differences between the different music instrument intervals. Aristotle (384-322 BC) was the first one to mention the relation of sound on contractions and expansions of the air. Around 20 BC, the Roman architect Vitruvius discussed the effects of echoes and revibration in his treatise about theatre design. Galileo Galilei and Marin Mersenne were first to understand most of the basic laws of the sound independently. Newton derived the equations of the sound wave velocity in solids in his book "Principia" in 1687.

Thermoacoustic-induced oscillations have been observed for centuries. Glass blowers produced heat generated sound when blowing a hot bulb at the end of a cold narrow tube. This phenomenon also has been observed in cryogenic storage vessels, where oscillations are induced by the insertion of a hollow tube open at the bottom end in liquid helium, called Taconis oscillations, but the lack of heat removal system causes the temperature gradient to diminish and acoustic wave to weaken and then to stop completely.

Byron Higgins made the first scientific observation of heat energy conversion into acoustical oscillations. He investigated the "singing flame" phenomena in a portion of a hydrogen flame in a tube with both ends open. Putnam and Dennis gave a survey of the related phenomena. Rijke introduced this phenomenon into a greater scale by using a heated wire screen to induce strong oscillations in a tube. Feldman mentioned in his related review that a convective air current through the pipe is the main inducer of this phenomenon[(2)]. The oscillations are strongest when the screen is at one fourth of the tube length.

Research performed by Sondhauss in 1850 is known to be the first to approximate the modern concept of thermoacoustic oscillation. Sondhauss experimentally investigated the oscillations related to glass blowers. Sondhauss observed that sound frequency and intensity depends on the length and volume of the bulb.

Lord Rayleigh gave a qualitative explanation of the Sondhauss thermoacoustic oscillations phenomena, where he stated that producing any type of thermoacoustic oscillations needs to meet a criteria: "If heat be given to the air at the moment of greatest condensation or taken

from it at the moment of greatest rarefaction, the vibration is encouraged". This shows that he related thermoacoustics to the interplay of density variations and heat injection.

The formal theoretical study of thermoacoustics started by Kramers in 1949 when he generalized the Kirchhoff theory of the attenuation of sound waves at constant temperature to the case of attenuation in the presence of a temperature gradient.

Rott made a breakthrough in the study and modeling of thermodynamic phenomena by developing a successful linear theory[3]. After that, the acoustical part of thermoacoustics was linked in a broad thermodynamic framework by Swift[4].

1.3 Linear theory of thermoacoustics

The formulation of the governing equations of thermoacoustics in a general linear theory was not developed until the 1970s, when Rott was able to present a unifying linear perspective that can easily be applicable to the thermoacoustic devices[1,3,5-7]. In this chapter, the linear theory of thermoacoustics is briefly presented. The linear theory of thermoacoustics makes use of several assumptions to simplify its formulations. It should be noted that operation of a thermoacoustic engine at high values of dynamics pressure amplitudes increases the actual performance deviation away from the predicted performance and introduces many losses that are not linearly accounted for, thus causing the engine performance to degrade. Nevertheless, the linear theory provides an important tool to simulate, design, and compare the performance of the thermoacoustic engines at low amplitudes.

1.3.1 Thermoacoustic phenomena

Acoustic oscillations in a media are a set of time depending properties, which may transfer energy along its path. Along the path of an acoustic wave, pressure and density are not the only time dependent property, but also entropy and temperature. Temperature changes along the wave can be invested to play the intended role in the thermoacoustic effect. The interplay of heat and sound is applicable in both conversion ways. The effect can be used to produce acoustic oscillations by supplying heat to the hot side of a stack, and sound oscillations can be used to induce a refrigeration effect by supplying a pressure wave inside a resonator where a stack is located.

In a thermoacoustic prime mover, a high temperature gradient along a tube where a gas media is contained induces density variations. Such variations in a constant volume of matter force changes in pressure. The cycle of thermoacoustic oscillation is a combination of heat transfer and pressure changes in a sinusoidal pattern. Self-induced oscillations can be encouraged, according to Lord Raleigh, by the appropriate phasing of heat transfer and pressure changes.

1.3.2 Thermodynamic cycle

The thermoacoustic cycle can be analyzed by focusing attention on what happens at a given parcel of a fluid while it oscillates in a resonator where a temperature gradient exists on the walls. Figure 1.1 shows the cycle of thermoacoustics in a device serving as (a) heat pump/refrigerator and a device serving as (b) prime mover. For simplicity, the parallel heat transfer process and compression or rarefaction are separated into different steps to give a clearer visualization of the cycle. The cycle is therefore found to be identical to the Brayton cycle.

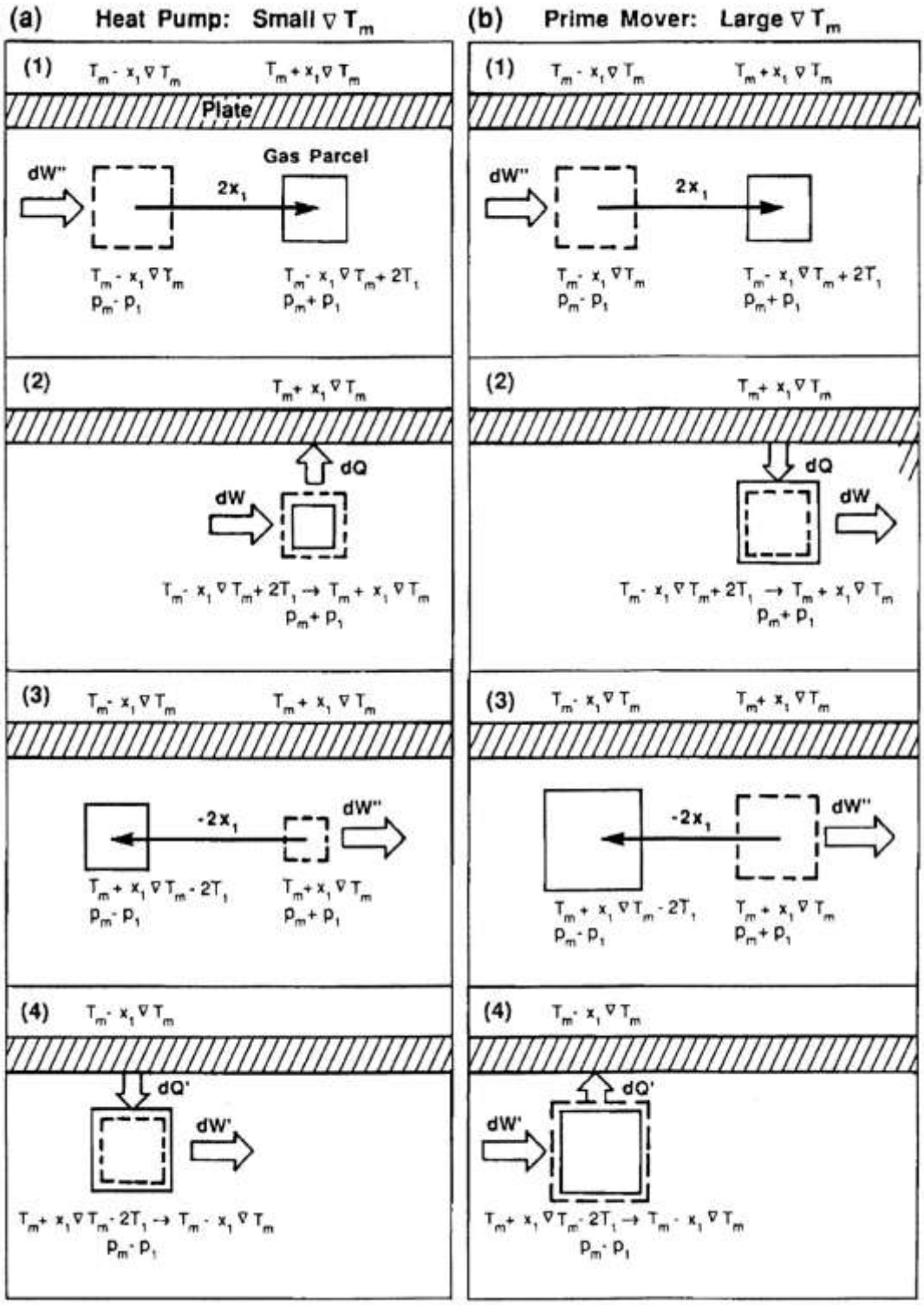

Figure 1.1: Typical cycle of (a) thermoacoustic heat pump and (b) thermoacoustic prime mover[4].

It is important to note that phasing in a traditional heat engine is critical. Pistons or valves have to move with correct relative motion for the working medium to be transported through the desired thermoacoustic cycle. Thermoacoustic devices do not contain moving parts to perform this function, yet the acoustic simulation of heat flux and generation (or absorption) of acoustic work point to some type of timed phasing of thermodynamic processes achieved

in a simple way. Phasing in acoustic devices depends on the presence of two thermodynamic media: fluid and solid walls.

The dynamic changes of the temperature in the fluid oscillating at the acoustic frequency come from two superimposed sources: the adiabatic compression and expansion of the fluid by the acoustic pressure, and the local temperature of the solid walls near the fluid. The heat flow between the solid walls and the fluid creates a time delay in temperature between temperature and pressure, which creates the necessary phase shift that drives the thermoacoustic cycle. Therefore, a rather poor thermal contact between the solid walls and the fluid parcel is intentionally required to achieve the correct phasing of the temperature oscillations of the working fluid and solid stack surface. For sinusoidal motion, parcels at a thermal penetration depth away from the solid walls have the critical phasing needed for the thermoacoustic effect. Parcels further away have no thermal contact with the walls and are simply compressed and expanded adiabatically by the wave, while parcels at a thermal penetration depth from the walls have good enough thermal contact with the walls to exchange heat with the solid walls but, at the same time, are in poor enough contact to produce the correct phasing for the cycle. Therefore, the gas at about δ_k away from the walls is the main contributor to the thermoacoustic effect as shown in figure 1.2. The thermal penetration depth is the distance through which the heat can diffuse through the gas in half a cycle. The thermal penetration depth is a parameter of the thermoacoustic effect, affected by the properties of gas and the frequency of oscillations. A gas with a high thermal conductivity, or a cycle with a lower frequency, allows a thicker layer of gas to be effective for the process.

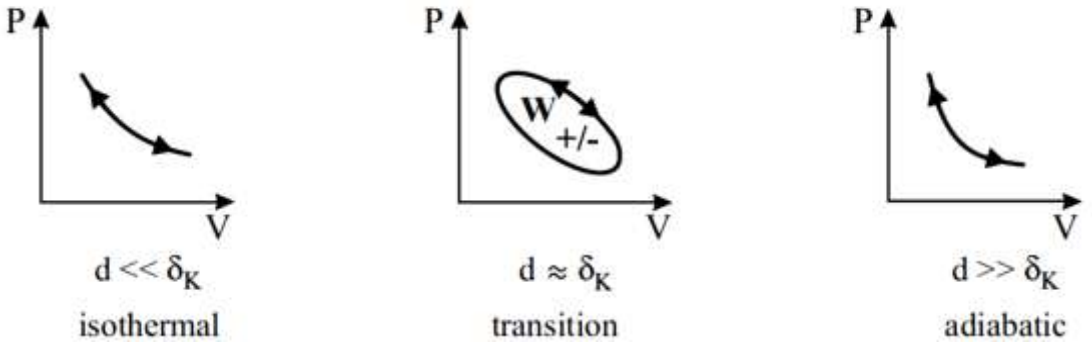

Figure 1.2: P-V diagrams for the thermodynamic processes of the gas parcels as the distance from the wall, d, increases.

The cycle needed for the heat pumping effect is illustrated in figure 1.1a. The heat pumping process is characterized by a low temperature gradient on the walls in contact with the gas parcel. It can be simplified into the following four processes: [1] Initially, the relatively cold gas parcel is compressed by the acoustic wave while moving. This reversible process causes the gas to warm up to the highest cycle temperature and move inwards to become in contact with the high temperature side of the wall. [2] Due to the low temperature gradient, the gas is warmer than the hottest portion of the wall. Heat flow irreversibly from the parcel to the wall. This heat rejection process is accompanied with further contraction that consumes more work. [3] The cycle continues as the parcel is displaced outwards reversibly to its initial location, causing the parcel to reach the lowest cycle temperature. The cold parcel is now in contact with the cold side of the stack wall. [4] However, the temperature of the gas is lower than that of the wall, thus heat flows irreversibly to the parcel.

In a thermoacoustic prime mover, [1] a reversible process of isentropic compression is done by the wave, consuming input work to the system, and causing the gas parcel to contract and warm up to a higher temperature. The movement of the parcel while contracting shall put it in contact with the high temperature wall section. [2] Heat flows from the wall to the parcel in an irreversible constant pressure process causing the parcel to reach the maximum cycle temperature. This causes the parcel to rarefy. [3] Consequently, the parcel moves outwards and work is obtained from the system. Now the parcel cyclic movement is going to make a reversible expansion process. Output work of this process is equal to the input work of the compression process, equalizing their share in net work. The parcel has now moved to be in contact with the coldest portion of the wall. [4] Heat irreversibly flows from the parcel to the solid walls and the parcel cools down and contracts to its initial condition. This attracts the parcel inwards again. However, needed work is less than produced work in the second process, producing net work. As a result, a standing wave is sustained due to the presence of a temperature gradient. The process follows the criteria of Lord Rayleigh as the addition of heat occurs when the pressure is high, and the heat is rejected when the pressure is low, thus encouraging the oscillations.

The main parameter that determines the type of the device (prime mover or refrigerator/heat pump) is the value of the temperature gradient. A *critical temperature gradient* is needed to induce the cycle in the direction of producing net work. This can be explained by considering processes [1] and [3] in the engine cycle (figure 1.1). The two adiabatic processes are needed to complete the cycle but result in no net work. The compression and expansion result in a certain temperature difference for the gas parcel in the two positions it reaches while expanding and contracting. For the whole media, this results in the need of a certain temperature gradient for these two processes to occur. The increase in the temperature gradient over its critical limit provides the necessary values for the two other isobaric processes to occur, producing the net work of the cycle.

The refrigerator cycle that uses acoustic work to produce adverse heat flow, results in a temperature gradient lower than the critical temperature gradient needed by the engine. The ratio of the temperature gradient to this *critical temperature gradient* is a very important parameter in the performance of thermoacoustic devices. Pressure oscillations are encouraged in the gas if a temperature gradient larger than this critical limit is imposed on the plate axial direction:

$$\nabla T_{crit} = T_m \beta \omega p_1 / u_1 c_p \rho_1 \qquad \text{Eq. 1.1}$$

where T_m is the mean gas temperature, β is the thermal expansion coefficient, p_1, ρ_1 and u_1 are dynamic pressure, density, and volumetric velocity of the gas respectively and ω is the angular frequency of oscillations. The ratio between the temperature gradient and the critical limit is less than one in the refrigerators and higher than one in prime movers. The thermoacoustic processes depend mainly on the interactions between the oscillating gas and the fixed, nearly isothermal solid surface. That suggests that the effective gas layer is the layer that can transfer heat to and from the wall. Gas oscillating far away from the wall undergoes an adiabatic process, gaining or losing no heat and making no contribution to the thermoacoustic effect. Gas in perfect contact with the solid surface can be assumed to follow the temperature of the walls and can be assumed to compress and expand isothermally, gaining and losing heat to the walls.

1.3.3 Acoustic Background

Acoustics is the branch of physics concerned with the mechanical pressure waves we call "sound". Acousticians study any mechanical wave that can be transmitted in any medium in any range of frequency, not only the audible range. Acoustic wave is a form of energy transfer: It carries energy from a location to another.

Acoustic wave is a type of harmonic oscillations. Harmonic oscillations are repeated movements where a particle moves around a position of equilibrium. The particle in acoustic waves is the matter particle and the energy is associated with its movement. The particle moves back and forth around a stationary position in the same direction of the wave movement, while the energy of the wave moves across the space.

The following paragraph discusses some of the main parameters that are used to define and acquire reasonable knowledge of the nature of an acoustic wave.

i. Full Cycle

A particle goes one full acoustic cycle when it reaches a certain position in its oscillatory movement twice, one moving forth and one moving back as shown in figure 1.3. After one cycle, the particle reaches its original position at the beginning of the cycle. A standard position agreed upon to be the typical start of a wave is the equilibrium position, where the movement around it in both directions are similar.

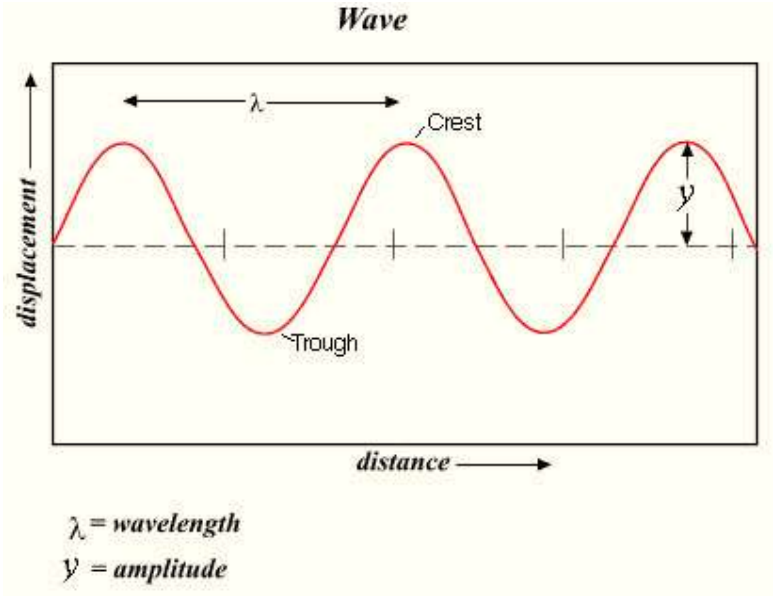

Figure 1.3: Wave characteristics for a typical sinusoidal wave

ii. Wavelength, frequency, time period, and wave number

Wavelength, λ, is the distance between the consecutive locations along the wave propagation direction, where the values of the pressure are the same. The frequency, *f*, of a wave is the number of cycles that pass through a fixed point in one second. Its unit (Hz) is named after Hertz and is equal to one cycle per second. The higher frequency is related to higher rate of energy transfer. For a fixed propagation speed: the higher the frequency, the shorter the wavelength. Time period, *T*, of a wave is the time taken by the gas particle to complete a full

cycle. It is the inverse of the frequency. The wave number is the number of wavelengths per 2π units of distance. It is sometimes termed the angular or circular wavenumber, but more often simply as wave number.

iii. Resonance

Resonance is the tendency of the system to produce higher amplitude oscillations at certain frequencies. These frequencies are known as the system resonance frequencies, or fundamental frequencies. The same driving force can produce higher pressure amplitudes at resonance frequencies than when operated at other frequencies.

In a mechanical system comprising an oscillating mass attached to a spring with certain stiffness, the system tends to oscillate with higher amplitudes at the resonance frequency that depends on the value of the mass and the stiffness of the spring. If the system is free to oscillate without external forces, it oscillates at the resonance frequency.

In an acoustic system, the geometry of the resonator in which the wave is contained will specify the values of the resonance frequencies. The system boundary conditions will specify a set of wave lengths, and frequencies, at which the particle will oscillate in a way that satisfies the boundary conditions. The frequencies of resonance of an iso-diameter resonator are multiples of the fundamental frequency, which is the lowest frequency of oscillations that satisfies the boundary conditions.

iv. Dynamic pressure amplitude

The amplitude of the wave is the difference between the maximum pressure and the equilibrium pressure. Although the amplitude of the wave depends mainly on the driving force which is not dependent on the factors mentioned above, the frequency and energy transfer are greatly associated with the amplitude. At low dynamic pressure amplitudes, the linear theory is valid. As the dynamic pressure amplitude increases, non-linear deviations become dominant.

v. Intensity

Intensity is the rate at which the energy is transferred along the wave path per unit area. It is mathematically dependent on the driving force along with the parameters of the wave and the fluid in which the wave moves.

vi. Standing waves

Standing (stationary) wave is a type of wave that remains fixed in space. The amplitude of oscillation of the particles of the wave for every position does not change with time. The dynamic pressure at the particles is noticed to have different values in time, but its maximum (i.e. amplitude) at every point is constant. This occurs as a result of the interference of two identical waves moving in *opposite* directions.

The properties of a standing acoustic wave in an air column are illustrated in figure 1.4. Standing wave contains an amount of energy that is fixed at the location of the wave. Standing wave needs energy to generate the pressure oscillations, but does not need further energy to sustain itself in a certain position, except to compensate for viscous losses. In contrast, traveling waves are not confined to a given space in the medium.

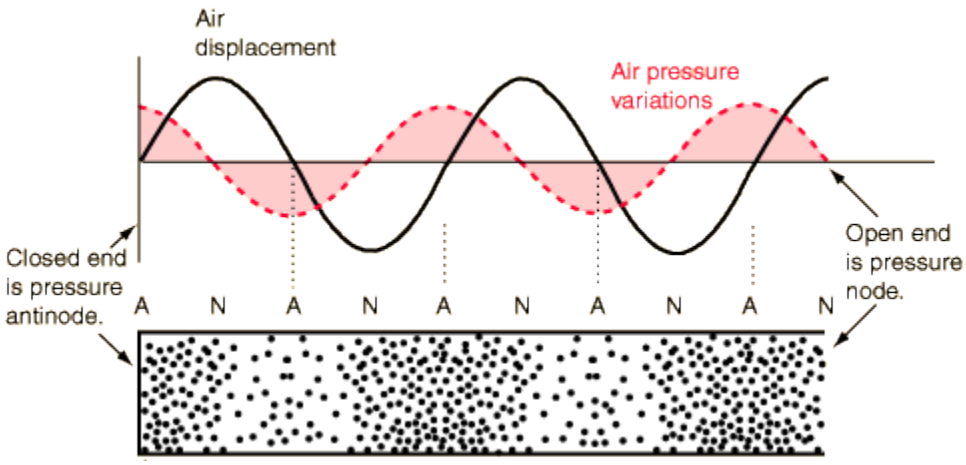

Figure 1.4: A standing wave in a column full of air.

1.3.4 General Thermoacoustic theory

Starting with Navier-Stokes and continuity equations, Rott developed a formula to describe the thermoacoustic oscillations that occur as a result of interactions of heat, viscosity, and thermal effects in fluids [1,3,5-7].

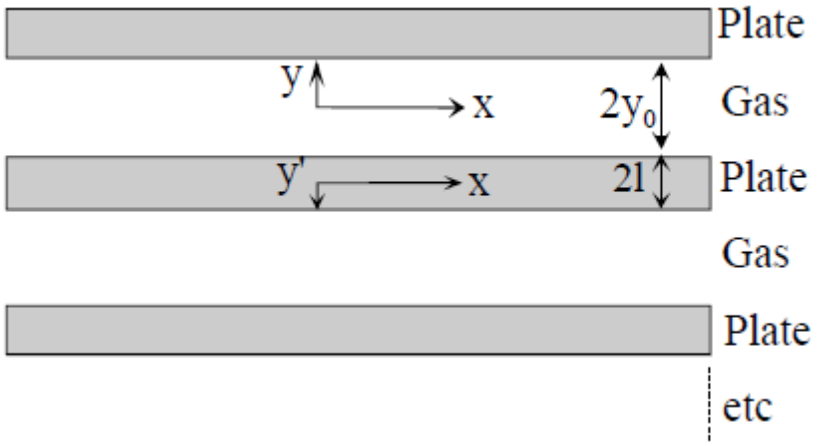

Figure 1.5: Geometry of the simplified parallel plate stacks.

Consider a stack of parallel plate placed in a gas-filled resonator as in figure 1.5. The plates are of thickness $2l$ and the spacing between every 2 layers of plates is $2y_0$. The x axis extends along the stack parallel to the wave propagation direction. The y axis is perpendicular to the layers of the stacks. The Rott wave equation is derived considering the following assumptions:

a. The theory only takes into consideration the linear effects. Any higher order effects, other than energy transport, which is a second order effect, are neglected. It is worth noting that second order effects, such as acoustic streaming and turbulence, can have high effects on performance and are not included in the linear assumption.
b. Oscillating phenomena oscillates harmonically at a *single* angular frequency (ω). This means that higher order harmonics of the wave is neglected.
c. The resonator walls and the plates of the stack or regenerator are assumed to be perfectly rigid.

d. The wave that propagates in the fluid is one dimensional and therefore the acoustic pressure, gas parcel displacement and velocity are assumed constant over every cross section.
e. The temperature span along the thermoacoustic stack or regenerator is small compared with the mean stack temperature. This guarantees that the properties can be evaluated at the mean stack temperature.

Acoustic quantities are presented as a mean value plus an oscillatory part. Therefore, complex notation is used for gas pressure, velocity, density, temperature, and entropy:

$$p = p_m + p_1 e^{i\omega t} \quad \text{Eq. 1.2a}$$

$$u = u_m + u_1 e^{i\omega t} \quad \text{Eq. 1.2b}$$

$$\rho = \rho_m + \rho_1 e^{i\omega t} \quad \text{Eq. 1.2c}$$

$$T = T_m + T_1 e^{i\omega t} \quad \text{Eq. 1.2d}$$

where u_m is usually zero (assuming no mean flow is present), and $i\omega t$ is used for the oscillatory time convention.

Acoustic power flow can be expressed as:

$$\overline{p(t)u(t)} = \frac{1}{2}Re[p\tilde{u}] = \frac{1}{2}p_1 u_1 \cos(\phi_1 - \phi_2) \quad \text{Eq. 1.3}$$

Where the tilde "~" denotes complex conjugation and ϕ_1, ϕ_2 denotes the phases of p_1 and u_1, respectively. For an ideal standing acoustic wave, the phase shift is exactly 90^o, resulting in no power flow. Power flow results from the small deviation in phase shift away from the 90^o value.

The continuity, Navier-Stokes, and energy equations respectively, can be expressed as:

$$\frac{\partial \rho}{\partial t} + \nabla.(\rho \mathrm{v}) = 0 \quad \text{Eq. 1.4a}$$

$$\rho\left[\frac{\partial \mathrm{v}}{\partial t} + (\mathrm{v}.\nabla)\mathrm{v}\right] = -\nabla p + \mu\nabla^2\mathrm{v} + \left(\xi + \frac{\mu}{3}\right)\nabla(\nabla.\mathrm{v}) \quad \text{Eq. 1.4b}$$

$$\frac{\partial}{\partial t}\left(\frac{\rho \mathrm{v}^2}{2} + \rho\epsilon\right) = -\Delta.\left[\rho \mathrm{v}\left(\frac{\upsilon^2}{2} + h\right) - \mathrm{K}\nabla\mathrm{T} - \mathrm{v}.\sum\right] \quad \text{Eq. 1.4c}$$

where ρ is density, v is velocity, p is pressure, μ and ξ are dynamic viscosity and bulk viscosity, respectively; K is the gas thermal conductivity, ϵ and h are internal energy and enthalpy per unit mass, respectively, and Σ is the viscous stress tensor, with components:

$$\sum_{ij} = \mu\left(\frac{\partial \upsilon_i}{\partial x_j} + \frac{\partial \upsilon_j}{\partial x_i} - \frac{2}{3}\delta_{ij}\frac{\partial \upsilon_k}{\partial x_k}\right) + \xi\delta_{ij}\frac{\partial \upsilon_k}{\partial x_k} \quad \text{Eq. 1.5}$$

Solving these equations with the boundary conditions as follows:

i) The temperatures in the plates and in the gas are coupled at the solid-gas interface where continuity of temperature and heat fluxes is imposed. These conditions are respectively expressed as:

$$T_1(y_0) = T_{s1}(l), \qquad \text{or} \qquad K\left(\frac{\partial T_1}{\partial y}\right)_{y0} = -K_s\left(\frac{\partial T_{s1}}{\partial \dot{y}}\right)_l \qquad \text{Eq. 1.6}$$

ii) No slip condition: $u_1(y_0) = 0$.

Solving the energy equation, the solid temperature can be expressed as:

$$T_{s1}(x,\dot{y}) = \frac{\varepsilon_s}{1+\varepsilon_s}\left[\frac{\beta T_m}{\rho_m c_p}p_1 + \frac{1}{\rho_m \omega^2}\frac{dT_m}{dx}\left(\frac{dp_1}{dx}\right)\left(\frac{1}{\sigma-1}\right)1 - \frac{f_v}{\sigma f_k}\right]\frac{\cosh(\alpha_s \dot{y})}{\cosh(\alpha_s l)} \qquad \text{Eq. 1.7}$$

, where

$$f_v = \frac{\tanh(\alpha_v y_0)}{\alpha_v y_0};\ \alpha_v = \frac{1+j}{\delta_v} \qquad \text{Eq. 1.7b}$$

$$f_k = \frac{\tanh(\alpha_k y_0)}{\alpha_k y_0};\ \alpha_k = \frac{1+j}{\delta_k} \qquad \text{Eq. 1.7c}$$

$$\varepsilon_s = \frac{\sqrt{K\rho_m c_p}}{\sqrt{K_s \rho_s c_s}}\frac{\tanh(\alpha_k y_0)}{\tanh(\alpha_s l)}, \quad \alpha_s = \frac{1+j}{\delta_s} \qquad \text{Eq. 1.7d}$$

$$\delta_k = \sqrt{\frac{2K}{\rho_m c_p \omega}}; \quad \delta_s = \sqrt{\frac{2K_s}{\rho_s c_s \omega}};\ \sigma = \left(\frac{\delta_v}{\delta_k}\right)^2 \qquad \text{Eq. 1.7e}$$

where δ_k is the thermal penetration depth of the gas, δ_s is the solid thermal penetration depth, and σ is the gas Prandtl number. The function f is called the Rott's function and it is geometry dependent. The time averaged can be derived as[8]:

$$\dot{E}_2 = \frac{A_g}{2}Rep_1\langle u_1^*\rangle\left(1 - \frac{\beta T_m(f_k - f_v^*)}{(1+\sigma)(1+\varepsilon_s)(1-f_v^*)}\right) \qquad \text{Eq. 1.8}$$
$$+ \frac{A_g \rho_m c_p |\langle u_1\rangle|^2}{2\omega(1-\sigma)|1-f_v|^2}\frac{dT_m}{dx}Im\left[f_v^* + \frac{(f_k - f_v^*)\left(1+\frac{\varepsilon_s f_v}{f_k}\right)}{(1+\varepsilon_s)(1+\sigma)}\right]$$
$$- \left[A_g K + A_s K_s\right]\frac{dT_m}{dx}$$

where A_s is the cross-sectional area of the stack material. This important result represents the energy flux along x direction (wave direction) in terms of $T_m(x)$, $p_1(x)$, material properties and geometry. For an ideal gas and ideal stack $\varepsilon_s = 0$, this result was observed obtained by Rott. As can be seen from the energy flux equation, the energy flux consists of three terms: the first term in p_1u_1 is the acoustic power, the second term in s_1u_1 is the hydrodynamic entropy flow, and the final term is simply the conduction of heat through gas and stack material in the stack region. The acoustic power absorbed in the stack is[8]:

$$\frac{d\dot{W}_2}{dx} = \frac{-A_g\omega}{2}\left[\frac{\rho_m Im(-f_v)}{|1-f_v|^2}|\langle u_1\rangle|^2 + \frac{(\gamma-1)Im(-f_k)}{\rho_m a^2(1+\varepsilon_s)}|p_1|^2 + \frac{\beta}{\omega(1-\sigma)(1+\varepsilon_s)}\frac{dT_m}{dx}Re\frac{(f_k^*-f_v^*)}{(1-f_v^*)}p_1\langle u_1^*\rangle\right] \quad \text{Eq. 1.9}$$

This is the acoustic power absorbed (or produced) in the stack per unit length. The subscript 2 is used to indicate that the acoustic power is a second-order quantity, i.e., the product of two first-order quantities, p_1 and u_1.

The first two terms in work equation are the viscous and thermal relaxation dissipation terms, respectively. These two terms are always present whenever a wave interacts with a solid surface, and they have a dissipative effect in thermoacoustics. The third term in the equation contains the temperature gradient dT_m/dx. This term can either absorb (refrigerator) or produce acoustic power (prime mover) depending on the magnitude of the temperature gradient along the stack. This term is the unique contribution to thermoacoustics.

i. Rott's function

The properties of the temperature and velocity fields of an oscillatory fluid inside a porous material are completely built in the thermoacoustic functions, f_k and f_v. Depending on surface geometry, the equations that yield these functions take different forms and some of the specific cases are discussed here. The function f_v includes the averaged influence of the viscous forces on the oscillating gas, in the presence of the walls. This expression is geometry dependent as shown in figure 1.7.

ii. Boundary layer and short-stack approximations

The thermoacoustic expressions presented in the previous section are complicated to use. Common theoretical assumptions are used to simplify these expressions[8].

First, in the boundary-layer approximation the stack pores are of a width $y_0 >> \delta_k$, so that the hyperbolic tangents in equation 1.6 can be set equal to unity.

Second, In the short-stack approximation, $L_s \ll \lambda$ the stack is considered to be short enough that the pressure and velocity in the stack do not vary appreciably.

In the standing-wave thermoacoustic engines, the correct phasing between the temperature of the walls and the gas needs that the absolute value of the imaginary part of f_k is high. As shown in figure 1.6, the optimum point occurs at the point where r_h/δ_k is about unity. The absolute value of the imaginary part is highest and occurs at r_h/δ_k of about 2 for the case of pin arrays which has the highest contact area with the gas.

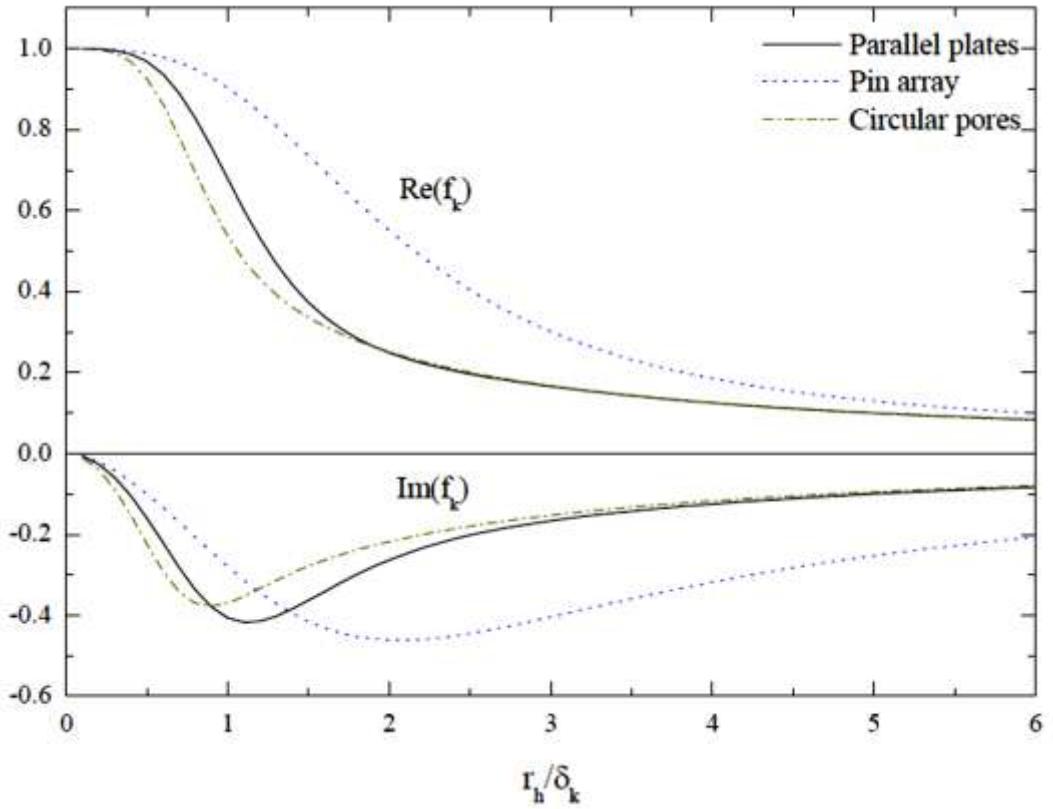

Figure 1.6: Imaginary and real parts of the Rott function f_k as function of the ratio of the hydraulic radius and the thermal penetration depth. Three geometries are considered. For pin arrays, an internal radius $r_i = 3\delta_k$ is used in the calculations[14].

The standing-wave acoustic pressure in the stack, p_1^s, is an appropriate reference for calculations, and thus, can be taken as real and is given by

$$p_1 = p_0 cos(kx) \qquad \text{Eq. 1.10a}$$

and the mean gas velocity in the stack in x direction is:

$$u_1 = j\left(1 + \frac{l}{y_0}\right)\frac{p_0}{\rho_m a} sin(kx) = j u_1^s \qquad \text{Eq. 1.10b}$$

where p_0 is the pressure amplitude at the pressure antinodes of the standing wave and k is the wave number. The factor $(1+l/y_0)$ accounts for the different gas cross sectional areas between the stack and the resonator, which requires that the velocity inside the stack must be higher than that outside by the cross-sectional area ratio $(1 + l/y_0)$. The Rott's function f in the boundary layer-approximation is given by[8]:

$$f_k = \frac{(1-j)\delta_k}{y_0} \qquad \text{Eq. 1.11a}$$

$$f_v = \frac{(1-j)\delta_v}{y_0} \qquad \text{Eq. 1.11b}$$

Equations 1.7 and 1.8 are converted into

$$Q_{cn} = \frac{\delta_{kn} D^2 \sin(2x_n)}{8\gamma(1+\sigma)\Lambda}\left(\frac{\Delta T_{mn}(x_n)}{(\gamma-1)BL_{sn}}\frac{1+\sqrt{\sigma}+\sigma}{1+\sqrt{\sigma}} - \left(1+\sqrt{\sigma}-\sqrt{\sigma}\delta_{kn}\right)\right) \quad \text{Eq. 1.12}$$

and $W_n = \frac{\delta_{kn} L_{sn} D^2}{4\gamma}(\gamma-1)B\cos(x_n)^2\left(\frac{\Delta T_{mn}\tan(x_n)}{BL_{sn}(\gamma-1)(1+\sqrt{\sigma})\Lambda}-1\right) - \frac{\delta_{kn} L_{sn} D^2}{4\gamma}\frac{\sqrt{\sigma}\sin(x_n)^2}{B\Lambda}$ Eq. 1.13

where $\Lambda = 1-\sqrt{\sigma}\,\delta_{kn}+\frac{1}{2}\sigma{\delta_{kn}}^2$ Eq. 1.13b

Boundary and short stack approximations are used to simplify the calculations required to describe the performance of the gas layers during the oscillations. While the initial forms are complicated and contain Bessel functions, using the short-stack and the boundary-layer approximations causes calculations of thermal and acoustic powers to be easier and require less effort. These approximations are valid in most practical cases.

1.4 Standing-wave Thermoacoustic Engine

The thermoacoustic engine (TAE) is a device that converts heat energy into work in the form of acoustic energy. A thermoacoustic engine is operating using the effects that arise from the resonance of a standing-wave in a gas. A standing-wave thermoacoustic engine typically has a thermoacoustic element called the "stack". A stack is a solid component with pores that allow the operating gas fluid to oscillate while in contact with the solid walls. The oscillation of the gas is accompanied with the change of its temperature. Due to the introduction of solid walls into the oscillating gas, the plate modifies the original, unperturbed temperature oscillations in both magnitude and phase for the gas about a thermal penetration depth $\delta = \sqrt{2k/\omega}$ away from the plate[4], where *k* is the thermal diffusivity of the gas and $\omega=2\pi f$ is the angular frequency of the wave. Thermal penetration depth is defined as the distance that heat can diffuse though the gas during a time $1/\omega$. In air oscillating at 1000 Hz, the thermal penetration depth is about 0.1 mm. Standing-wave TAE must be supplied with the necessary heat to maintain the temperature gradient on the stack. This is done by two heat exchangers on both sides of the stack.

Thermoacoustic engines still suffer from some limitations, including that:

- The device usually has low power to volume ratio. Very high densities of operating fluids are required to obtain high power densities,
- The commercially-available linear alternators used to convert acoustic energy into electricity currently have low efficiencies compared to rotary electric generators, and only expensive specially-made alternators can give satisfactory performance.
- TAE uses gases at high pressures to provide reasonable power densities. This imposes sealing challenges particularly if the mixture has light gases like helium.
- The heat exchanging process in TAE is critical to maintain the power conversion process. The hot heat exchanger has to transfer heat to the stack and the cold heat exchanger has to

sustain the temperature gradient across the stack. Yet, the available space for it is constrained with the small size and the blockage it adds to the path of the wave. The heat exchange process in oscillating media is still under extensive research.

- The acoustic waves inside a thermoacoustic engines operated at large pressure ratios suffer many kinds of non-linearities such as turbulence which dissipates energy due to viscous effects, harmonic generation of different frequencies that carries acoustic power in frequencies other than the fundamental frequency.

The performance of thermoacoustic engines usually is characterized through several indicators as follows:

- The first and second law efficiencies, defined in section 3.4.3
- The onset temperature difference, defined as the minimum temperature difference across the sides of the stack at which the dynamic pressure is generated,
- The frequency of the resultant pressure wave, since this frequency should match the resonance frequency required by the load device, either a thermoacoustic refrigerator/heat pump or a linear alternator,
- The degree of harmonic distortion, indicating the ratio of higher harmonics to the fundamental mode in the resulting dynamic pressure wave, and
- The variation of the resultant wave frequency with the TAE operating temperature

1.5 Applications

Although the field of thermoacoustics is still in the technical development stage, some effective devices were built investing the thermoacoustic effect in applications involving refrigeration or power generation.

In 2007, Babaei and Seddikui[9] presented a thermoacoustic air refrigeration system designed for automotive applications, working with helium and investing the engine waste heat with an overall efficiency of 18.8%.

In 2004, Symko *et al.*[10] proposed a small, high-frequency thermoacoustic refrigerator that is driven by a thermoacoustic engine that uses the waste heat of microelectronic components to pump heat or produce spot cooling. They proposed using the waste heat from a microelectronic processor to drive a small scale thermoacoustically-driven thermoacoustic refrigerator to produce spot cooling for the surface of the processor. Cooling power densities of 0.1 to 0.6 Watts for every cm^2 of resonator cross sectional area were achieved.

In 2004, Hatazawa *et al.*[11] designed a thermoacoustically-driven thermoacoustic refrigerator that uses waste heat from a gasoline engine. In 2007, Babaei *et al.*[12] proposed a similar system to use in a gas turbine trigeneration system, operating with the gas turbine waste heat. In 2005, Zoontjens *et al.*[13] investigated the feasibility of using the automotive motor waste heat to power a thermoacoustic air conditioner to replace the fuel consuming conventional system.

In 1998, the first solar-energy powered standing wave thermoacoustic engine was built by Chen and Garrett[14]. Adeff and Hofler[15] built and tested a prototype thermoacoustic system that operates on the solar energy. Chen[16] constructed the first solar powered thermoacoustic cooler which was heated by a parabolic dish collector. Shen *et al.*[17] investigated the performance of a solar-powered thermoacoustic engine working with different gases under different solar tilt angles.

1.6 Thesis Scope

The present study aims to:

[1] build, operate and test a standing-wave engine prototype,

[2] simulate the performance of the built prototype using DELTAEC,

[3] operate the prototype with different gases and gas mixtures, and record the relevant parameters in transient and steady-state phases,

[4] analyze the engine performance in time and frequency domain in transient and steady-state phases,

[5] evaluate the performance of the engine and identify the major power losses,

[5] identify the major losses in the engine and its source, and

[6] develop and test a technique to eliminate or reduce the losses in the engine.

In this work, the major source of losses in the engine was identified as the existence of higher harmonics in the output acoustic wave. The loss in higher harmonic generation was reduced using inserts of different shapes, blockage areas and positions along the wave.

2. Review of Related Literature

The field of thermoacoustic built up a solid base of available literature in the recent decades. In this chapter, studies of the standing-wave thermoacoustic engines are presented, describing the history, experimental performance, and simulation results of thermoacoustic engines. Several studies discuss the validity of the currently accepted theoretical model, the linear theory. Some authors discuss the possibility of introducing the non-linear terms in the theory.

In the presented literature, experimental performance of many prototypes is compared with the numerical simulations of DELTAEC software. Other presented studies describe the losses related to the generation of higher harmonics. Performance and description of several prototypes built to make use of solar or waste energy are presented.

2.1 Historical background of thermoacoustic engines

The first description of the acoustic-oscillation production using thermoacoustics is described by Sondhauss in 1850, who detected sound generation in a duct where sufficiently large axial temperature gradient is imposed. After Byron Higgins made the first observations and investigations of organ-pipe type oscillations, known as .singing flames, in 1777, the physics of thermoacoustic were investigated by Kirchhoff in 1868.

No noticeable further progress was made until the thermoacoustic theory was first developed by Rott[5-7] and reviewed later by Swift[4]. In this series of theoretical studies, Rott managed to build the thermoacoustic theory that describes the interactions of acoustic waves and temperature variations and the thermodynamic processes associated with the existence of waves in a fluid. Several research teams aim to improve the effectiveness of this technology to provide effective alternatives for conventional power production and conversion technologies.

From as early as 1962, it was experimentally found by Carter *et al.* that by properly inserting a solid substrate in the Sondhauss tube, the oscillations were enhanced. Merkli and Thomann[18] found that during a thermoacoustic cycle, heat is transferred along a resonator from a region near the velocity antinode to a region near the adjacent pressure antinode. These phenomena were studied by Rott[1,3,5-7] who extended the qualitative explanation by Lord Rayleigh by giving a quantitative explanation for the phenomena.

2.2 Performance of standing-wave thermoacoustic engines

Standing-wave thermoacoustic engines have been going under extensive research. Although there has been much progress in the field of travelling-wave engines that is promising regarding the higher efficiencies, the standing-wave engines possess a lot of advantages that makes it still competitive. These advantages include simplicity, ease of design and manufacture, and higher understanding of the physics. Investigations on the non-linear performance of standing-wave engines still need more work to clearly understand and describe losses and deviation from the linear theory.

2.2.1 Experimental investigations on thermoacoustic engines

Swift[4] systematically expanded and summarized the theory of linear thermoacoustics. The theory supposes that the time dependence of all fluctuating quantities, such as pressure, velocity, temperature is purely sinusoidal. Swift[19] introduced viscous resistance, thermal-relaxation resistance, inertance, compliance and proportionality coefficient of a controlled source to thermoacoustics, and sound-current analogy was carried out.

Arafa *et al.*[20] studied the effect of mean pressure and stack length, position, and porosity, on the performance of a standing-wave engine working with helium from 1 to 10 bar. They suggested that the engine should work using an inert gas with high speed of sound and low Prandtl number; the engine should also be operated at a ratio of pore half width to thermal penetration depth in the approximate range of 3 - 5 for low onset temperature and high conversion efficiencies.

The use of a dimensionless framework was carried by Olson and Swift[21] who used dimensionless parameters to analyze thermoacoustic devices. Dimensionless numbers are used to reduce the number of independent parameters in their experiments and for scaling purposes.

The review by Swift[4] in 1988 described the theoretical performance of thermoacoustic engines. Theoretical predictions of the linear theory showed that the efficiency and work flux decrease when the stack is located closer to the velocity node for the same wave length ratio due to the higher viscous losses and longitudinal thermal conduction. Swift also noticed that the maximum relative efficiency and maximum work flux do not coincide, but there is a wide range of acceptable operating conditions. Measurements confirmed the validity of calculations. The square of normalized pressure increased linearly with the input power at low amplitudes. Swift expected that at higher amplitudes the nonlinearities will appear, but couldn't operate the engine to prevent catastrophic damage due to oscillation-caused cavitation.

In their paper that describes a solar–driven standing-wave thermoacoustic engine, Chen and Garrett[14] confirmed the linear behavior of the square of pressure versus heat input that is predicted by the linear theory as shown in figure 2.1. The results also showed that the temperature difference across the stack is essentially independent of input heater power above onset.

Jin *et al.*[22] investigated the performance of a standing wave engine of low onset temperature. Results of experiments showed the operating characteristics of their prototype. Results confirmed that the onset temperature of the present system can be lower than 100 °C. The structural parameters, including stack position and tube inclination, may also affect the onset temperature. The lowest value can be observed at a proper stack position in a horizontal resonant tube. As to operating frequency, the resonant tube length is its crucial factor, while there is little influence from heat input and stack's position.

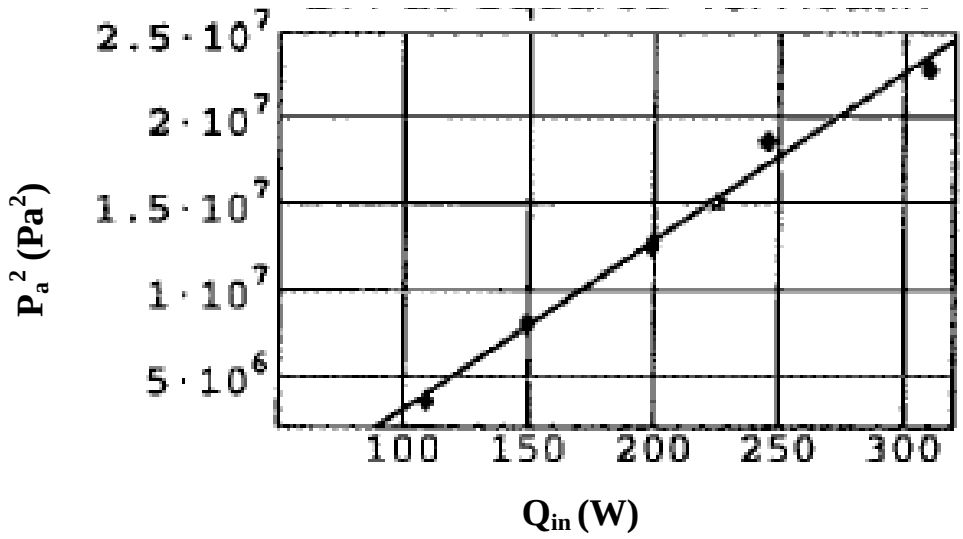

Figure 2.1: Square of pressure wave amplitude versus heat input to the standing-wave engine by Chen and Garrett[14].

In a detailed work, Swift[23] presents measurements and analysis of a 13-cm diameter standing-wave thermoacoustic engine. The engine uses Helium at 13.8 bar. The engine delivers up to 630W of acoustic power. Swift's measurement agreed with the predictions of linear theory within 4% at low acoustic amplitudes. The measurements of the square of the amplitude, shown in figure 2.2, differ from the predictions by 20%, twice the uncertainty. Swift suggests some reasons of this deviation including resonance-enhanced harmonic content in the acoustic wave, and a first order temperature defect in thermoacoustic heat exchangers. It was observed that at low pressure amplitudes, steady-state operation of the engine was not possible, because as the heater heated the hot heat exchanger and nearby parts, causing the engine to begin oscillation quickly reaching high dynamic pressures, and then these high-amplitude oscillations quickly cooled the hot-stack side causing the oscillations to stop.

Ibrahim and Abdel-Rahman[24] presented experimental data on the issues related to operating the engine by various heat sources at different temperatures. They demonstrated how the use of gas mixtures affected the onset temperature, the acoustic power output, the operating frequency, and the change in operating frequency with temperature.

Belcher *et al.*[25] numerically assessed thermoacoustic engines using different gases and concluded that if all losses outside the stack are negligible (in the heat exchangers and resonator), the minimum onset temperature would occur for gases having a specific-heat ratio γ close to one, which is characteristic of polyatomic gases.

2.2.2 Numerical studies on thermoacoustic engines using DELTAEC

Ward and Swift[26] developed a program for thermoacoustic computation, i.e. DELTAEC (Design Environment for Low-amplitude Thermoacoustic Energy Conversion), which can be used to simulate and design thermoacoustic engines and refrigerators, and is helpful for practical application of linear thermoacoustics.

Valuable contributions by Swift and Ward[27] to the simulation of thermoacoustics focused on the theoretical performance of porous stacks, the influence of turbulent flow on viscous resistance, local loss caused by the variety of flow area, entrance effect and joining condition.

Their work improved the veracity accuracy of the simulation of thermoacoustic machines within linear thermoacoustics.

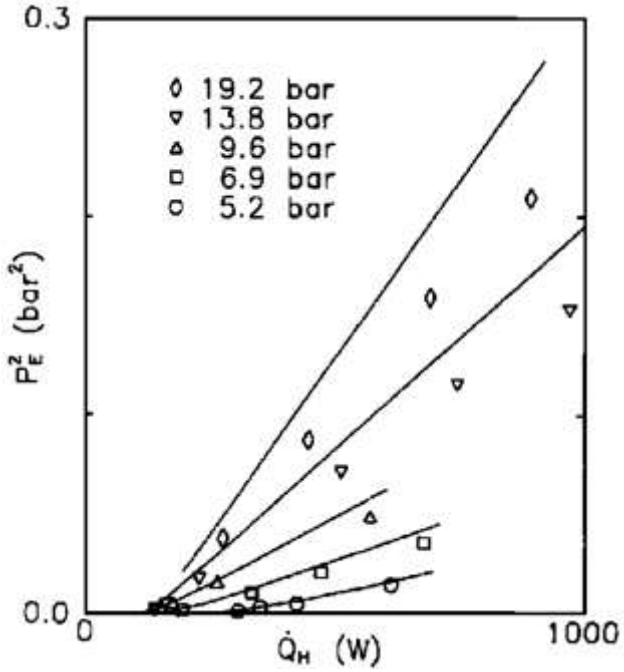

Figure 2.2: Square of end pressure amplitude versus input heat for different Helium mean pressures. Lines are calculations and points are measurements[23].

Gardner and Swift[28] used DELTAEC to calculate values with which to compare the measurements in their investigation of a cascade thermoacoustic engine. For one of the data sets, they compared the calculated results for ‘‘as-built’’ dimensions and ‘‘as-running’’ dimensions, to investigate whether thermal expansion of the hot parts and consequent compression of the bellows were significant. Differences were only of the order of 0.1% and 0.1°, so they performed all other calculations using as-built dimensions. Figure 2.3 shows that DELTAEC results were close to the experimental measurements. It is important to note that swift used the minor losses factor as an adjusting parameter for the DETAEC calculations to meet the measurements.

Ibrahim *et al.* used DELTAEC to study the performance of a standing-wave thermoacoustic engine[29]. They concluded that mean pressure, stack spacing, stack mid-position and stack length have a noticeable effect on energy conversion efficiency. By compromising the effects of these parameters, the first law efficiency of their modeled engine could be increased from 9.6% to 16%.

Arafa *et al.*[30] used DELTAEC to investigate the sensitivity of the mean pressure, stack spacing, stack mid-position and stack length on the engine performance. They indicated the relative importance of these parameters and their effect on the engine performance.

Babaei and Siddiqui used DELTAEC as verification for a design procedure for thermoacoustic devices. A good agreement is observed between the developed procedure and the DELTAEC simulations[31]. Both Wetzel[32] and Besnoin[33] discussed thermoacoustic device optimization in their works. While Wetzel focused on the optimal performance of a thermoacoustic refrigerator, Besnoin targeted heat exchangers. In addition to these

optimization efforts, Zoontjens *et al.*[34] illustrated the optimization of thermoacoustic devices; they used DELTAEC to vary individual parameters to determine optimal designs. Ueda[35] determined the effect of a variation of certain engine parameters on pressure amplitudes. Another work that made use of DELTAEC is Tijani *et al.*[36], who attempted to optimize the spacing of the stack.

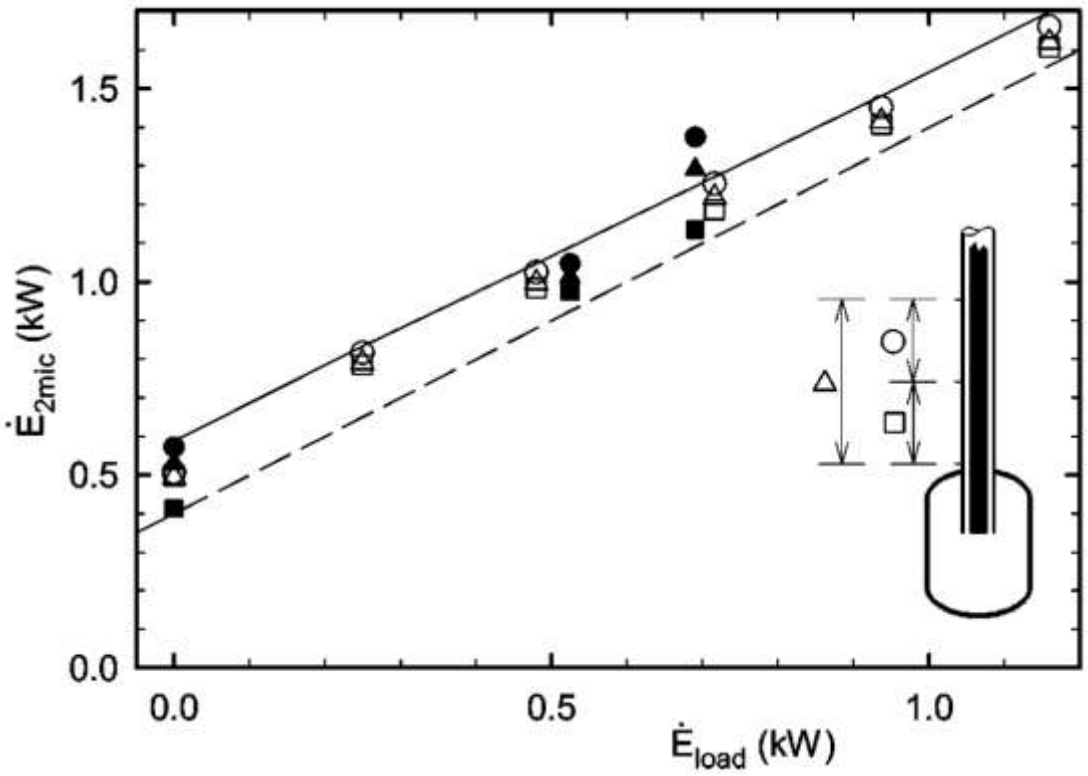

Figure 2.3: Acoustic power flowing through the resonator in terms of the acoustic power dissipated in an acoustic load. Symbols are measurements and the solid line is DELTAEC calculations[28].

Babaei and Siddiqui[31] developed a comprehensive design and optimization algorithm for designing thermoacoustic devices. The results from the algorithm are in good agreement with that obtained from the computer code DELTAEC. Figure 2.4 describes the results of model in the study. It shows that at a given stack position, the acoustic power produced by the engine decreases with an increase in the stack length, whereas, as a given stack length, the acoustic power produced by the engine increases as the stack moves away from the pressure antinode.

The results show that at a certain combination of certain stack position and length, the stack performance is the best. Figure (2.4a) shows that every combination of stack positions and lengths has a limit on the possible acoustic power.

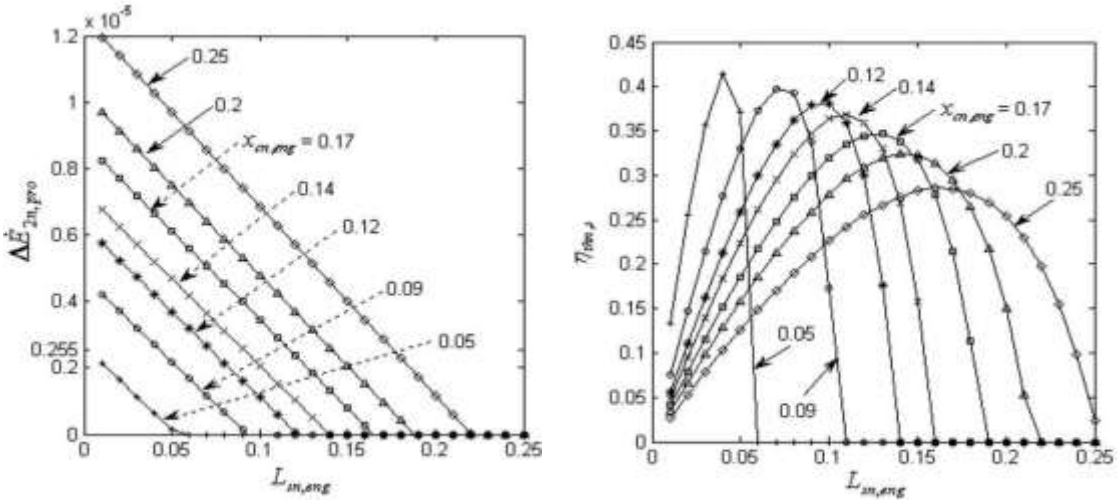

Figure 2.4: Normalized length of the engine stack (L_{sn}) versus **(a)** normalized acoustic power produced **(b)** normalized thermal efficiency of engine stack, at different normalized stack center positions (x_{cn}) at normalized temperature difference= 0.7.[31]

2.2.3 Nonlinear effects

There have been many observations[23,37,38] demonstrating that at high amplitudes measurements deviate significantly from predictions by linear theory. Streaming, turbulence, and harmonics are mentioned as main causes for these deviations.

Streaming [39,40] refers to a steady mass-flux density or velocity, usually of second order, that is superimposed on the larger first-order oscillations. With the addition of a steady non-zero mean velocity, the gas moves through the tube in a repetitive manner including a difference in the forward and backward flows as described by Swift[19].

Nonlinear thermoacoustics, as a branch of nonlinear acoustics, was developed in the last decade[41-44]. Karpov and Prosperetti have studied these effects extensively [41-43]. They adapted the momentum, continuity and energy equations with nonlinear terms to build a nonlinear thermoacoustic model in the time domain. Their model may describe quantitatively the evolution of the initial linear instability to the nonlinear regime and finally to the steady-state amplitude, and may also supply a quantitative explanation on the frequency shift of thermoacoustic systems. In addition, some modifications on the model improve the stability of the numerical computation.

Smith and Swift reported valuable Measurements of the spatial distribution of the time-averaged second-order pressure in a plane standing wave in atmospheric air[45]. Accurate measurements of the second-order time averaged pressure in a standing wave in atmospheric air have been made at two frequencies and at pressure amplitudes as large as 17.5% of pm using piezoresistive pressure transducers built into the resonator walls. Results shown in figure 2.5 suggest that the streaming pressure is small compared to the fundamental pressure, but still has an important effect on losses.

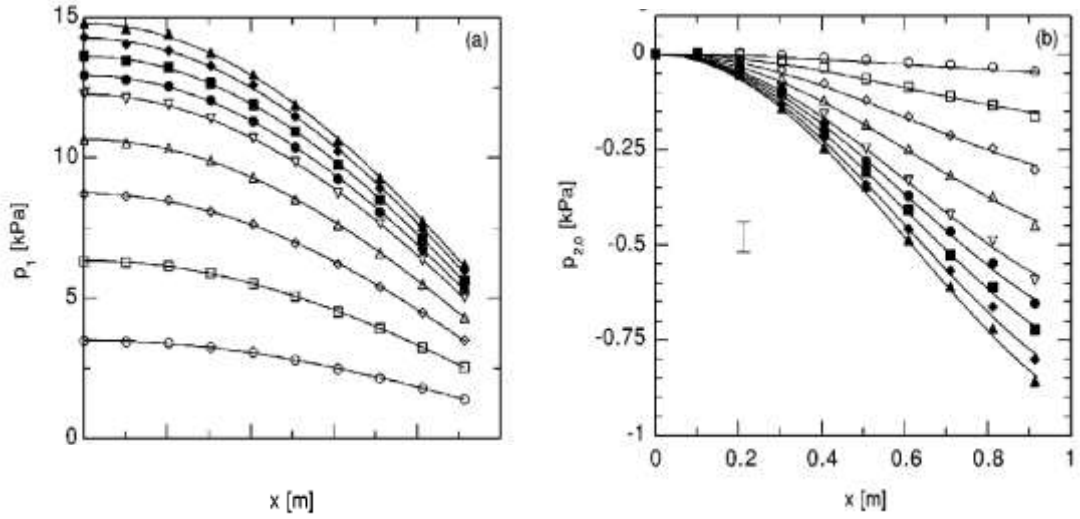

Figure 2.5: Measurements of the fundamental pressure and the streaming time averaged pressure in a 70 Hz standing wave by Smith and Swift[45].

Higher harmonics oscillate at integer multiples of the fundamental frequency, and can become quite important at high amplitudes. Atchley *et al.*[46], noticed experimentally that the generation of higher harmonics can cause highly nonlinear waveforms that degrade the performance significantly. The impact of the harmonics is greatest when excited near resonance, but Gaitan and Atchley[47] suggested that this can be suppressed by careful tuning of the resonator. A complete numerical extension would require going up to fourth order in the asymptotic expansion[48].

Swift[23] investigated a way to suppress the losses that dissipate with the harmonics of the fundamental. He inserted some objects at positions where the amplitude of the first harmonics is high. The result, plotted in figure 2.6, showed a constant relationship between the first harmonic amplitude versus the square of the fundamental amplitude, both normalized by the mean pressure. The constant of the linear relationship decreased when the inserts were used. Swift[23] also noticed that inserting blockage in the way of the thermoacoustic wave can affect its harmonic content. The blockage suppressed the first harmonic when it was put in a point of the system where the first harmonic has maximum gas-particle velocity. However, Swift did not discuss the geometry of the insert or its effect on the acoustic-power output of the system.

Turbulence arises at high Reynolds numbers, where the assumption of laminar flow is no longer valid. Turbulence may also arise due to abrupt changes in the shape or direction of the channels, which leads to the shedding of vortices[49,50] and can cause significant losses. Gardner *et al.*[51] gave some suggestions on how to include turbulence into the modeling, but they are by no means complete. The available literature suggests therefore that it is still a challenge to include the effects of turbulence, hysteresis and higher harmonics systematically into the analysis.

Ibrahim et al.[52] experimentally investigated the excitation of higher harmonics. They observed that operating the engine at a temperature just above the onset temperature generates an acoustic wave at the fundamental mode with no harmonics observed but with relatively low dynamic pressure amplitude. When they operated the engine at higher

temperature differences across the stack, up to 30 % of the generated acoustic power was contained in the first mode, in their range of operation.

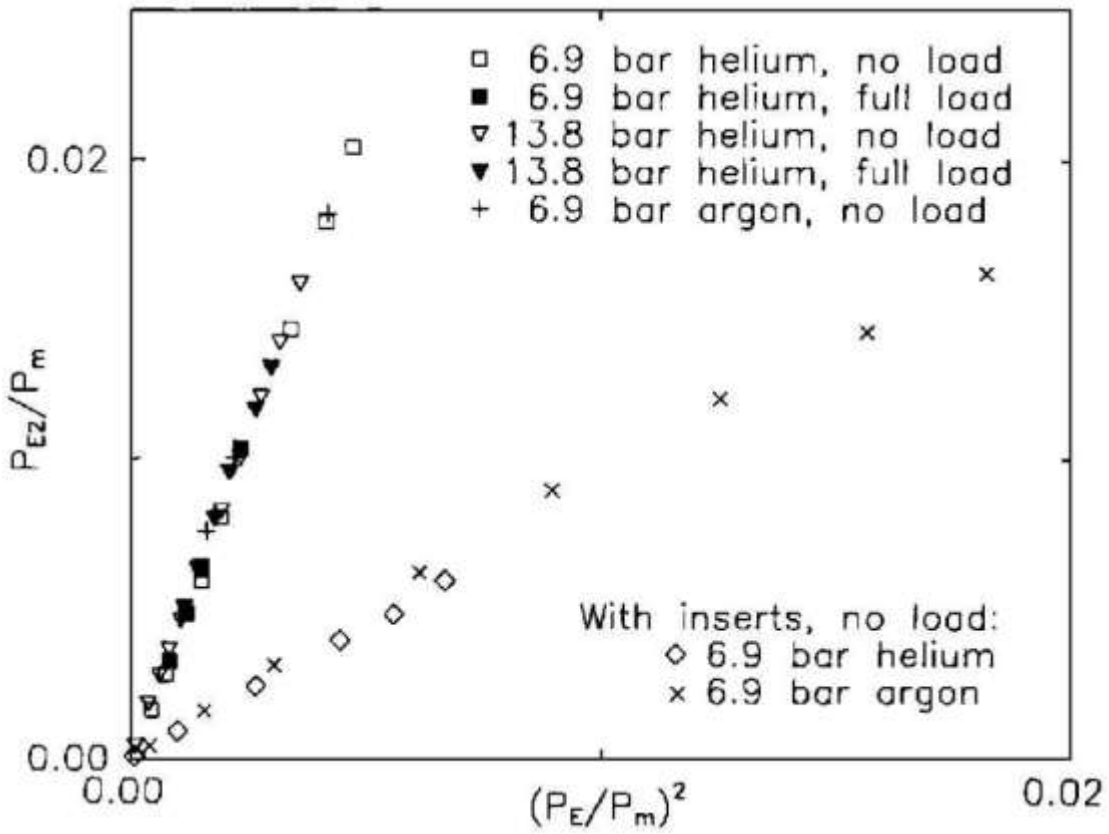

Figure 2.6: Effect of inserts on the first harmonic normalized amplitude vs the square of the normalized fundamental amplitude[23].

2.3 Applications

As a result of more than two decades of attempts, thermoacoustic conversion efficiencies have been improved to levels that rival what can be obtained from internal combustion engines[53]. Some thermoacoustic devices have been successfully applied on space shuttles and navy warships, but more extensive commercial applications are still restricted by the power density and actual efficiency [54].

In the 1980s, Los Alamos Natioal Laboratory started to develop thermoacoustic devices including a standing wave thermoacoustic engine build and studied by Swift[23]. The length and inner diameter of its resonant tube is 4320 mm and 127 mm, respectively. The system was charged with gas helium of 13.8 bar. The acoustic power of 630 W was obtained from a heat input of 7 kW, i.e. its efficiency reached 9%.

Due to the low energy density of thermoacoustic devices, the priority was given to inspecting their potential to be driven by waste heat or solar energy.

In 1998, the first solar energy powered standing wave thermoacoustic engine (shown in figure 2.7) was built by Chen and Garrett[14]. Sunlight was focused, by a 3-feet-diameter lens, to one end of a ceramic stack, which was located inside resonant tube of 40 cm in length. This ¼ wavelength resonant can emit sound at 420 Hz, with an intensity of 120 dB at a point

1 m distance from the open end of the tube. The onset for the quarter-wavelength mode occurred at 35 W. This demonstrative prototype proved the feasibility of thermoacoustic engines driven by solar energy, which is clean and environmentally friendly. The promising project accords with the global policy of sustainable development and energy saving.

Adeff and Hofler[15] built and tested a prototype of a thermoacoustically-driven thermoacoustic refrigerator that operates by solar energy. Chen[16] constructed a solar powered thermoacoustic cooler which was heated by a parabolic dish collector. The operating gas was a mixture of 18% argon and 82% helium at a pressure of six bar absolutes. However, the cooler just achieved 1.5 ^{o}C temperature span due to gas leakage and thermal losses. Shen *et al.*[17] investigated the performance of a solar-powered thermoacoustic engine working with different gases under different solar tilt angles. Efforts have been made to explore the possibility of using thermoacoustic engines in waste heat management.

A wide variety of standing-wave engines has been built making use of Rott's Theory. Hatazawa *et al.*[11] designed a thermoacoustically-driven thermoacoustic heat pump that uses waste heat from a gasoline engine. The performance of the engine is almost equal to the use of an electric-heater at a thermal input of 300 W, which corresponds to slightly more than 1% of the heat quantity of exhaust gas provided under typical automobile engine working conditions. Babaei *et al.*[12] proposed a similar system to use in a gas turbine trigeneration system, operating with the gas turbine waste heat. They proposed system including a standing-wave engine that drives a standing-wave refrigerator. Preliminary results show that the thermoacoustic refrigeration system is capable of achieving an overall theoretical efficiency of 36%. The trigeneration system overall efficiency was enhanced by 5% after the introduction of the thermoacoustic device. Zoontjens *et al.*[13] investigated the feasibility of using the automotive motor waste heat to power a thermoacoustic air conditioner to replace the fuel-consuming conventional system. They argue that this proposed system has a strong potential to replace the conventional automotive air conditioning systems. Symko *et al.*[10] proposed a small, high-frequency thermoacoustic refrigerator that is driven by a thermoacoustic engine that uses the waste heat of microelectronic components to pump heat or produce spot cooling. They suggest that devices like that can be operated in the range of ultrasonic frequencies thus working on high power densities.

2.4 scope of the present study

This work aims at developing a thermoacoustic engine, to characterize the engine performance using different gases and to improve the engine performance by inserting specially-designed inserts of different blockage area, shapes, thicknesses, and at different positions inside the resonator. These inserts are designed to suppress the excitation of harmonics. This is partly a continuation of the work of Swift[23] in order to study the effect of these inserts on the harmonic suppression.

3. Experimental Setup and Procedure

The experimental setup consists of an iso-diameter resonator filled with a gas mixture. It contains a thermoacoustic stack and hot and cold heat exchangers. Measurement devices included pressure, temperature are used and connected to sensors to measure signal conditions and data acquisition. Data is manipulated and analyzed using codes written using MATLAB programming language. Detailed description of the apparatus, methods, measurement procedures, data manipulation and analysis is included in this chapter.

3.1 Standing wave thermoacoustic engine

The used engine is described in figure 3.1. It consists of a resonator with a length of 0.95 m and a uniform inner diameter of 0.127 m. A stack of length 0.04 m is positions at a center position of 0.05 m measured from the blind flange. Heat is provided to the system by an electric heater, connected through a variable resistance, at the stack end closer to the blind flange. A finned tube heat exchanger is attached to the other side of the stack to absorb the rejected heat load and to maintain the temperature gradient along the stack. The components of the apparatus, shown in figure 3.2, and the procedures of measurements and operation are detailed in the sections of this chapter.

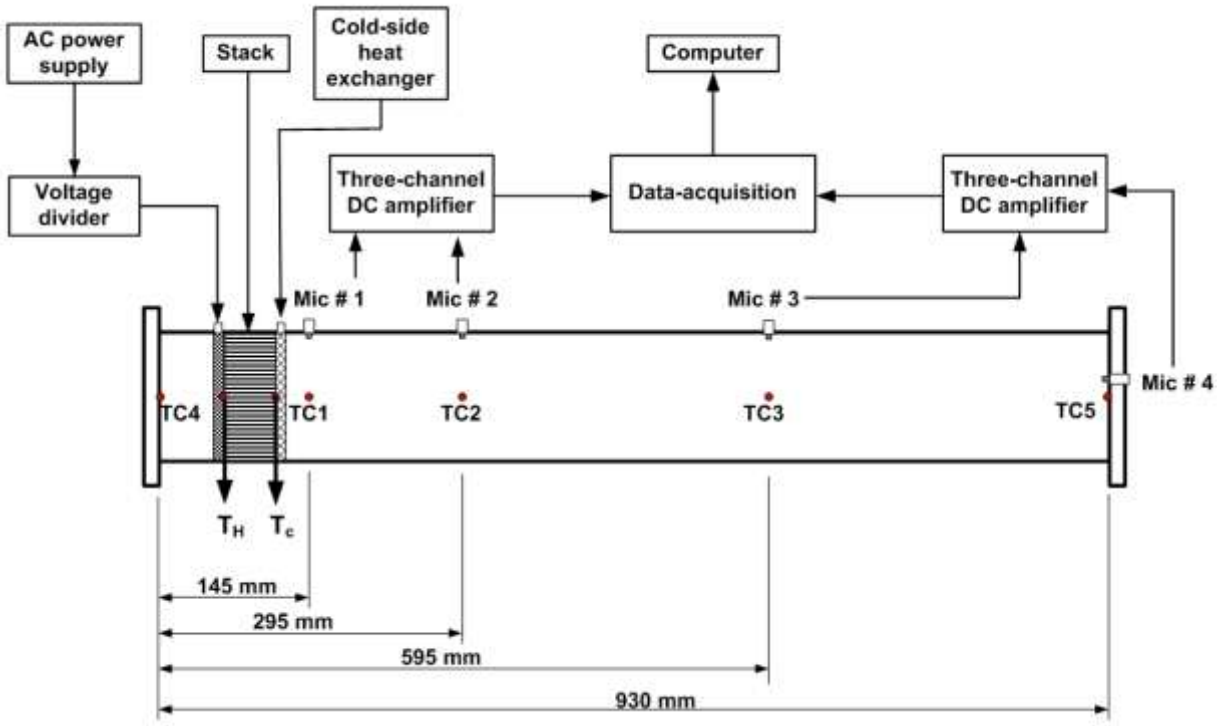

Figure 3.1: A schematic drawing of the engine and measurement instrumentation

3.1.1 Resonator

The resonator is responsible for housing the working gas, the stack, and the hot and cold heat exchangers. The resonator used is made of a stainless steel tube of 0.950m in length and 0.127m (5 in) in diameter. The resonator shape and dimensions determine the characteristics

of the wave. The modes of the wave depend on the boundary conditions at the resonator ends. For the case of an iso-diameter resonator with blind flanges in both sides, the wave fundamental mode will be in the form of half a wave length, and its harmonics (n * λ/2, where n is an integer).

The resonator is filled with the working gas. The low diameter to length ratio (0.13) guarantees the validity of the one-dimensional assumptions used in DELTAEC.

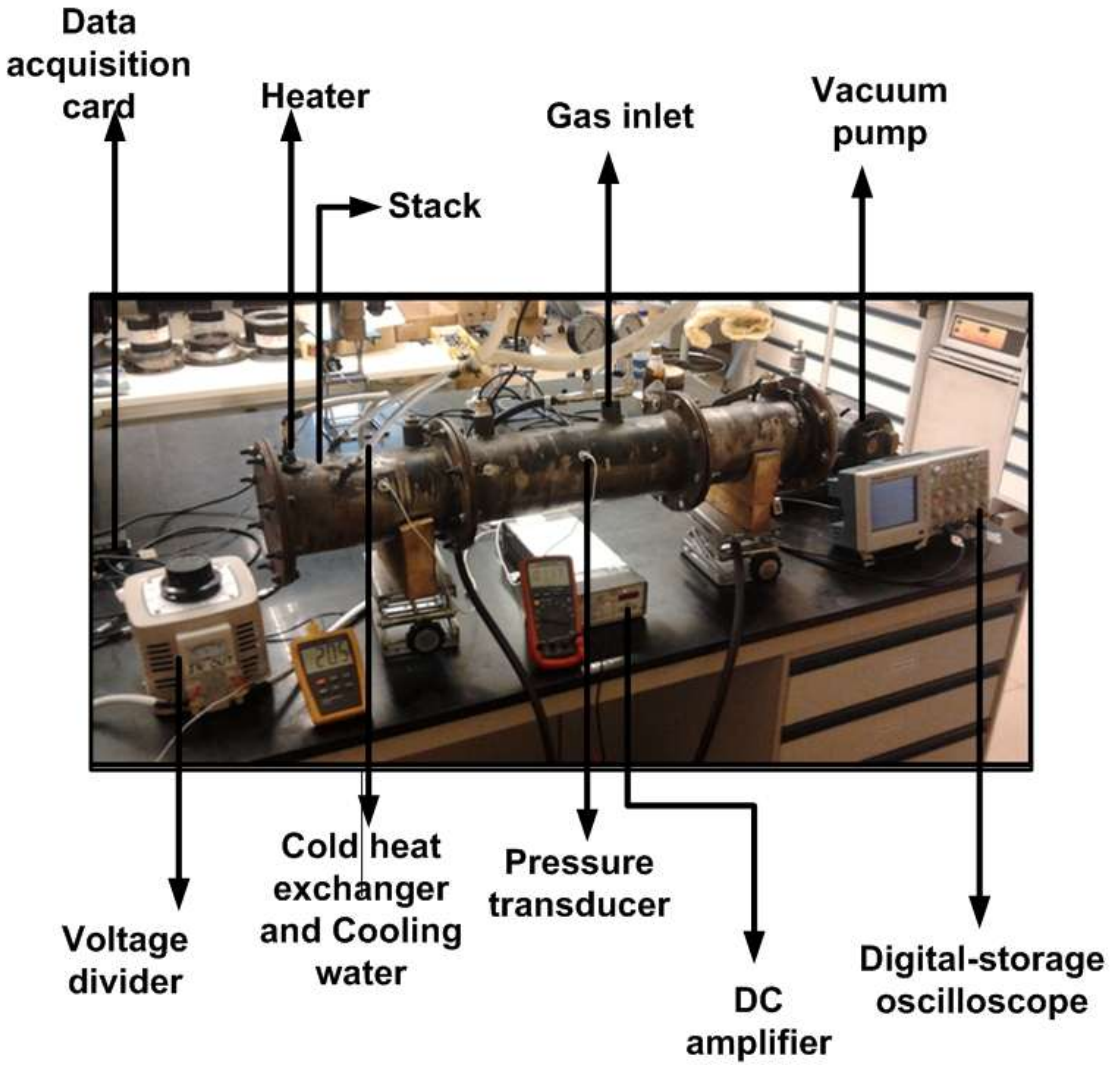

Figure 3.2: The apparatus of the engine in the lab showing the resonator and the measurement instrumentation.

3.1.2 Thermoacoustic Stack

The stack which consists of many parallel passes for the air of specially selected dimensions keeps the operating gas in an effective thermal contact with the walls. The gas carries heat from adjacent pore walls and transfers it along the stack. Stacks as in figure 3.3 in the used apparatus have square pores of different sizes detailed in table 3.1.

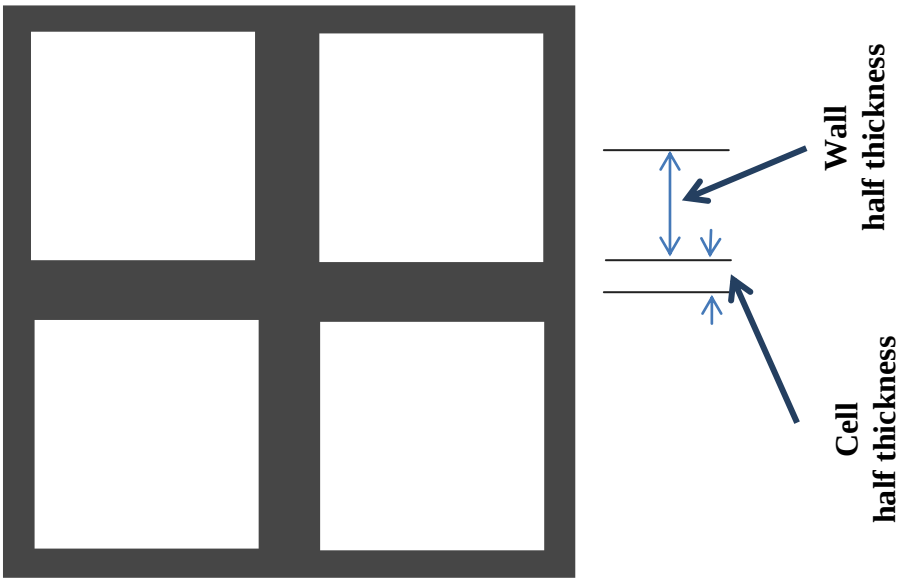

Figure 3.3: Cell geometry of rectangular stack cross section.

The stack is made of celcor. This material shows a high mechanical strength at high operating temperature, thermal stability and a uniform porosity. This material has a wide range of applications in many areas such as diesel filter panticulates[55]. It was supplied by companies that produce them for this purpose. Celcor has a thermal conductivity *k* of 2.5 W/K m and its specific heat c_p is 896 J/Kg K[55].

The used stacks are cut into pieces of 0.05 m in length and of diameter close to the inner diameter of the system (0.127 m) using a center lathe and wrapped in a layer of insulating cloth to decrease the heat transfer between the stack and the conductive resonator body and to provide good sealing between the stack and the resonator body. Table 3.1 lists the parameters of resonator and the available stack used throughout the experiments.

3.1.3 Heat exchangers

The heat exchangers are one of the main components of any thermoacoustic device. Energy input and rejection from the device are vital to keep the temperature gradient along the stack higher than the critical temperature gradient needed to maintain the thermoacoustic effect. In a thermoacoustic heat exchanger, thermoacoustic oscillations are the main motion of the gas that enhances heat transfer[4]. Swift recommends that the dimension of the heat exchanger parallel to the wave propagation direction, i.e. its length, should be equal to one peak-to-peak gas displacement ($2\times TD + 2 \times \delta_k$). Where TD is the gas parcel displacement through half a cycle, and δ_k is the thermal penetration depth[4].

In contrast to a steady-flow device, heat transfer cannot be enhanced by lengthening the traditional heat exchanger passages more than one peak-to-peak gas displacement because some of the gas in the heat exchanger will never contact the end of the regenerator to deliver heat where it is required. Instead, the effective way to increase the heat transfer depends on increasing the number of passages in which the gas flows[57]. Each passage must be hermetically sealed from the external fluid passage. The higher the number of passages, the higher the probability of failure and the cost of fabrication become. In steady-flow devices,

the heat exchangers can be well separated by piping runs, but the small gas displacement also forces the heat exchangers to be located close together. The compact size and high heat flux of traditional oscillating-flow heat exchangers often leads to high thermal gradients and high thermal stresses that promote failure.

Table 3.1: Resonator and stack dimensions

Main Dimensions			
Resonator length	92.5 cm	Hot duct length	12.5 cm
Resonator diameter	12.7 cm	Cold duct length	80 cm
Stack center position	15 cm	Stack length	5 cm
Hot heat exchanger length	1 cm	Cold heat exchanger length	1 cm

Dimensions of used stacks			
CPSI	**200-CPSI**	**400-CPSI**	**600-CPSI**
Plate spacing (μm)	771	559	481
Plate thickness (μm)	127	76	38
Porosity	73.7%	77.5%	85.8%

The heat exchanger used in the apparatus is shown in figure 3.4. It consists of 11 parallel vertical copper tubes of 1 cm diameter. Circular copper rings of 1 mm thickness are attached around each tube at spacing of 1mm. The heat exchanger width (in direction of resonator axis) should be selected equal to the particle displacement which is around 2mm in this case[(19)]. However, due to the simple manufacturing techniques used, the width of 1cm is used. The extra width does not help as heat transfer surface area, but it allows for wider tubes and minimizes cooling water flow resistance.

3.1.4 Working gas

Working gas is selected upon the working case conditions. For a certain frequency and mean pressure and temperature, every gas has its thermal and viscous penetration depths. The selection of stack pore dimension depends on these depths.

The power densities that can be transferred in a gas depend on its density and molecular weight. This suggests that for a certain level of output power required, a gas of proper density will be needed. Practical thermoacoustic devices use high pressure gases as mean gas pressure can alter the density, but it increases the weight, viscosity, and leakage probability of the gas.

Figure 3.4: The finned tube heat exchanger inside the resonator developed specially for this study.

No certain mixture is known to give the best performance in thermoacoustic devices. Mixtures of low Prandtl number is suggested to give higher performance, but the best performance are not necessarily obtained by using the mixture of lowest Prandtl number. The engine efficiency increase is a consequence of two effects:

i. The Prandtl number decrease.

ii. the output power is proportional to the acoustic velocity u and thus inversely proportional to the product of the density and velocity of sound ρa (in a standing wave: $u \sim p/\rho a$).

Lowest Prandtl number usually occurs in mixtures of binary gases. As the gases are not of the same density, the mixture with the lowest Prandtl number is not the mixture with lowest possible density, and the best performance is obtained by using a gas mixture that achieves the needed compromise between density and Prandtl number[8].

In this study, air, helium and argon are used at atmospheric mean pressure. Atmospheric pressure minimizes leakage, preventing the change of gas-mixture composition during experiments. Air is readily available, which minimizes the cost of this component. Helium and helium-argon mixtures will provide the ability to vary the properties of the mixture including Prandtl number.

3.1.5 Harmonic suppression inserts

The inserts used in this apparatus were made of three different gas areas: 0.75, 0.5, 0.25 of the resonator area. The insert with half resonator gas area was made of 2 different thicknesses: 1 cm and 3 cm which are small enough compared with wave length which is

about 1.8m. The insert open area was in form of an open ring or a circle full of holes. The different inserts used are shown in figure 3.5.

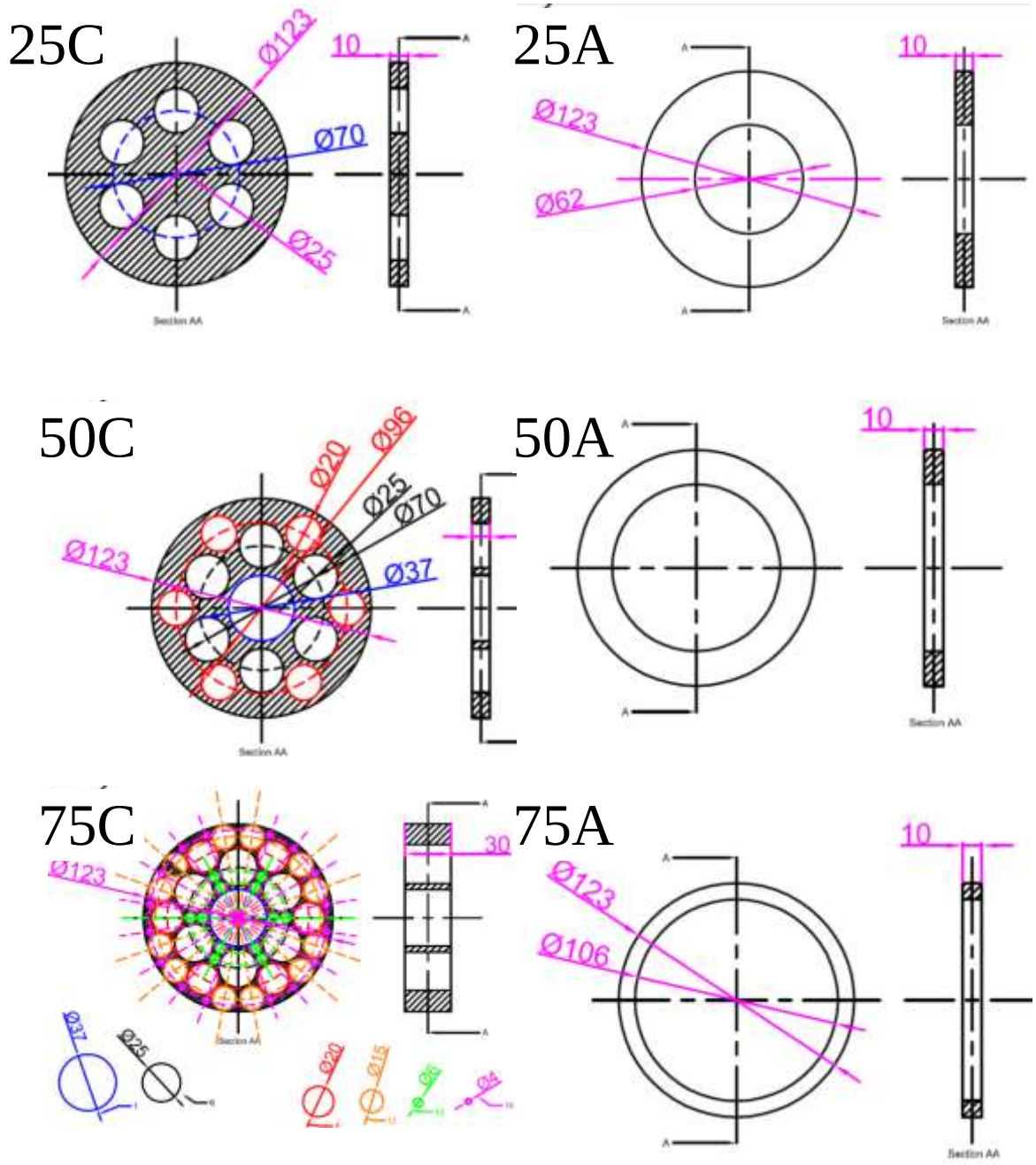

Figure 3.5: Shapes of inserts used in this experiment

Every experiment is named as XYZ-N, where X is the gas area as a percentage of the resonator area, Y is the shape code: either A which is a hollow ring or C which is multiple holes, Z is the thickness of the insert in cm, and N is the distance in cm between the insert center and the hot-side blind flange. For example, The experiment 50C3-60 was done using a stack which contains multiple holes, the stack open area is half the area of the resonator area, the stack thickness is 3 cm, and the insert is placed 60 cm away from the blind flange.

3.2 Measurement system

The measurements done on the system include pressure, temperature, and electric current and voltage. The collected data is used to calculate important parameters such as acoustic power and efficiency.

3.2.1 Pressure measurements

The pressure of the gas in the system is an important parameter of the performance, indicating power, blockage, and harmonic content. Measurement of pressure waves in two different points in the system with reasonable accuracy provides information about the acoustic power flux in this region. The value of the pressure in the system will indicate the mode and the blockage in the resonator. Analyzing the complex shape of the pressure waves indicates the harmonic content which causes a nonlinear loss in the system.

The pressure microphones used are piezo-resistive Meggitt microphones (Model 8510B-2, range 0-2 psi gage, individually calibrated, sensitivity of about 20 mV/kPa, resonance frequency of 70 kHz and high stability over temperature transients). The signals from the pressure transducer are fed into a three-channel, 200 kHz bandwidth, programmable-gain DC amplifier model 136. Both the sensor and the amplifier are shown in figure 3.6. The signal is also visualized and saved using the oscilloscope as shown in figure 3.7. The programming code is used then to calculate the wave frequency and analyze the wave into its different modes and to obtain the acoustic power.

Figure 3.6: The power sensor model 8510B-2, and the amplifier model 136 used in pressure signal detection and processing.

The Pressure consists of two components: a mean value and a dynamic value. The dynamic part of the wave is the result of the fundamental of the wave and the addition of the different harmonics of the wave. The dynamic pressures at different axial locations 14.5 cm, 30.5 cm, 59.5 cm and 93 cm) inside the engine are measured using pressure microphones. The axial locations where the microphones are positioned correspond to 0.78 %, 1.64 % and 3.2 %, respectively of the wave length. The determination of the pressure magnitude and phase of each mode at each microphone location allows estimation of the average acoustic power between any two microphones[56] for the fundamental mode and the first harmonic. The two microphone method is limited by the fact that phase mismatch between the two measuring microphones can introduce significant error. It is suggested that the microphones should be placed such that there is at least one degree in phase difference between the two pressure signals[56].

3.2.2 Temperature Measurements

The temperature of the stack sides is an important parameter of the system performance. Temperature of the gas mixture within the system also determines the thermal and viscous properties of the gas which is used to evaluate other performance characteristics such as the power and the efficiency.

The temperatures at the hot and cold sides of the stack are measured with thermocouples (type K, 147 μm in diameter, supplied by Omega Engineering). The data is fed to the system using the data acquisition device USB-6343. The programing software Labview then processes the signal and uses its predefined calibration characteristics to evaluate the temperature various locations in in the system.

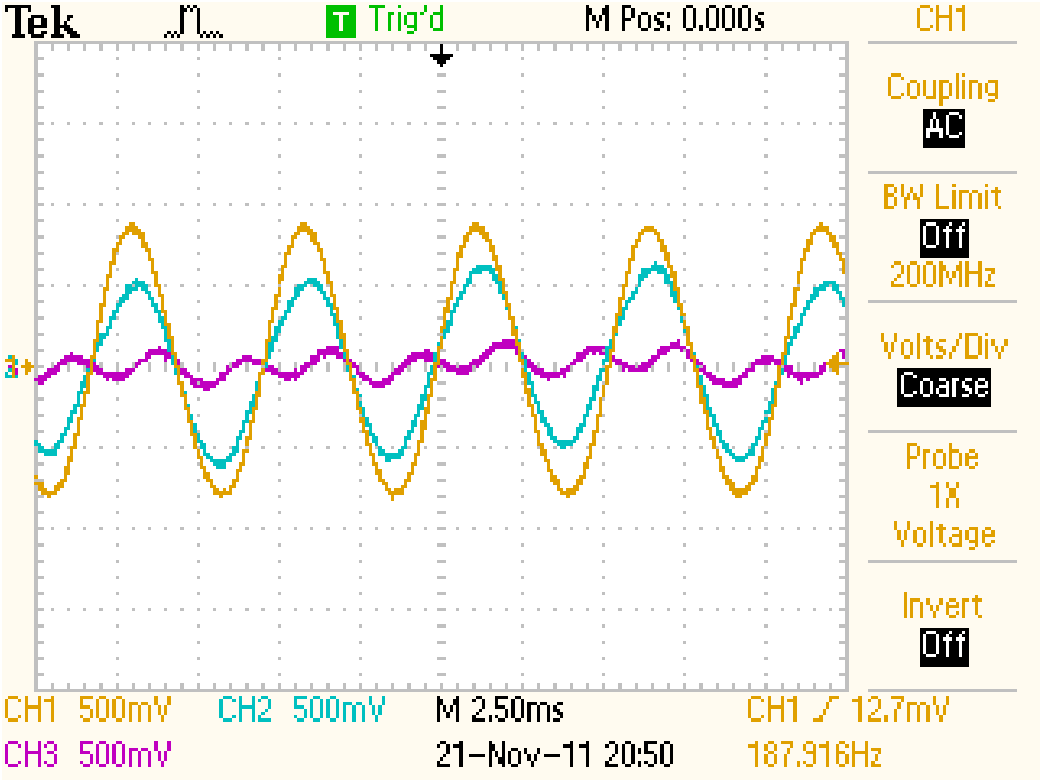

Figure 3.7: Oscillations at three different locations visualized simultaneously on the oscilloscope screen. The figure includes 3 waves obtained from 3 different microphones.

The pressure measurement data is acquired in two ways: For the long full-run experiments, it is delivered directly to the data acquisition system. For the pressure wave data analysis, a pressure wave is visualized and saved (in column data form .ascii) using the oscilloscope. Both types of data is then processed by programming codes to obtain information about the pressure wave during the run. Pressure and temperature data during full runs of the engine was recorded. The data included the pressure wave with a rate of 1000 scan per second, which is more than 5 times the wave frequency to avoid aliasing errors.

3.3 Measurement Procedure

i. Data acquisition

Both temperature and pressure signals are acquired simultaneously using a USB data acquisition board (Omega model OMB-DAQ-3005, 16-bit, 16differential channels, 1-MHz band width, with programmable gain).

ii. Gas mixture preparation

The components of the mixture that fills the engine are determined by totally evacuating the engine before filling using a vacuum pump. The engine is then filled with the gas with the larger partial pressure until the pressure in the engine reaches the value of the needed partial pressure. After that, the other gas is added until the pressure reaches the required value of 1 bar of absolute pressure.

iii. Engine start-up

The engine, filled with the operating gas, is then started up by connecting the required voltage to the heater rod. The hot and cold stack side temperatures start to increase above the room temperature. When the temperature difference between the sides of the stack reaches the onset temperature difference, pressure waves are detected by the microphones along the resonator. Heater voltage is kept constant during the process.

iv. Steady state

The measured temperature and pressures are monitored during the experiment. The system is operated at a steady state to record steady-state operation data.

v. Shut-off

To record data during the shut-off process, the voltage on the heater rod is turned off completely. The pressure waves starts to decrease in amplitude. Temperatures and pressures are recorded until the hot and cold temperature come down to the atmospheric state.

3.4 Data analysis

The collected data is analyzed using programing codes to obtain information about the performance of the engine. In this section, theoretical background for the analysis is presented.

3.4.1 Onset temperature

To calculate the onset temperature of the experiment, the amplitude of the wave is calculated throughout the experiment as an average for every one second. The mean pressure P_m and fundamental amplitude P_0 are calculated by the equations:

$$P_{mean} = \frac{\sum_n (P_i)}{n} \qquad \text{Eq. 3.1a}$$

$$P = \frac{\sqrt{2}\ \sum_n abs(P_i - P_{avg})}{n} \qquad \text{Eq. 3.1b}$$

Where n is the number of samples in one second, typically 1000. The amplitude is calculated as a constant multiplied by the root mean square of the signal. The square root of two is used assuming that the wave is dominated by a single frequency sine wave. An example for the amplitude during a full run of the system is shown in figure 3.8.

The onset temperature is defined as the temperature difference across the stack sides at which the working gas starts to oscillate thermoacoustically. The experiment starts at cold state where the temperatures of the cold and hot sides of the stack are both at room temperature. As the temperature increases, a sudden increase in amplitude is detected when the wave is initiated. The temperature difference calculated at the moment when the wave starts is used as the onset temperature difference.

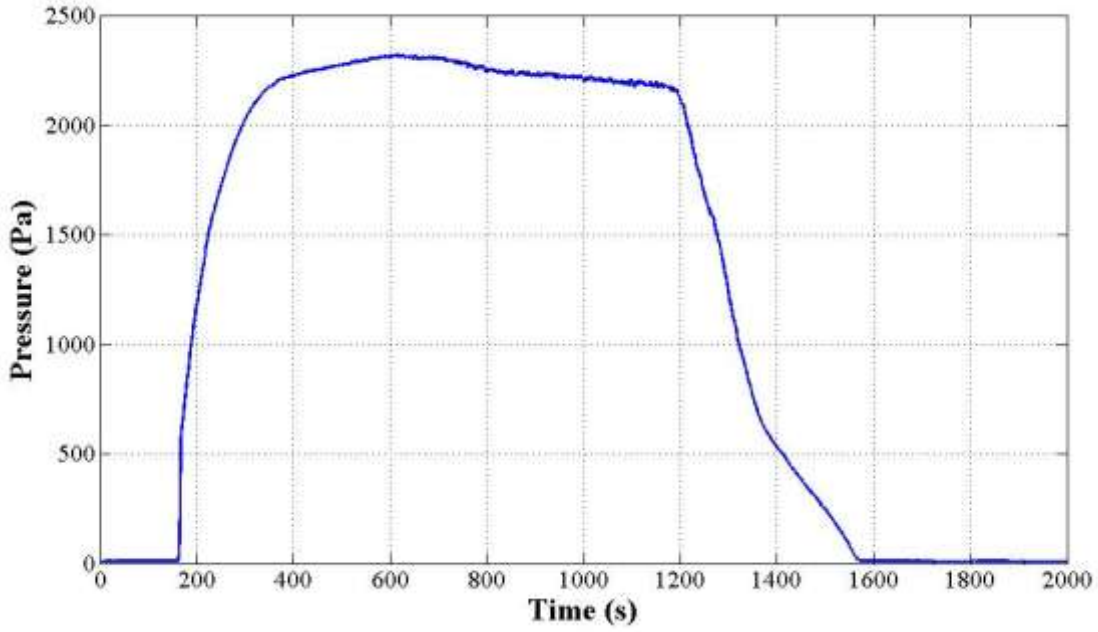

Figure 3.8: The pressure amplitude versus time during a full run of the engine including startup, steady oscillations, and shut-down.

3.4.2 Acoustic power

The acoustic power of the wave is an important measure of the effectiveness of the system. It is measured using the two microphone method formulated by Biwa[65]. This method determines the acoustic intensity of a gas in a wide duct from measurements of pressure. Simple formulae for the method are based on boundary layer approximation. This method uses the relationships of standing wave complex pressure P and velocity V , which determines the intensity I in the form:

$$I = PV = \frac{1}{2} Re[\tilde{p}v] \qquad \text{Eq. 3.2}$$

where $P = p(x)e^{-i\omega t} \quad and \quad V = (x)e^{-i\omega t}$ Eq. 3.2b

The two microphone intensity measurements have a clear advantage to the direct methods that requires measurement of velocity. Pressure measurements are much simpler and easier than the LDV and PIV methods that require seeding particles and transparent ducts. However, the measurements are sensitive to the measured phase angle between the two pressures[56]. The method requires the determination of the pressure amplitudes and phases at two known locations in the wave.

The intensity is formulated by Biwa *et al.*[56] as:

$$I = \frac{1}{8\omega\rho}\{Im[H](|P_A|^2 - |P_B|^2) + 2Re(H)|P_A||P_B|\sin\theta\} \quad \text{Eq. 3.3}$$

Where $\theta = \arg[\frac{p_A}{p_B}]$ is the phase lead of p_A relative to P_B

Complex variable H is evaluated through:

$$H = \frac{kF}{\cos\left(\frac{\tilde{k}\Delta x}{2}\right)\sin\left(\frac{k\Delta x}{2}\right)} \quad \text{Eq. 3.3b}$$

The complex variable k in its general form is obtained through:

$$k = -i\frac{\omega}{a}\sqrt{\frac{J_0\left(\frac{i^{1.5}\sqrt{2}r_0}{\delta}\right)}{J_2\left(\frac{i^{1.5}\sqrt{2}r_0}{\delta}\right)}}\sqrt{\gamma + (\gamma-1)\frac{J_2\left(\frac{i^{1.5}\sqrt{2\sigma}r_0}{\delta}\right)}{J_0\left(\frac{i^{1.5}\sqrt{2\sigma}r_0}{\delta}\right)}} \quad \text{Eq. 3.3c}$$

and the other complex variable, F, is obtained as:

$$F = 1 - \frac{2J_1\left(\frac{i^{1.5}\sqrt{2}r_0}{\delta}\right)}{\left(\frac{i^{1.5}\sqrt{2}r_0}{\delta}\right)J_0\left(\frac{i^{1.5}\sqrt{2}r_0}{\delta}\right)} \quad \text{Eq. 3.3d}$$

If the boundary layer approximation is used, these variables will turn into the following simpler forms:

$$k = \frac{\omega}{a}\left\{1 + \frac{1-i}{2}\left(1 + \frac{\gamma-1}{\sqrt{\sigma}}\right)\right\} \text{ and } \quad F = 1 - \frac{1-i}{\frac{r_0}{\delta}} \quad \text{Eq. 3.4}$$

A MATLAB code is used to import the data from the files saved by oscilloscope, calculate pressure amplitudes and phases, plot and save the wave harmonics, and calculate the power in the duct knowing its diameter. The code is included in the appendices.

3.4.3 First and second law efficiencies

Knowing the power output, the thermal to acoustic first law efficiency of the engine is defined as

$$\eta_I = \frac{E_{out}}{Q_{in}} \qquad \text{Eq. 3.5}$$

where $E_{out}$is the calculated average acoustic power passing in the region between the two microphones used for the two microphone method measurements. Q_{in} is the heat power input delivered to the engine. This power input is calculated as

$$Q_{in} = P_{elec} = \frac{V^2}{R} \qquad \text{Eq. 3.6}$$

where R is the value of the resistance of the used heater coil. It is assumed to be constant during the experiment and does not depend on the temperature.

The second law efficiency is a measure of the quality of the system and is calculated using the limit of Carnot efficiency as a reference. Knowing the temperatures on both sides of the stack, T_h and T_c, Carnot efficiency is calculated as:

$$\eta_C = \frac{T_h - T_c}{T_h} \qquad \text{Eq. 3.7}$$

and then the second law efficiency is $\eta_{II} = \frac{\eta_I}{\eta_C}$ Eq. 3.8

3.4.4 Harmonic content and frequency calculation

The measured frequency is used in the calculation of the acoustic power and other characteristics of the system. Angular frequency is a value used as a reference parameter in dimensionless analysis. The frequency spectrum of the wave is obtained by a MATLAB code that handles the data saved by oscilloscope. An example is shown in figure 3.9.

The information about frequency content is obtained using Fast Fourier Transform analysis (FFT). The exact value of the fundamental frequency is obtained from the regression of the wave to a function of the form:

$$P = \sum_n P_n \sin(\omega_n t + \varphi_n) \qquad \text{Eq. 3.9}$$

Where P_n , ω_n, φ_n are the amplitude, angular frequency, and phase of the n^{th} harmonic. The regression was performed by a code that used the sum of eight terms, producing the amplitudes and phases of the fundamental and the first seven harmonic components. The code, that is included in the appendices, produces high regression factors (R^2) of more than 0.99. Early attempts also showed that in our iso-diameter resonator, the harmonics are usually of a frequency that is a integer multiple of the fundamental frequency. The fundamental frequency that comes out as a result from regression was in good agreement with the oscilloscope and FFT values.

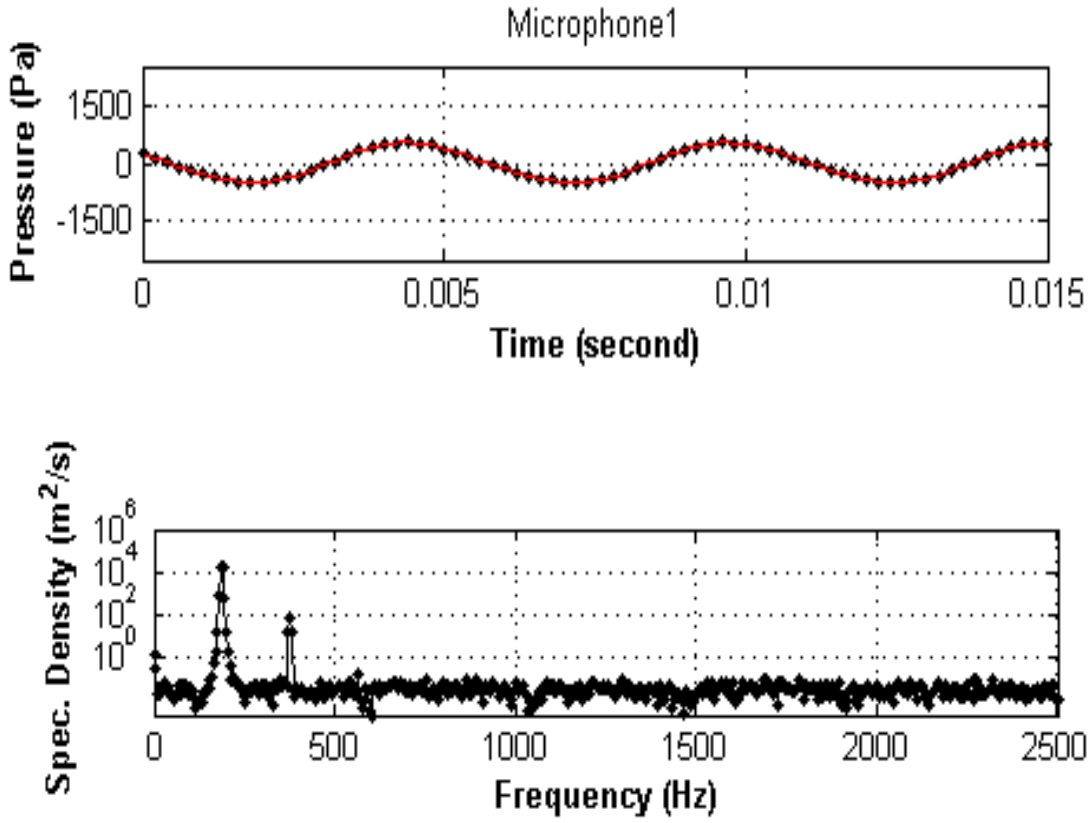

Figure 3.9: Thermoacoustic wave in time and frequency domain.

3.5 DELTAEC model

DELTAEC, or Design Environment for Low-Amplitude Thermoacoustic Energy Conversion, is a computer program that can calculate details of how thermoacoustic equipment performs. These calculations can help the user to design equipment to achieve desired performance. Input data can be modified or entered via a user interface or by using any text editor. Results can be examined via the user interface, built-in graphics displays, the operating system text utilities, or any spreadsheet or graphics software.

DELTAEC numerically integrates the single-frequency wave equation and other equations such as the energy equation, in a gas (or a very compressible, thermodynamically active liquid), in a geometry given by the user as a sequence of segments such as ducts, compliances, transducers, and thermoacoustic stacks or regenerators. With its multi-parameter shooting method to satisfy a variety of mixed boundary conditions, DELTAEC gives the user considerable freedom in choosing which variables are computed as solutions. For example, in a simple acoustic resonator, DELTAEC can compute the input impedance as a function of frequency, or the resonance frequency for a given geometry and gas, or the length required to give a desired resonance frequency, or even the concentration in a binary gas mixture required to give a desired resonance frequency in a given geometry.

The latest version of DELTAEC is freely available for noncommercial, educational, and evaluation use from www.lanl.gov/thermoacoustics. DELTAEC is under continual development, so regular users should update their copies occasionally. A full description of DELTAEC, tutorials for its use, derivation of its theoretical background is available in its user guide which is downloaded with it.

In this work, the thermoacoustic engine is modeled using the DELTAEC segment. The model is verified by comparing the calculated results from the model with the results from the measurements. The model of the system gets the input voltage to the heaters and the geometry as inputs. DELTAEC then calculates output acoustic power, thermal to acoustic efficiencies, and resonance frequency. The model in the DELTAEC code consists of 20 segments. The model starts from the cold end flange. Begin segment (number 0) defines the mean temperature at the start, the frequency, the mean pressure, and the used gas. It also states that the velocity is zero as a boundary condition of the flange. Segments 1,6,8,10,18 are duct segments of 5" diameter representing the resonator parts. Segment 2 is the insert: a duct with lower gas area. Segments 14, 17 represent the cold heat exchanger and the heater as heat exchangers of constant surface temperature. Segment 19 is a boundary condition of infinity acoustic resistance, to represent a flange where no gas velocity can occur. The remaining segments are RPN segments, a type of segments with no physical existence. These segments contain calculations of the important parameters such as pressures, powers, temperature differences, and efficiencies.

4. Results and Discussion

4.1 Stable engine performance

This section describes the performance of the prototype of the thermoacoustic engine. The section presents and compares the numerical and experimental results when the engine was operated with air at 1 bar and a 600-CPSI stack. The engine was driven with heat supplied by an electric heater of heating power up to 1680 W.

First, the engine is modeled using DELTAEC. Figure 4.1 shows the DELTAEC schematic of the engine. The model includes surfaces at the location of microphones to be able to read the simulated dynamic pressures at these locations to compare with the measurements.

4.1.1 Wave characteristics

Using air at 1 bar, the DELTAEC model predicts that at input heat of 1680 W, the 600-CPSI stack produces a standing wave in the resonator. The standing wave, whose components are shown in figures (4.2a) and (4.2b), has dynamic pressure anti-nodes at the two blind flanges of the resonator.

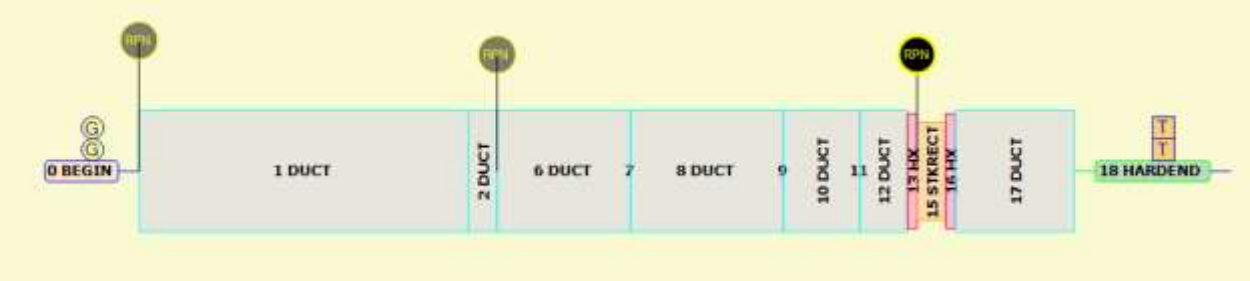

Figure 4.1: DELTAEC schematic of the engine.

The dynamic pressure amplitude reaches 10753 Pa at the hot-side flange and 10570 Pa at the cold-side flange. The pressure at the center of the stack is 10128 Pa. Using a heat input of 1680 W, the model shows that the engine produces a pressure ratio of 10.1% at the center of the stack, which is high enough to suffer non-linearities.

The volumetric velocity is found to be lagging the dynamic pressure by 90^{o} as the imaginary part is dominant, whereas the real pressure is dominant in the dynamic pressure. The volumetric velocity has an anti-node in the middle of the resonator and two nodes at the two blind flanges of the resonator, which corresponds to a half wavelength mode of operation. The maximum amplitude of the volumetric velocity simulated by the DELTAEC model is found to be 0.35 m^3/s.

Figure 4.3 shows the flow of acoustic and total power inside the resonator. The acoustic power produced at the stack flows to both sides of the resonator to make up for the viscous losses due to viscosity of the air. At these conditions, DELTAEC predicts that the stack produces about 36 W of acoustic power. This power is used to sustain the wave against the viscous losses which are distributed as follows: 10 W at the hot heat exchanger, 2 W at the hot duct, 10 W at the cold heat exchanger, and 14 W at the cold duct. The engine contains no acoustic-to-electric power converters. Thus, all the acoustic energy generated by the stack is consumed in the form of viscous dissipation.

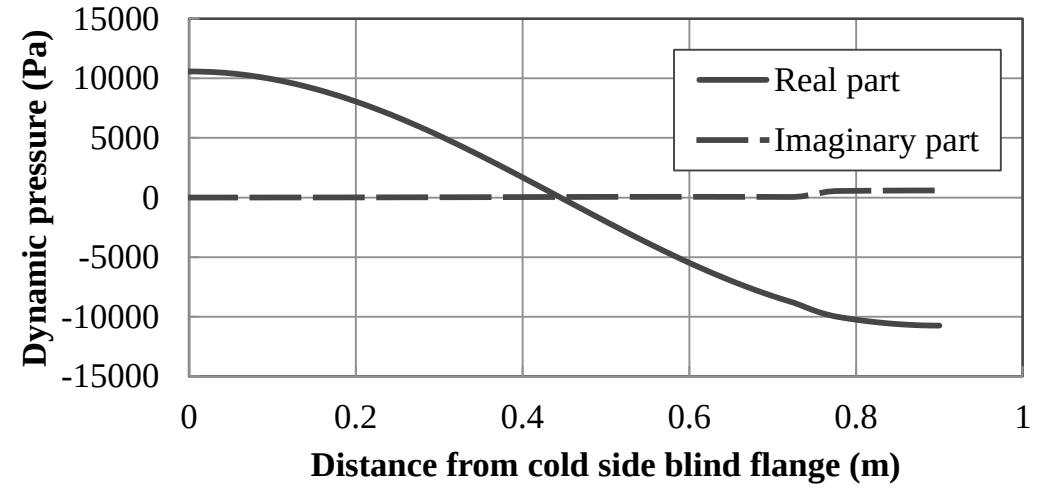

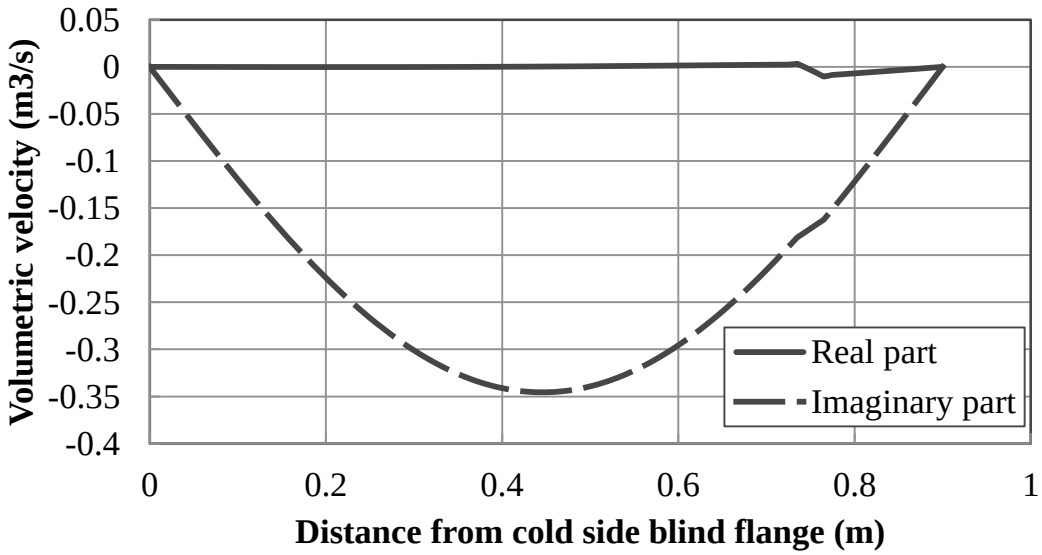

Figure 4.2: (a) Real and imaginary components of dynamic pressure inside the resonator as predicted by DELTAEC using air at 1 bar and 600-CPSI stack. **(b)** Real and imaginary components of volumetric velocity inside the resonator as predicted by DELTAEC using air at 1 bar and 600-CPSI stack.

Because DELTAEC can model certain features of the thermoacoustic engine, including the output acoustic power, the onset temperature difference, the operating frequency and the dynamic pressure amplitude, it is of interest to compare these modeled features with their measured counterparts. Figures 4.4, 4.5 and 4.6 present these comparisons for the effect of input heat on output acoustic power, pressure ratio, and frequency respectively.

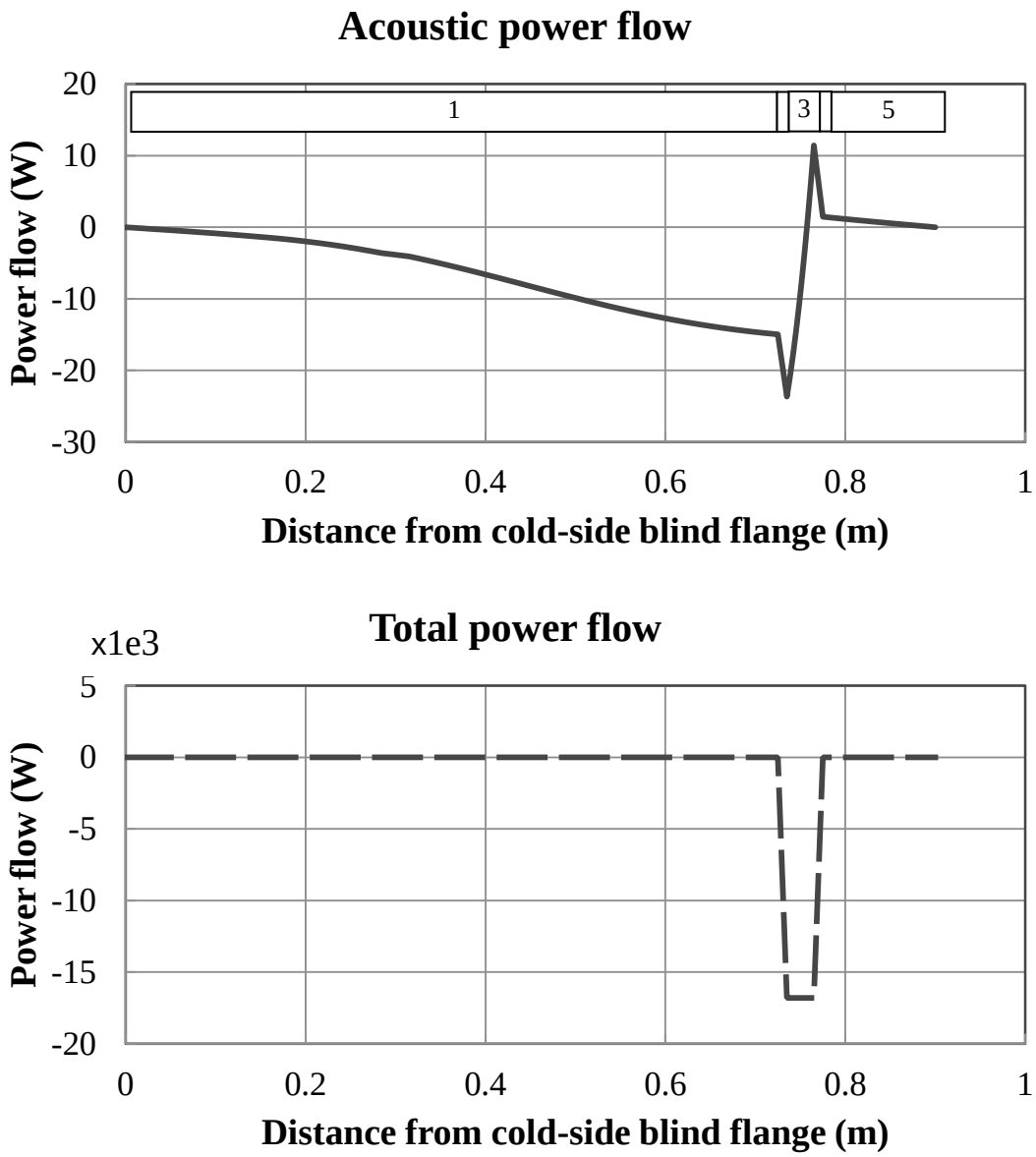

Figure 4.3: The acoustic and total power flows inside the resonator as predicted by DELTAEC. Negative values refer to flow in the –x direction. 1:cold duct, 2: cold heat exchanger, 3:stack, 4:hot heat exchanger, 5:hot duct

4.1.2 Acoustic power output

In figure 4.4, the measured acoustic power increases with the increase of input heat power to the engine. The results of the DELTAEC model showed good agreement with the experimental data. However, the measured output acoustic power is less than the DELTAEC model results by 65%. The reasons may include that DELTAEC does not model non-linearities, such as harmonic generation. It also does not account for minor losses. Moreover, heat losses to the surroundings are not accounted for.

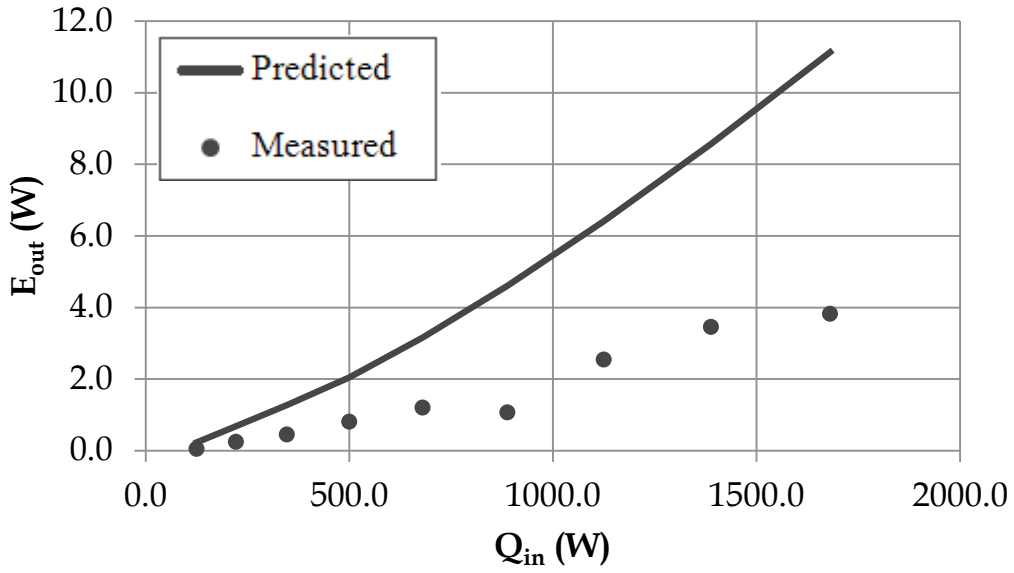

Figure 4.4: Effect of input heat power on acoustic power output of the engine for air at 1 bar using a 600-CPSI stack.

4.1.3 Dynamic pressure amplitude

In figure 4.5, the square of the pressure ratio, where the pressure ratio is defined as the dynamic pressure amplitude divided by the mean pressure, is shown to increase *linearly* with the input heat power as predicted by the linear theory. This indicates that the nonlinearities in the model are not dominant. The model calculates the pressure trend to be increasing linearly, but fails in predicting the amplitude of the dynamic pressure correctly. The calculated pressure amplitude is 108% higher than the measured value.

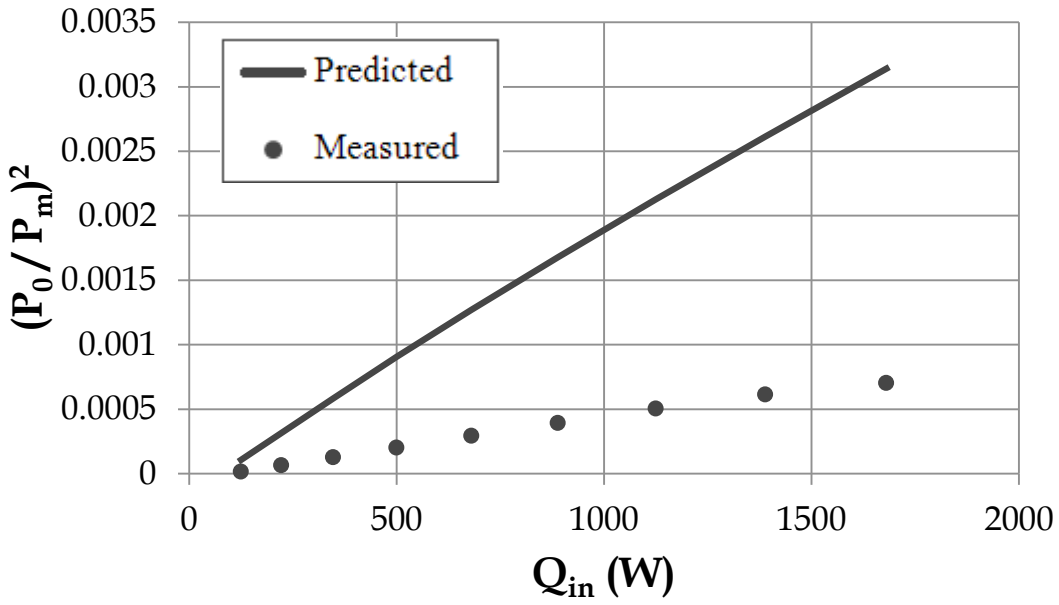

Figure 4.5: Effect of input heat power on the square of the normalized fundamental frequency for air at 1 bar using a 600-CPSI stack.

4.1.4 Frequency

The frequency of the fundamental mode of the standing wave in the resonator in DELTAEC simulation shows a little change with input heat, ranging from 193.1 Hz at 500 W of input heat to 193.5 Hz at 1680 W of input heat. It should be noted that the modeled and measured frequencies increase slightly with the increase of input heat due to the increased mean air temperature, affecting the speed of sound, hence the frequency of operation. In addition, the measured values are less than the modeled values, as shown in figure 4.6, since DELTAEC does not account for many losses in the system.

The experimental results show a good agreement with the *trend* of the results of DELTAEC. The measured acoustic power, dynamic pressure amplitude and working frequency are less than DELTAEC results due to the losses that are not accounted for as mentioned above.

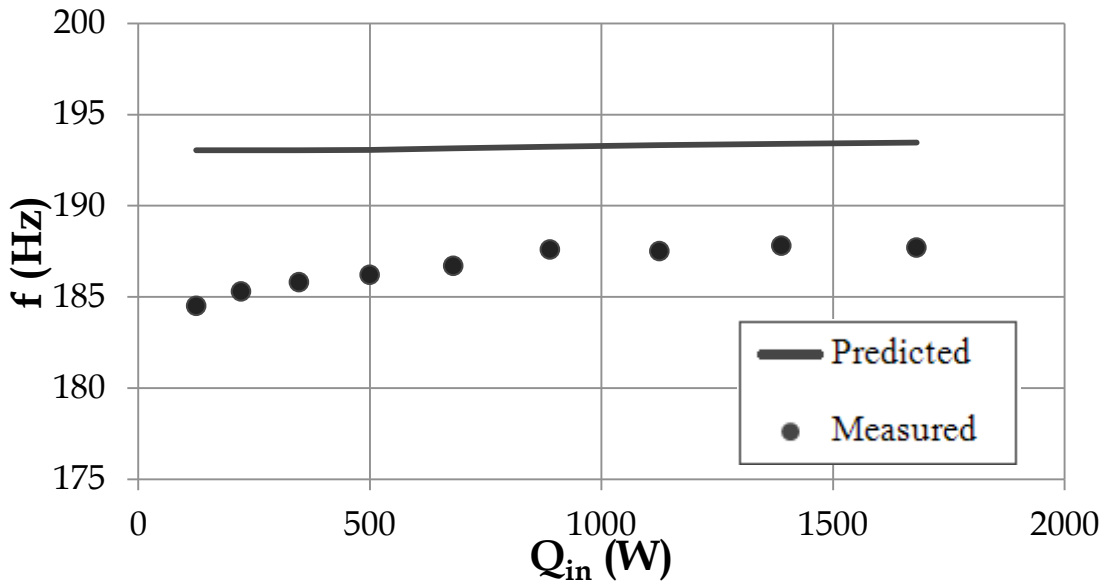

Figure 4.6: Effect of input heat power on the frequency of the fundamental acoustic wave for air at 1 bar using a 600-CPSI stack.

4.2 Sustainability of operation

An important issue in designing and operating thermoacoustic engines is the ability to sustain the temperature gradient across the stack, which in turn sustains the generation of the acoustic wave. This is mainly a function of the thermal conductivity of the stack, the working gas, the resonator holding the stack material and, more importantly, how well the cold heat exchanger removes heat from the cold stack side. Figure 4.7 shows the thermal network inside the stack. The heat leakage through the stack flows through the stainless-steel resonator wall, the stack solid, and the gas inside the pores of the stack.

For the case of a 600-CPSI stack filled with gas at mean temperature of 400K. The resonator outer diameter is 6”. The expected resistances when filled with air and helium are shown in table 4.1. The low values of the resistance of the resonator wall show that the leakage through it is dominant. The change of gas properties made no significant change in the total resistance. The stack thermal resistance is also small compared to the gas resistances in both cases.

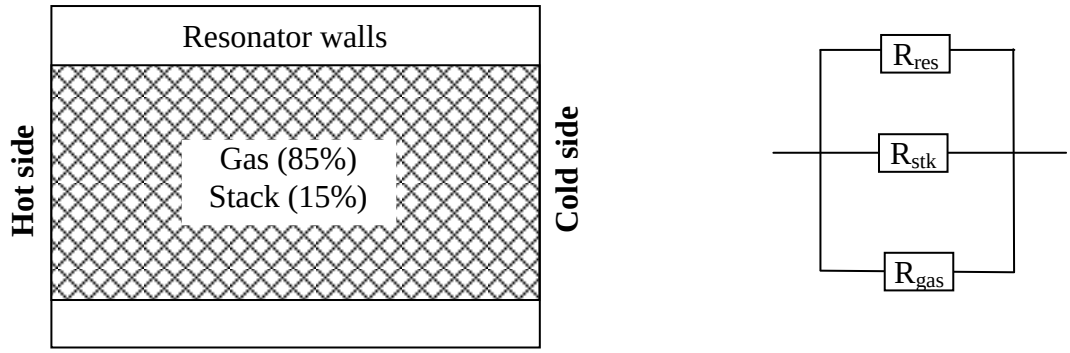

Figure 4.7: The thermal network for the resonator walls, the 600-CPSI stack and the gas filling it. R_{res} is the resonator wall thermal resistance, R_{stk} is the stack walls thermal resistance, and R_{gas} is the gas thermal resistance.

At the hot and cold heat exchangers, the gas side heat transfer coefficient depends on the oscillations of the gas. Garrett[32] suggest that an approximate estimation of the convective heat transfer coefficient (*h*) between gas and solid wall of thermoacoustic heat exchangers can be achieved on the basis of a simple "boundary layer conduction heat transfer" model. The convective coefficient h should be roughly equal to:

$$h = \frac{k}{\sqrt{2}\delta_k} \qquad \text{Eq. 4.1}$$

Table 4.1: Thermal resistance components in a 600-CPSI stack

	Air	Helium
R_{res}	0.556 KW^{-1}	
R_{stk}	10.5 KW^{-1}	
R_{gas}	137 KW^{-1}	24.7 KW^{-1}
R_{total}	0.526 KW^{-1}	0.516 KW^{-1}

Simple calculations show that for air at atmospheric pressure oscillating at 190 Hz, the heat transfer coefficient *h* is found to be 93 W/m^2K, while helium at the same pressure result in a better heat transfer process with *h* = 185 W/m^2K. Compared with the higher heat transfer of internal water flow in a finned tube heat exchanger (h ~ 750W/m^2K), it is clear that improvements should be done to increase the heat transfer coefficient and area at the gas side.

The increase in pressure gives better heat transfer coefficient. At 20 bars, air gives a heat transfer coefficient *h* = 415 W/m^2K, while helium gives *h* = 827 W/m^2K. This shows that improvements at the water side become effective in increasing the effectiveness of the heat exchanger.

Full runs of the engine show that the engine works at a stable condition for long periods of time (7200 s). In figure 4.8, the hot heat exchanger raises the hot-side temperature to 685^oC in 2000 s. This starts with a rapid increase in temperature from 30 to 600^oC during the time from 0 to 500 s. The cold heat exchanger takes a similar trend. It starts at 30^oC then reaches 90^oC at 500 s and finally reaches 111^oC at 2000 s.

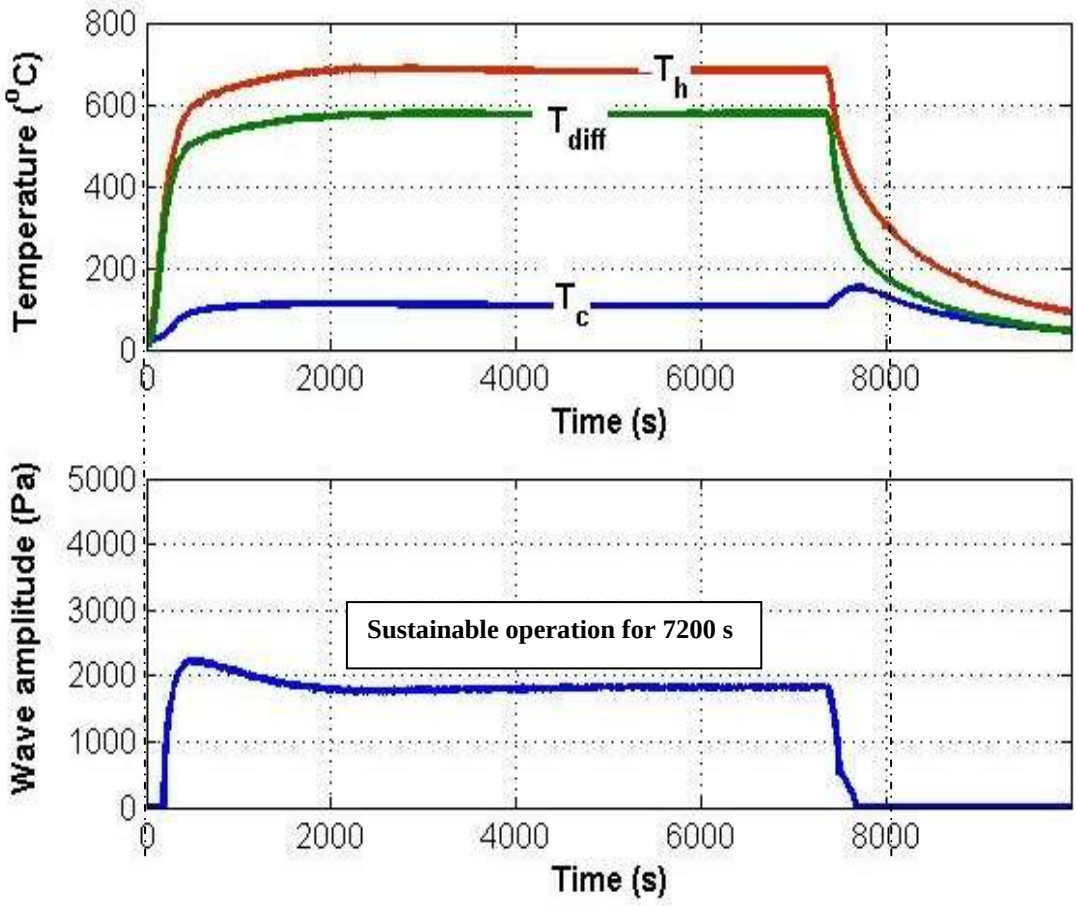

Figure 4.8: Performance of the thermoacoustic engine using air at 1 bar and a 600-CPSI stack during a 7200 s run. **(a)** Temperature of air at the hot and cold sides of the stack and temperature difference across the stack. **(b)** Dynamic pressure amplitude of the fundamental wave measured at 14.5 cm from the hot side blind flange during the experiment.

The hot and the cold side temperatures stay stable at 685°C and 111°C during the rest of the run until the engine is turned off. The pressure wave starts to exist when the temperature difference on the side of the stack reaches the onset value of 309°C after 200 s from the start of the run.

The pressure wave starts with a high increase in amplitude, taking a time of 374 s from the onset to reach its maximum of 2220 Pa. The dynamic pressure amplitude then decreases until it reaches its stable value of 1757 Pa after 2000 s from the start of experiment. The stable temperature difference of 574°C, resulting from the input heat of 1680 W, causes the dynamic pressure amplitude to stay stable at 1757 Pa until the shutoff of the engine.

Figure 4.9 shows the dynamic pressure amplitude versus the temperature difference across the stack during one full run. This particular representation omits time in favor of demonstrating the hysteresis. The curve takes two different curves during startup and shutdown process.

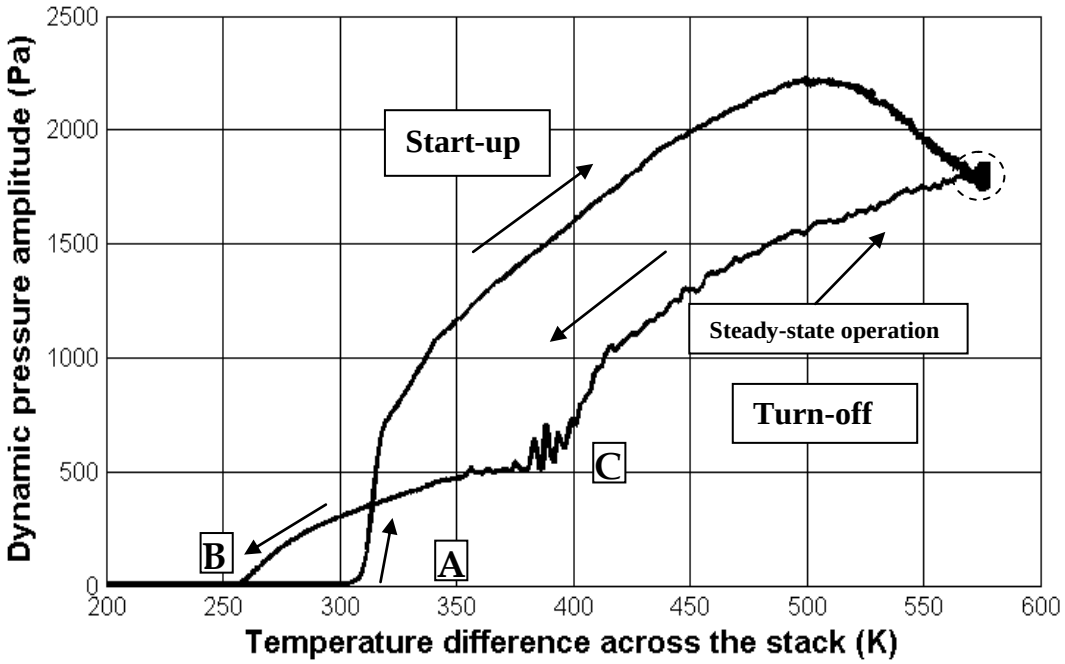

Figure 4.9: Dynamic pressure amplitude of the fundamental wave versus the temperature difference across the stack during a full run of 7200 seconds. The engine uses air at 1 bar and a 600-CPSI stack. Dynamic pressure is measured at 14.5 cm from the hot side blind flange.

4.3 Transient operation and hysteresis

Due to the time-dependent development of the gradient across the stack during long cycles, hysteresis is observed during startup and shutdown. In this section, the full-cycle performance of the engine is investigated, using several gas mixtures, stacks with different pore sizes, different start-up conditions, and different operating times of the engine.

4.3.1 Hysteresis characteristics for cycles of different running times

In this experiment, the engine is operated for several cycles starting from the same initial conditions. Each cycle consists of a start-up stage, a steady-state stage, and a shut-down stage. Every cycle has its different operation time. The engine is started each time from cold state, where hot and cold sides of the stack are at the same temperature and the engine has not been operated before the experiment for time enough to guarantee that the whole stack and resonator temperatures are homogenous. The objective of this set of experiments is to demonstrate the effect of the operating time which affects the development of the stack temperature gradient on the size of the system's loop.

In figure 4.10, temperatures of hot and cold sides and dynamic pressure amplitudes versus time are presented, and the dynamic pressure amplitude is shown versus the temperature difference across the stack. Cycles of 300 and 500 seconds show continuously increasing dynamic pressure amplitude till shut down. Starting from the cycle of 1700 seconds, the cycle shows a peak in the dynamic pressure amplitude that is followed by a mild decrease in pressure.

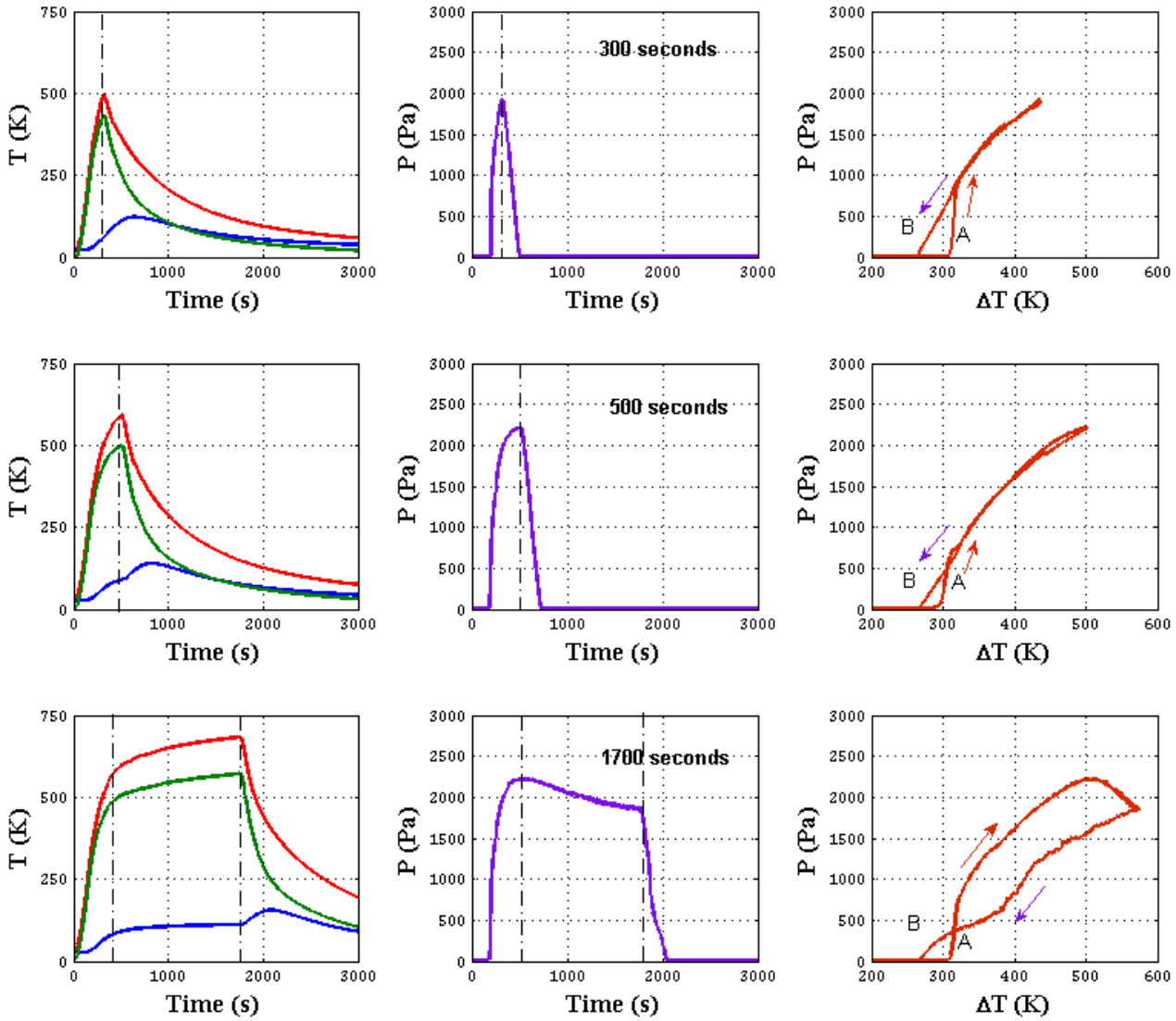

Figure 4.10a: Full cycles of engine operating for different times of 300,500, 1700 seconds, showing transient path of temperature and dynamic pressure amplitude, and the hysteresis loop of dynamic pressure amplitude with temperature difference.

Further increase in the operating time shows steady-state operation at an operation time of 7200 s as shown in the bottom set of graphs of figure 4.9b.

4.3.2 Hysteresis characteristics for cycles of different starting conditions

Two cycles with operation time of 3000 second with different starting conditions are presented to clarify the effect of starting at hot versus cold conditions. One of the cycles starts from cold state, while the other starts just after the engine was turned-off from a previous experiment. The performance of the engine during these two runs is shown in figure 4.11. The two cycles of the same operating time, 3000 seconds, showed that for the cycle that started with stack at room temperature, the peak amplitude is much higher than the one that started at hotter stack temperature (2223 Pa and 1912 Pa respectively) , while the steady temperature reached after that is nearly the same (582 ^{o}C). This implies that the different mean temperature of the stack during start-up has a significant effect on the hysteresis characteristics of the dynamic pressure of the engine.

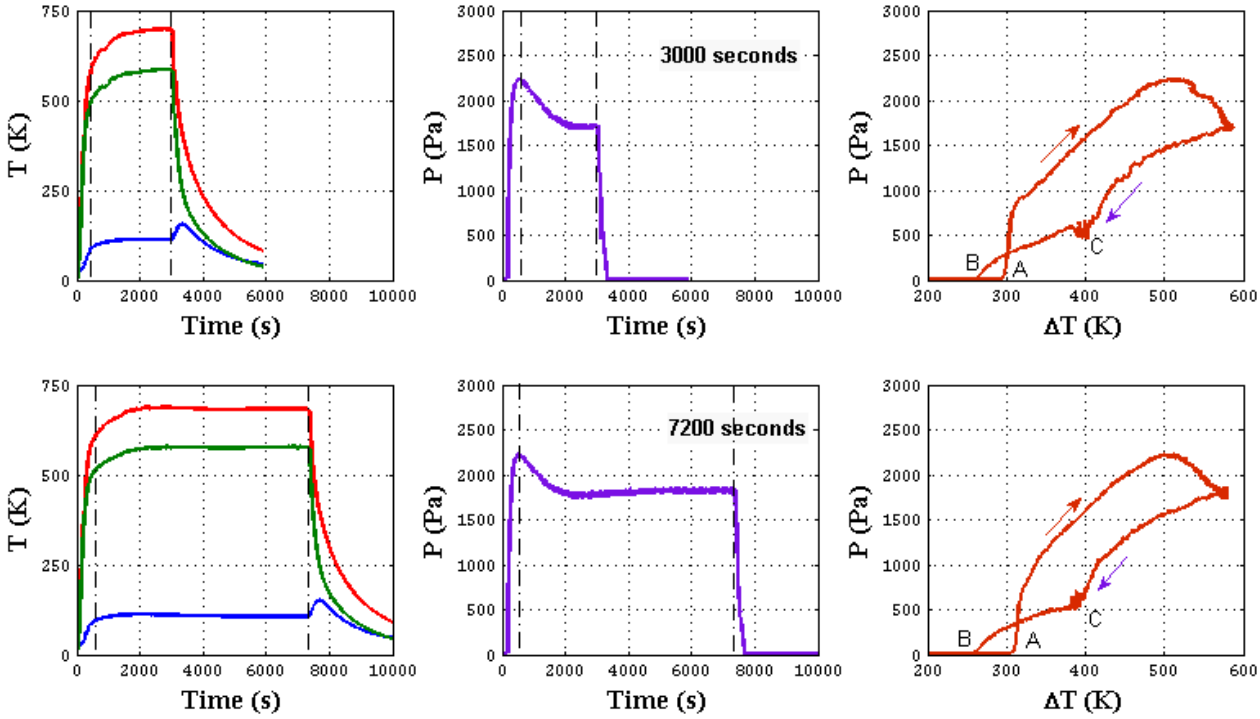

Figure 4.10b: Full cycles of engine operating for different times of 3000 seconds, and 7200 seconds, showing transient path of temperature and dynamic pressure amplitude, and the hysteresis loop of dynamic pressure amplitude with temperature difference.

4.3.3 Hysteresis in onset temperature

For all cycles, it is noticed that the wave starts at a temperature difference across the stack during the start-up process (about 305 K at point A in figures 4.9, 4.10 and 4.11) and stops at a lower temperature difference across the stack during the shut-off stack (about 270 K at point B in figures 4.9, 4.10 and 4.11). Both temperature differences are higher than the theoretical temperature difference suggested by DELTAEC which is 173 K. This behavior demonstrates that the onset process has hysteresis characteristics. When the wave already exists, it is easier to sustain it than to start its existence. This behavior is related to the change in the parameters that control the onset temperature difference which are the mean temperature T_m, gas heat capacity ratio γ and thermal expansion coefficient β.

An inspection of the cold-side stack temperature in figures 4.10 and 4.11 shows that when the engine is turned-off, the temperatures of the cold side increases, although the heat input to the engine is turned-off. The increase takes place over a period of approximately five minutes, before it starts to cool down and approach the ambient temperature. This observation is important for the design of the cold-side heat exchanger because it suggests that the resultant wave actually helps in cooling the cold-stack side. This implies that at these operational conditions, the rate of cooling on the cold stack side by the convection in oscillating flow conditions is higher than the rate of heating by conduction. At the hot stack side, the rate of cooling caused by the oscillating wave is negligible compared to the heat generation rate by the heater. Therefore, upon the spontaneous shut down of the engine, the hot stack side does not experience a similar phenomenon.

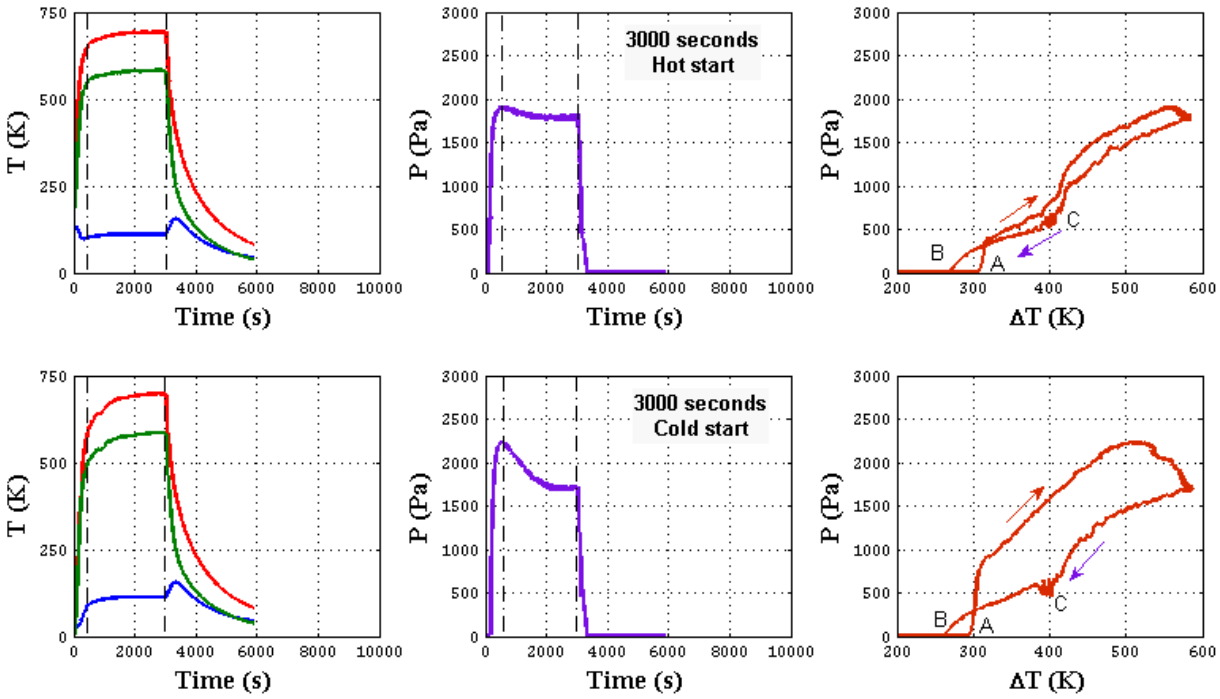

Figure 4.11: Full cycle of the engine operating for 3000 s starting from hot condition (upper row) and cold conditions (lower row) showing transient path of temperature and dynamic pressure amplitude, and the hysteresis loop of dynamic pressure amplitude with temperature difference.

Figure 4.11 also shows that the cycles with operating time of 3000 seconds or more starting from cold condition have approximately the same hysteresis size of hysteresis loop. The dynamic pressure amplitude starts to increase with a high pressure to temperature difference rate at a temperature difference of 310 K. The rate of pressure increase then decreases a little and stays constant for temperature differences between 350 and 500 K. At that point, the dynamic pressure amplitude reaches it maximum value of 2214 Pa. The dynamic pressure amplitude then starts to decrease until it reaches its steady state value of 1790Pa.

At a temperature difference of about 400 K during shutdown, the system dynamic pressure amplitude and temperature difference stays constant for a short period of time. This behavior is not related modifications to the hardware of the system. It may be due to a transition in heat transfer mode which causes a decrease in heat transfer efficiency due to lower oscillation amplitude. After this short time, the dynamic pressure amplitude decreases in a different rate, not equal to the increase rate, but much lower. Therefore, the dynamic pressure amplitude reaches zero at a temperature difference lower that the onset temperature difference measure at the start-up.

The different rates of cooling agree with the observations of De Waele on the numerical simulation of transient effects in the engine during shut-down. De waele argues that when the hot-side temperature decreases, the wave production decreases as well until the oscillations become weak enough that the heat transfer coefficient is decreased so that the hot-side temperature decreases at a lower rate and the rate of the decrease of oscillations also decreases [58].

4.3.4 Hysteresis characteristics for different gas mixtures

The hysteresis characteristics of the engine when operated using different gas mixtures is investigated. Runs in this section, shown in figure 4.12, are performed using a 600-CPSI stack. The mixtures used are air and mixtures of air and helium with air molar fractions of 80%, 70% and 50%. All experiments were operated for more than 1000 seconds.

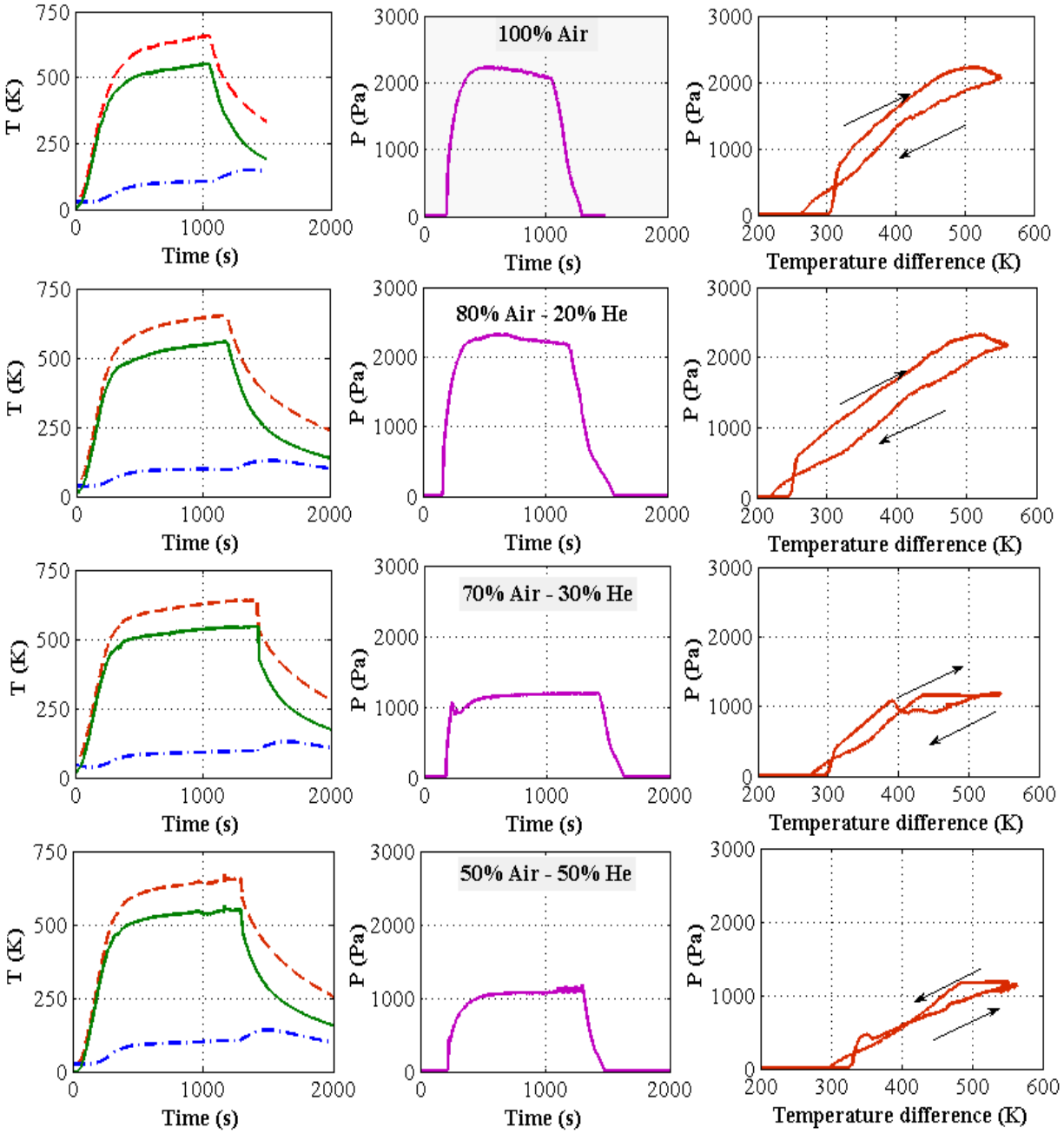

Figure 4.12: Full cycles of engine operating for different gas mixtures of air and Helium, showing transient path of temperature and dynamic pressure amplitude, and the hysteresis loop of dynamic pressure amplitude with temperature difference. Red and blue dashed lines are hot and cold temperatures, while green continuous line is the temperature difference.

As shown in figure 4.12, it is observed that the difference in onset temperature between start-up and shut-down discussed in the previous section 4.3.1 is present. In all cases, the onset temperature during start-up is higher than the temperature at which oscillations stop during shut-down. The change in rate of amplitude decrease while shutting down is noticed at about the same temperature difference of about 350 K in all experiments.

Due to properties changes of the operating mixture, major changes occur in hysteresis characteristics. First, the onset temperature at start-up and shut-down is different for every mixture. For start-up, it is 306 K for air, 250 K for 80% air, 300 K for 70% air, 329 K for 50% air. Shutdown onset temperature difference is 266 K for air, 222 K for 80% air, 279 K for 70% air, 302 K for 50% air. This suggests that the mixture of 80% air and 20% Helium molar fractions is favorable because:

i) it gives lower onset temperature, this allows it to be used with lower quality heat sources that would otherwise be wasted, and

ii) as the onset temperature of the fundamental mode decreases, the onset temperatures of higher modes are reduced as well. Then, operating TAE at a hot-end temperature much higher than the onset temperature of the fundamental mode excites the higher harmonics.

Figure 4.12 also shows the dynamic pressure amplitude versus time where the dynamic pressure amplitude increases after the onset and experiences an overshoot before it settles to a lower quasi-steady value. The results indicate that as the helium fraction increases, the overshoot decreases until it disappears at high helium fraction.
The right column in figure 6 shows the hysteresis loop plotted as the variation between the dynamic pressure amplitude versus the temperature difference across the stack. This reflects evidence of hysteresis where the onset temperature difference at start-up is always higher than at shut down, and the size of the hysteresis loop clearly decreases as the helium molar fraction increases. Figure 4.12 shows that the dynamic pressure amplitude reaches a peak then decreases to the steady value for the 100% air and the 80% air – 20% He mixtures. The difference between the peak and the steady amplitude is higher for 100% air than the 80% air-20% He mixture. For mixtures with higher Helium content, the peak is not recorded at all. This may be due to the higher thermal conductivity of Helium. The non-uniform distribution of temperature gradient contributes in this phenomenon, and the higher thermal conductivity of Helium helps transferring temperature along the stack in a higher rate. Although this is regarded a loss in potential driving input, it may be of use to reach the steady state in a faster manner that does not allow the dynamic pressure amplitude to increase then decrease again.
The steady dynamic pressure amplitudes are different for every mixture. The amplitude stabilizes at 2059 Pa for air, 2170 Pa for 80% air, 1191 Pa for 70% air, and 1102 Pa for 50% air. This supports the suggestion that the mixture of 80% air and 20% Helium molar fractions is favorable.

4.3.5 Hysteresis characteristics for different pore sizes

The hysteresis characteristics of the engine when operated using stacks of different pore sizes is investigated. This is done by recording two nuns with 600-CPSI and 400-CPSI stacks. The two experiments use pure air as an operating fluid as it is seen that it has more obvious hysteresis paths. All experiments are operated for 4000 seconds, which is enough.

Figure 4.13 shows two runs that show the same behavior in the ascending and descending rates. They also have the same phenomena that result in higher onset temperature in start-up

than in shut-down. For the 600cpsi stack which has lower hydraulic radius, the peak pressure reaches 2229 Pa and the steady state pressure is 1804 Pa with a ratio of 1.236. For the 400cpsi stack, the peak pressure is 2419 Pa and the steady state pressure is 2085 Pa with a ratio of 1.16. This suggests that the hydraulic radius of the 400cpsi stack is favorable for the air mixture at the experiment temperature and pressure.

The run with 600cpsi stack also experiences a longer period of stability while the pressure is decreasing (at 395 K of temperature difference) before the dynamic pressure amplitude continues to decrease at a lower rate. The run with 400cpsi stack has no stop at the point where the rate changes while the pressure is decreasing (at a lower temperature difference of 345 K).

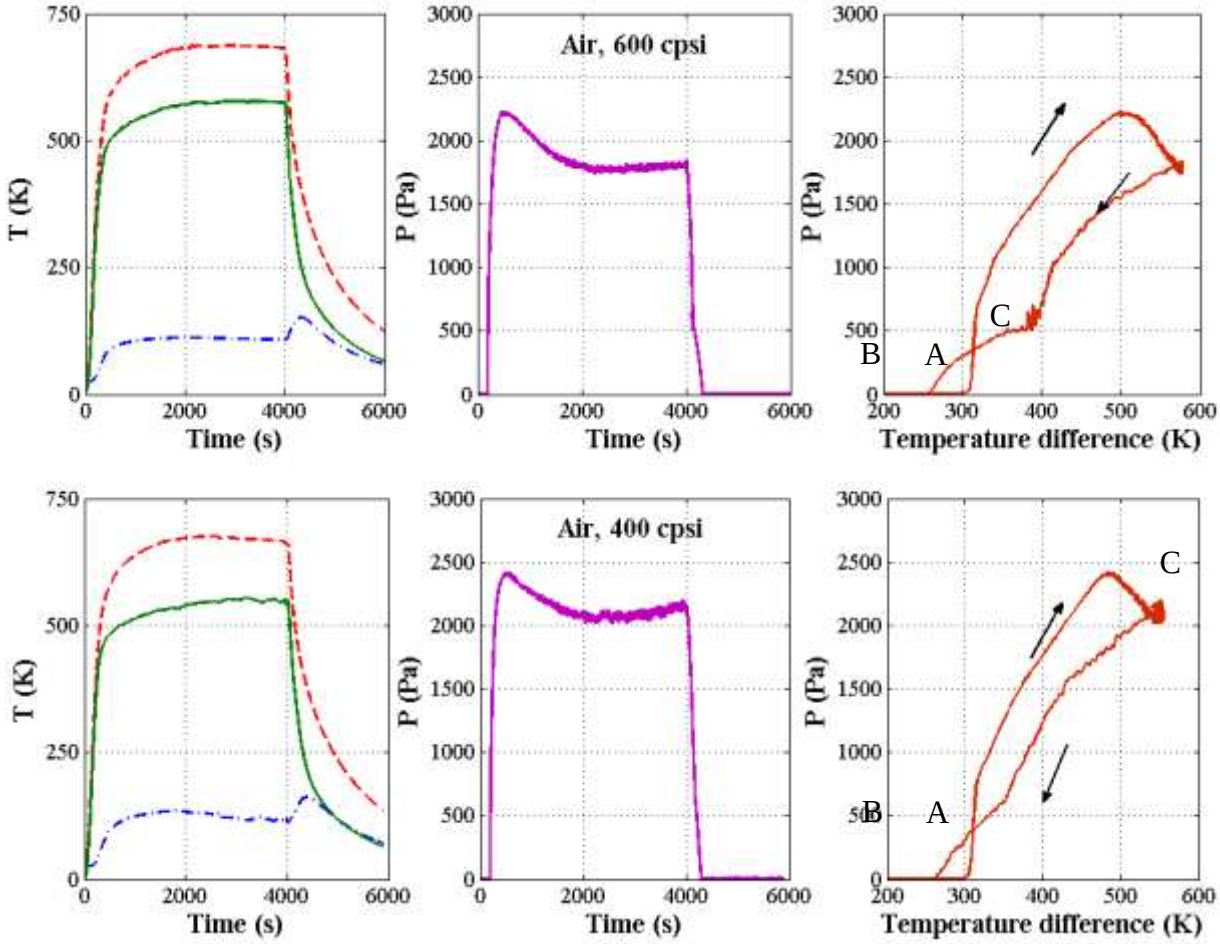

Figure 4.13: Full cycles of engine operating for different gas mixtures of air and Helium, showing transient path of temperature and dynamic pressure amplitude, and the hysteresis loop of dynamic pressure amplitude with temperature difference. Red and blue dashed lines are hot and cold temperatures, while green continuous line is the temperature difference.

The onset temperature at start-up and shut down are not significantly different. At start-up, it is 307 K for the 600cpsi stack, and 304 K for the 400cpsi stack. At shutdown, it is 259 K for the 600cpsi stack and 262 K for the 400cpsi stack. This implies that the components of the operating gas are the main factor affecting the onset temperature.

4.3.6 Wave characteristics during a full run

The characteristics of the resulting wave from the engine have a high importance when it comes to energy harvesting. The power production technologies available use single frequency and other higher frequencies are regarded as a loss. Therefore, the frequency content of the wave is described in detail here.

A) T_h= 340^{o}C
T_c= 105^{o}C
T_h-T_c = 235 ^{o}C

B) T_h= 432^{o}C
T_c= 90^{o}C
T_h-T_c = 342 ^{o}C

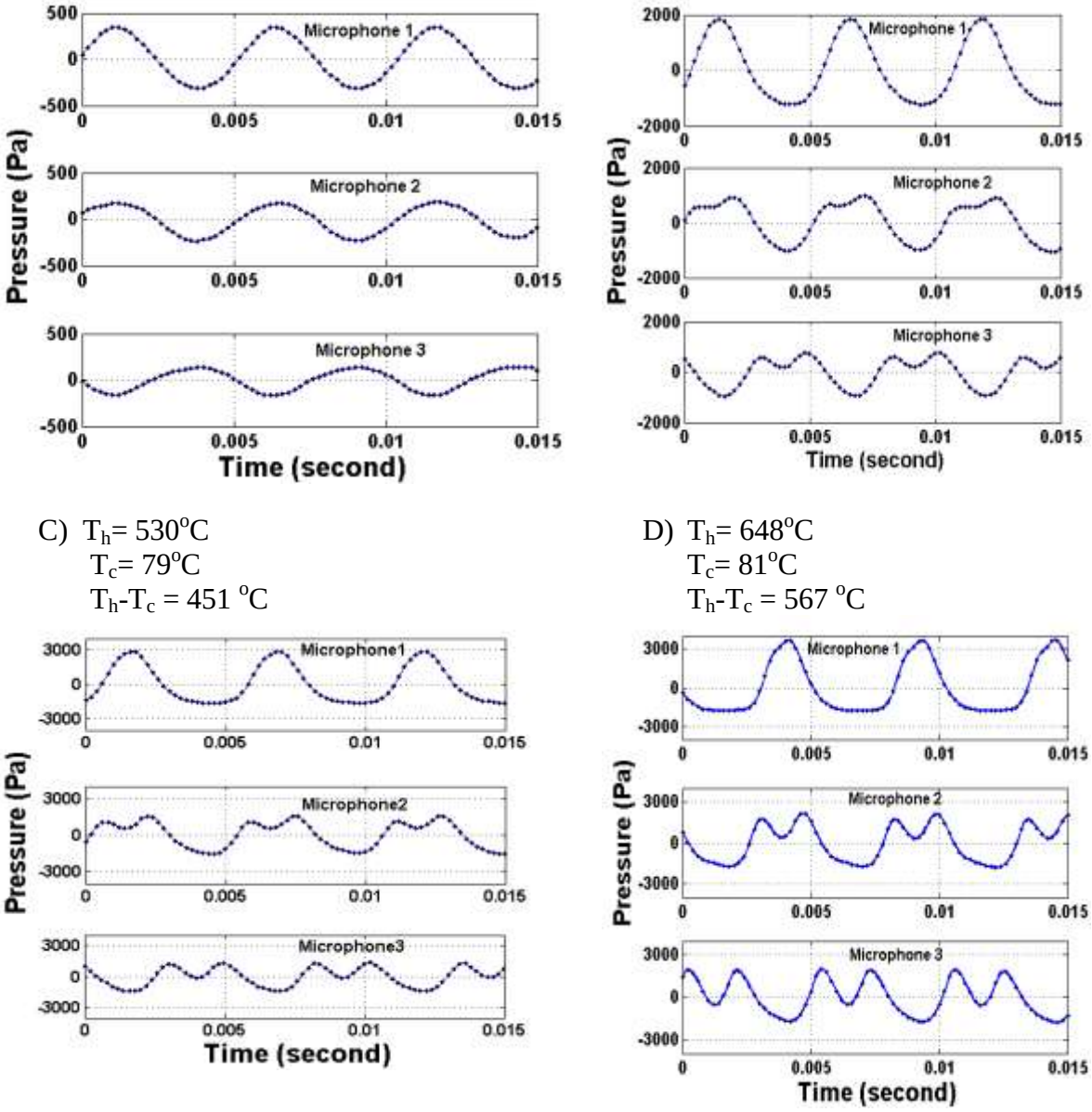

C) T_h= 530^{o}C
T_c= 79^{o}C
T_h-T_c = 451 ^{o}C

D) T_h= 648^{o}C
T_c= 81^{o}C
T_h-T_c = 567 ^{o}C

Figure 4.14: AC-coupled pressure waves in the time domain at different temperature differences across the stack at three different axial locations along the resonator

Figure 4.14 shows the resulting dynamic AC-coupled pressure waves in a range of hot-end temperature from 340 ^{o}C to 648 ^{o}C for the first, second and third microphones. Looking at the pressure data presented in case (A), where the engine is operating at a temperature difference of 235 ^{o}C, just 6% above its onset temperature difference of 221 K, it is observed that the wave measured with the first microphone, the nearest to the pressure antinode, indicates a

pure sine wave with an amplitude of 328 Pa and a frequency of 190.4 Hz. At the same operating conditions but further along the axis of the resonator, the amplitude reduces and the wave is more and more distorted. For example, the third microphone located the farthest from the pressure antinode reads an amplitude of 150.6 Pa and its harmonic analysis show two frequencies, namely190.4 Hz and 380.9 Hz.

A) T_h= 340^{o}C
T_c= 105^{o}C
T_h-T_c = 235 ^{o}C

B) T_h= 432^{o}C
T_c= 90^{o}C
T_h-T_c = 342 ^{o}C

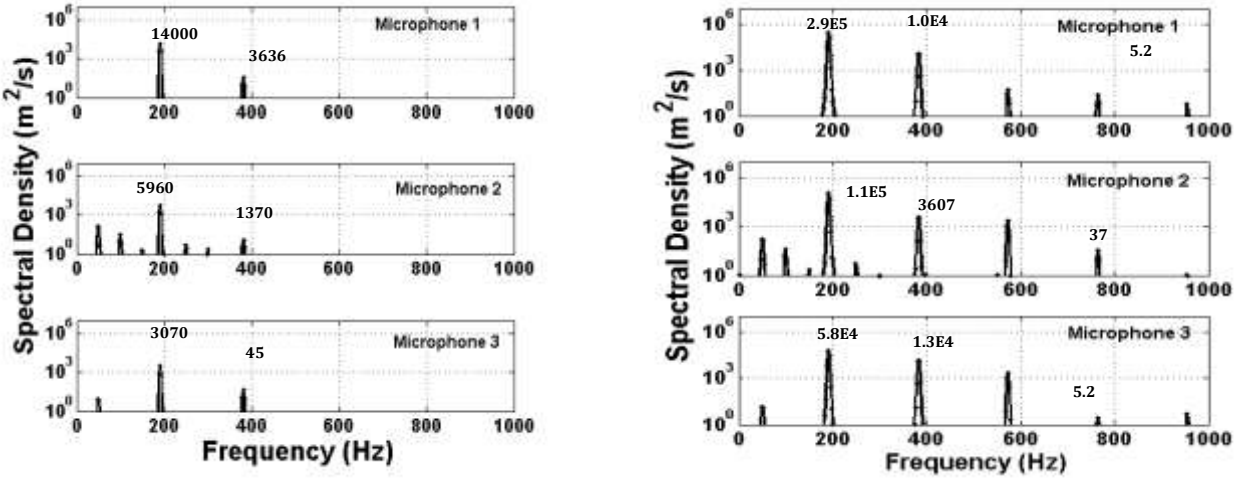

C) T_h= 530^{o}C
T_c= 79^{o}C
T_h-T_c = 451 ^{o}C

D) T_h= 648^{o}C
T_c= 81^{o}C
T_h-T_c = 567 ^{o}C

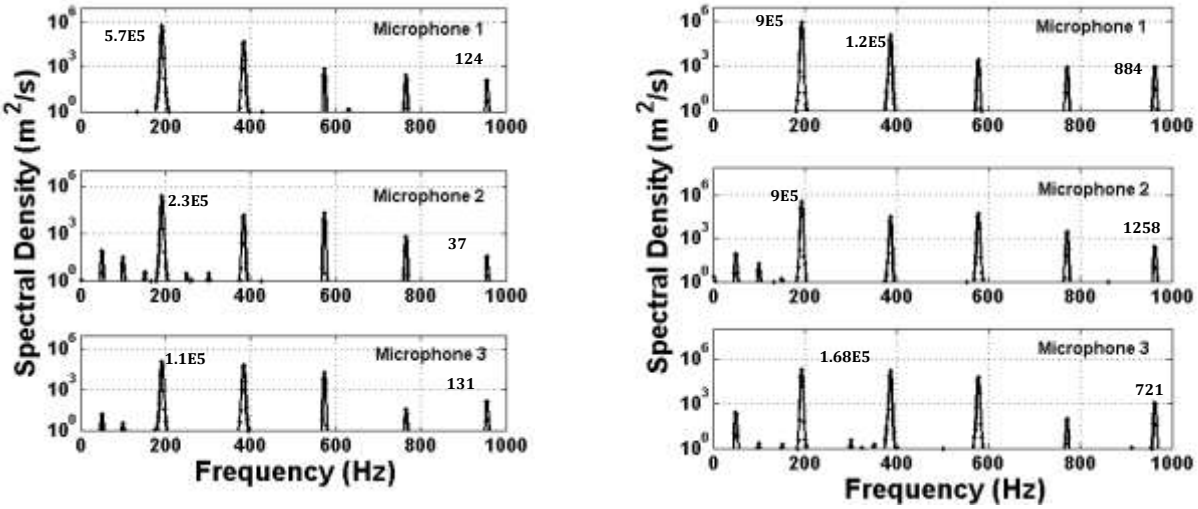

Figure 4.15: AC-coupled pressure waves in the time domain at different temperature differences across the stack at three different axial locations along the resonator

The reduction of dynamic pressure amplitude along the resonator axis is because of the nature of pressure distribution along the resonaotor axis for different modes. The increase in the harmonic content in the third microphone with respect to the first microphine is because the first harmonic has its pressure antinode at the resonator middle, as opposed to the fundamental mode which has its pressure antinodes at the resonator ends. Therefore, around the middle of the resopnator the first harmonic dominates over the fundamental mode which

explains the increase in the wave distortation as the pressure measurements approach the middle of the resonator.

As the hot-end temperature increases, the pressure wave measured by the first microphone experiences more distortions, indicating higher excitation of the harmonics. The pressure wave captured by the second and third microphones always shows more distortion than that measured by the first microphone, as explained above.

Comparison between cases (A) and (D) in figure 4.14 shows that as the temperature difference across the stack increases from 235^{o}C to 567^{o}C, the pressure magnitude of the fundamental component P_0 increases from 301 Pa to 2577 Pa, while the pressure magnitude P_1 of the first harmonic component increases from 13 Pa to 972 Pa. The P_1/ P_0 ratio indicates the relative strength of the first harmonic to the fundamental mode increases by an order of magnitude, from 0.04 to 0.38. Similarly, the ratio of the pressure magnitude of the third harmonic to that of the fundamental (P_3/P_0) increases by more than an order of magnitude from 0.2% to 3%. This illustrates how the increase in the operating temperature causes an increase in the dynamic pressure of the resulting pressure wave but also causes increased excitation of the harmonics.

The data presented in the time domain in figure 4.14 is further analysed in the frequency domain and the results plotted in figure 4.15. In this analysis, a set of 2048 data points are used for each case with a sampling rate of 5 kS/s, yielding a frequency resolution of 2.4 Hz. In figure 4, a vertical logarithmic scale is used extending from 1 to 2E6 to showing the large range of the spectral density of the components of the pressure wave, particularly at high temperatures. The results show the frequency of the fundamental mode (190.4 Hz) and the frequency of the higher harmonics (382.6 Hz, 574.2 Hz and 770.8 Hz). The progression of the harmonics with the increase of hot-end temperature is demonstrated.

4.4 Steady state operation using different gases and gas mixtures

The working gas used in thermoacoustic devices is the main component of the device. No certain mixture will give what can be described as a best engine performance. This is because the performance is characterized by several features, including the available power density, the first and second-law conversion efficiencies, the required onset temperature and the corresponding limitation on the available heat sources, the frequency of operation, and the degree of complexity required to solve sealing issues.

An ideal working gas[(59)] should [1] have high speed of sound, *a*, since the power density of the device is proportional to the speed of sound. It should be noted that for fixed engine geometry and operating conditions, the working frequency is proportional to the square root of the sound speed of the working gas; [2] have low thermal conductivity, *k*, to reduce the heat transfer from the hot side of the stack to the cold side across the working gas. A large thermal conductivity, however, increases the thermal penetration depth, which facilitates the manufacturing of the stack; [3] have a specific-heat ratio γ close to one to retain low onset temperature; [4] have low Prandtl number, to allow thick thermal penetration depth (to increase the thermal interactions between the gas and the stack) together with a thin viscous penetration depth (to reduce viscous losses by shear in the viscous penetration depth); [5] be leak tight. Light gases are more difficult to seal than heavy gases and this difficulty increases as the mean pressure increases and should not be underestimated in the design and assembly of the different resonator modules, or during the welding of heat exchangers or flanges or thorough the fittings of the engine accessories.

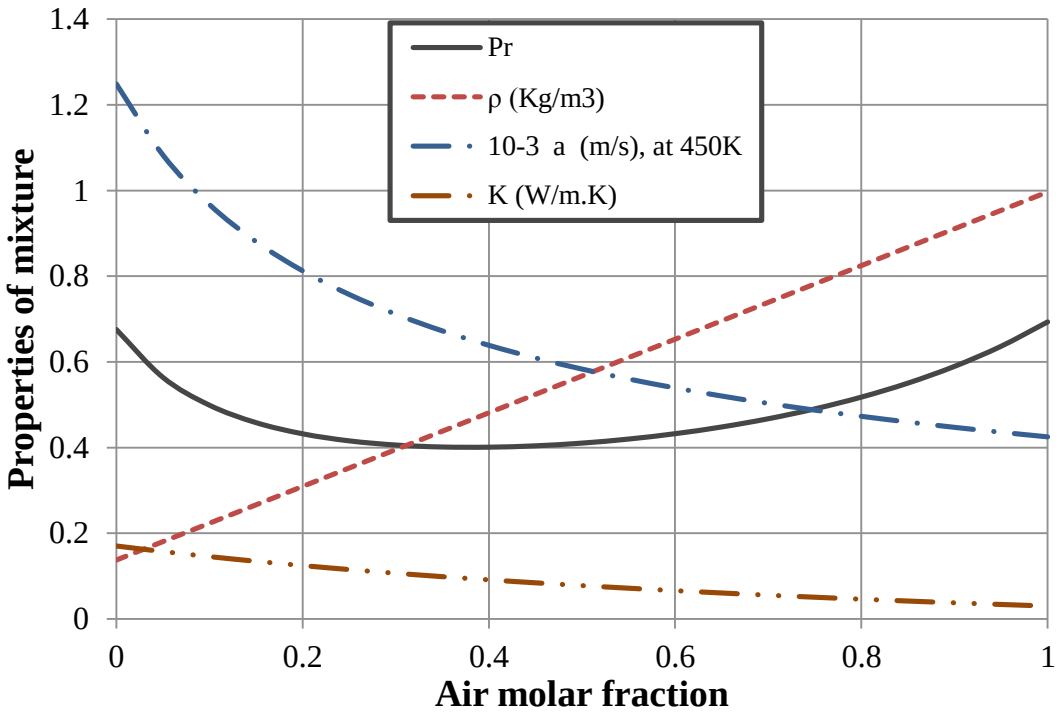

Figure 4.16: Density, speed of sound, Prandtl number and thermal conductivity for air/helium gas mixtures.

These contradicting requirements indicate that the optimum mixture of gases in a thermoacoustic engine should be selected according to the particular design objective (for example, the engine should have high first-law conversion efficiency η or low onset temperature) with careful consideration of the temperature of the available heat source. Helium, for example, is a commonly-used working gas in thermoacoustic engines and refrigerators, thanks to its large sonic speed but its high specific-heat ratio requires large onset temperature difference which eliminates several potential heat sources, its high thermal conductivity increases the conduction heat losses and makes it more difficult to maintain the temperature gradient across the stack, its small molecule is harder to seal than other inert gases and its low density makes the power density very low unless operating at high mean gas pressure. Figure 4.16 shows how a gas mixture of two gases (air and helium in this case) enjoys a wide range of speeds of sound, thermal conductivity, density and a minimum Prandtl number at a certain mixture composition.

Gases and gas mixtures used in this study are:

- pure air
- 80% air - 20% He
- 70% air - 30% He
- 60% air - 40% He
- 40% air – 60% He
- Argon

Appendix A lists the thermal properties of the air and Helium mixtures used in experiments.
In this section, the results of the experiments done to investigate effect of gas mixture composition and the stack pore size on the engine performance and harmonic content are presented.

4.4.1 Effect of gas mixture composition on output acoustic power

The linear theory predicts that for a thermoacoustic engine with no heat input or output losses, i.e. , the heat input is completely delivered to the stack and the system has no viscous or thermal losses, the power output increases linearly with the heat input starting from the origin. The introduction of losses in this theory causes the liner relation between power and heat input to intersect with the heat input axis in a non-zero value representing the average heat input loss that is not converted into output acoustic power and leaks out from the system.

The two microphone method used for power determination gives the average power intensity in the area between the two microphones. The average power flow from the stack is calculated by multiplying the intensity by the area of the resonator. Power flow is measured for different mixture by two microphones located at 14.5 cm and 30.5 cm respectively from the hot blind flange.

It is important to note that the power flow output of the engine is not only controlled by the working gas properties, but also by the position of the stack within the wave. In this engine, the stack position is kept fixed.

Figure 4.17 shows the power flow measured at different heat input to the engine. For every gas mixture, the measured output power flow starts with a linear increase with the increase of input heat. After that, as the pressure ratio of the engine increases and goes beyond the linear limit, a mild decrease in the slope of the acoustic power output line is detected. The limit where nonlinear behavior is detected is near $Q_{in}/P_m aA=10^{-3}$ which is about 750 Watts of input heat in this engine.

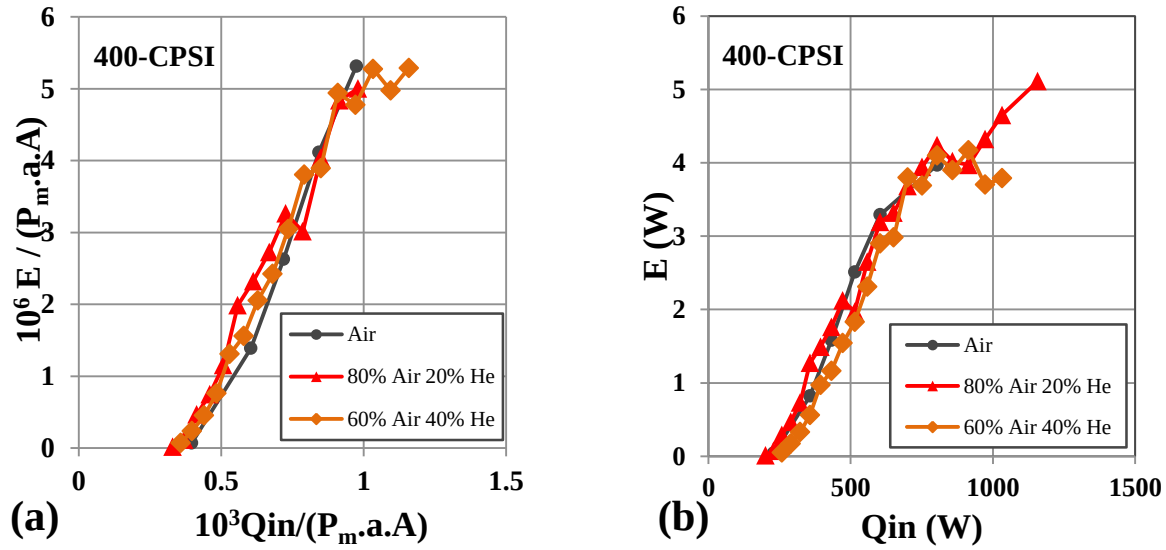

Figure 4.17: Engine output acoustic power flow at three different gas compositions. **a.** normalized power and input heat. **b.** absolute power and input heat.

Figure 4.17 shows that results at the linear region shows that the power flow output are not significantly affected by the composition of the mixture. This is possibly due to the low pressure used in the experiment which gives properties with no significant properties variations. However, significant differences are detected in the pressure components within the system as the next sections discuss.

4.4.2 Effect of gas mixture composition on pressure amplitudes.

The engine is operated using different stack pore sizes. Three different pore sizes are used to clarify the role played by the ratio of the pore hydraulic radius to the thermal penetration depth (r_h / δ_k). Stacks of 4 cm length and pore sizes of 600, 400, and 200 CPSI are used at the same location in the engine. Different gas compositions are included in the experiments. Figure 4.18 shows the linear relation observed between square of the drive ratio $(P/P_m)^2$ and the normalized heat input.

Results in Figure 4.18 show that the engine works at pressure ratios dependent on the heat input to the system. The square of the pressure ratio, which is an indication of the acoustic power produced in the stack, increases linearly with the heat input in the linear region.

Table 4.2 includes the dimensionless parameter (r_h / δ_k) for the experiments in figure 4.17. A standing wave thermoacoustic device needs this value to be more than one to provide a low blockage path for the wave inside the stack. Values of 3-5 are typical for thermoacoustic engines. In our case, the value ranges from 2.50 and 5.4 which is acceptable range.

The results indicate that the square of the pressure ratio is higher for the mixtures of gases than pure air or Argon. Mixture of 80% air and 20% He has better performance in both 600-CPSI and 400-CPSI stacks than other mixtures of air and Helium and pure air. This is an indication that the mixture with 80% Air and 20% Helium has preferable characteristics, which is a suitable trade-off between the Prandtl number (0.47), the mixture density (0.82 Kg/m^3), the thermal conductivity (0.046 W/mK) and the speed of sound (472 m/s) .

The 600-CPSI and 400-CPSI stacks operate at pressure ratios with no significant differences for each gas. This is related to the fact that the values of (r_h / δ_k) have no significant differences. On the other hand, the cases operated with 200-CPSI stack indicate lower pressure ratios than those operated with 400-CPSI or 600-CPSI stack for all gas mixtures used. This behavior is a result of the high values of (r_h / δ_k) associated with the 200-CPSI stack, with respect to the 400-CPSI or 600-CPSI stacks as reported in table 4.2.

Table 4.2: The average hydraulic radius to thermal penetration depth ratio for experiments in figure 5.3. The values are all calculated at mean temperature of 400^oC.

Gas	CPSI	r_h / δ_k	Gas	CPSI	r_h / δ_k
Air	600	3.37	Air	400	3.92
80% air - 20% He	600	2.71	80% air – 20% He	400	3.16
70% air - 30% He	600	2.50	60% air – 40% He	400	2.74
40% air – 60% He	600	2.04			
Air	200	5.4			
Argon	200	5.41			
40% Ar – 60% He	200	3.13			

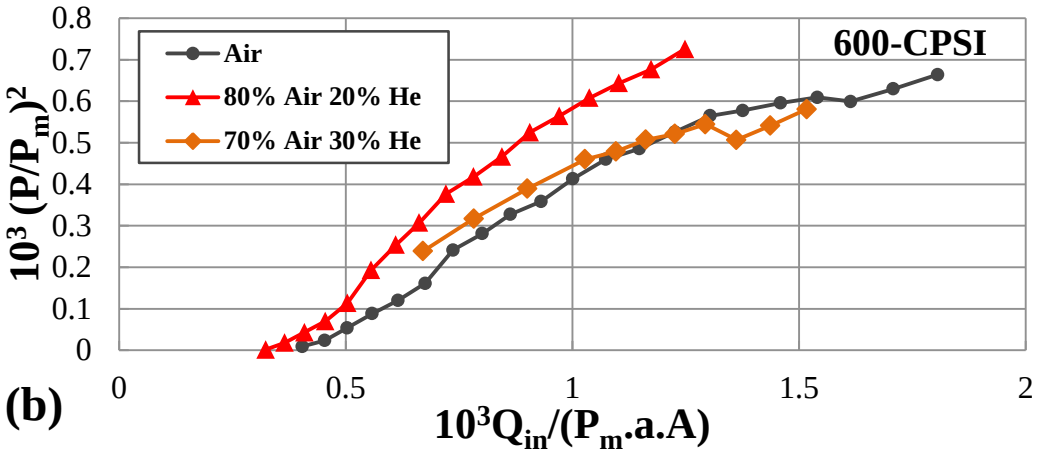

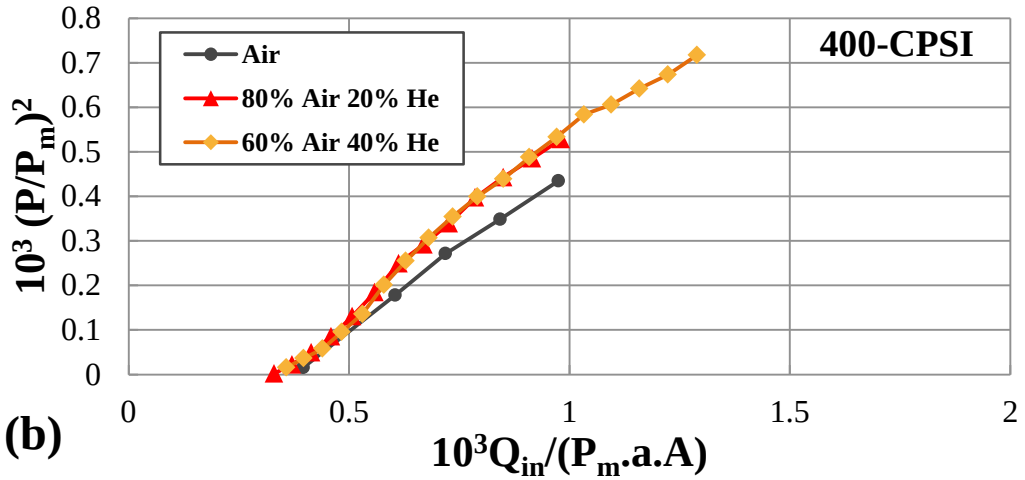

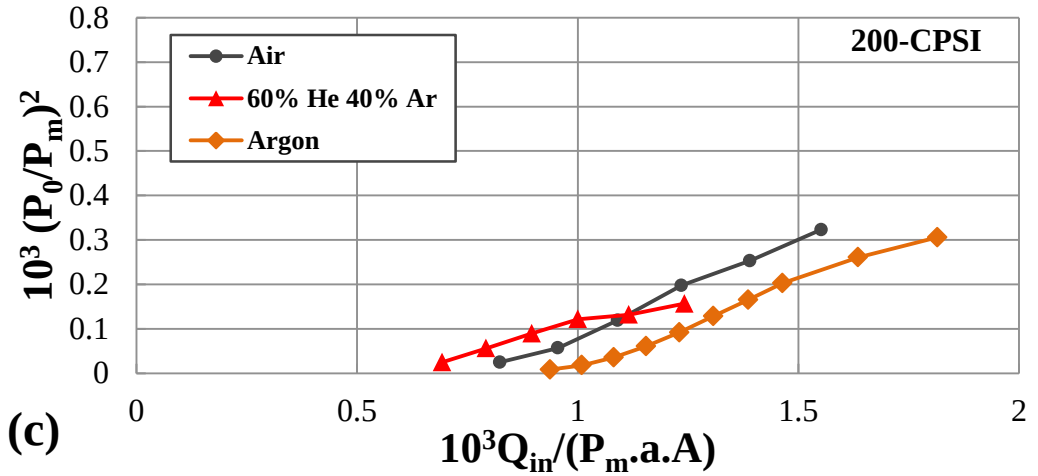

Figure 4.18: Pressure ratio at different gas compositions and different pore sizes. a. 600-CPSI, b. 400-CPSI and c. 200-CPSI measured at 14.5 cm from hot-duct flange.

4.4.3 Effect of gas mixture composition on harmonic distortion

The wave produced by the engine is a result of the addition of the fundamental wave to its harmonics. The energy collection from the engine is usually through a single frequency device. Therefore, the harmonics is regarded as a loss for the output acoustic power.

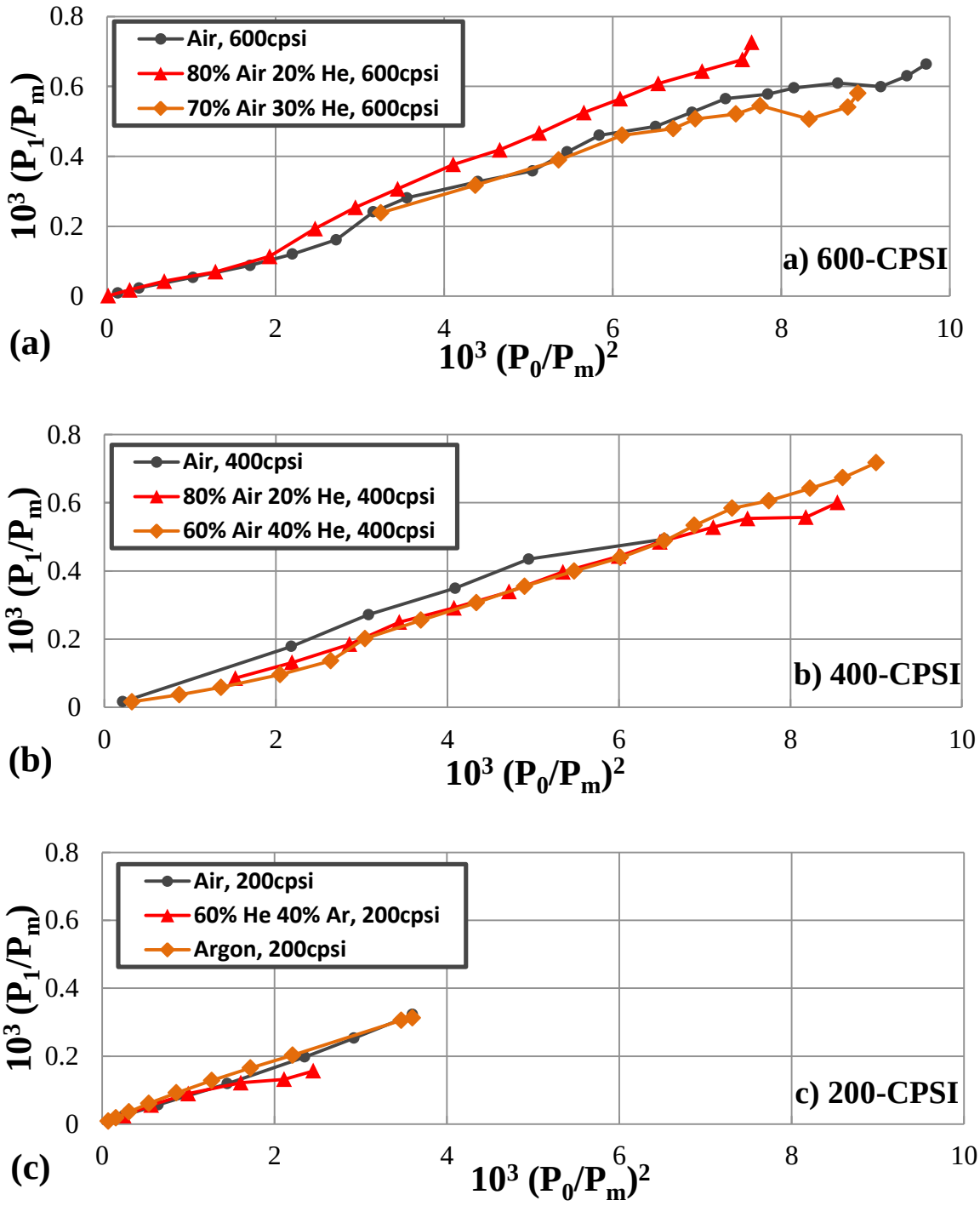

Figure 4.19: Normalized first harmonic amplitude versus normalized squared fundamental amplitude at different gas compositions and different pore sizes. **a.** 600-CPSI, **b.** 400-CPSI and **c.** 200-CPSI

The harmonic content is the most obvious nonlinear effect present in the present system. For example, at the highest power recorded using 600-CPSI stack with air mixture, the amplitude of the first harmonic P_1 is 972 Pa, which is 0.378 of the amplitude of the fundamental of this case, both measured using the same transducer at 14.5 cm from the hot-duct flange.

Figure 4.20 shows the relationship between the first harmonic pressure ratio to the square of the fundamental pressure ratio for the same experiments in figure 4.19. Remarkably, the results show that the relationship between the first harmonic and fundamental pressure ratios is linear. The linear relationship for all experiments has nearly the same slope. The different lines for different gas compositions and stack pore sizes start from the origin.

It can be concluded that the relationship is neither related significantly with the gas composition nor the stack pore size. Whatever the source of P_1 is, it is present and large. Its thermoacoustic effect should be accounted for. It causes a DC flow and transports heat along the stack. This requires a higher temperature difference between the two sides of the stack for the same output acoustic power.

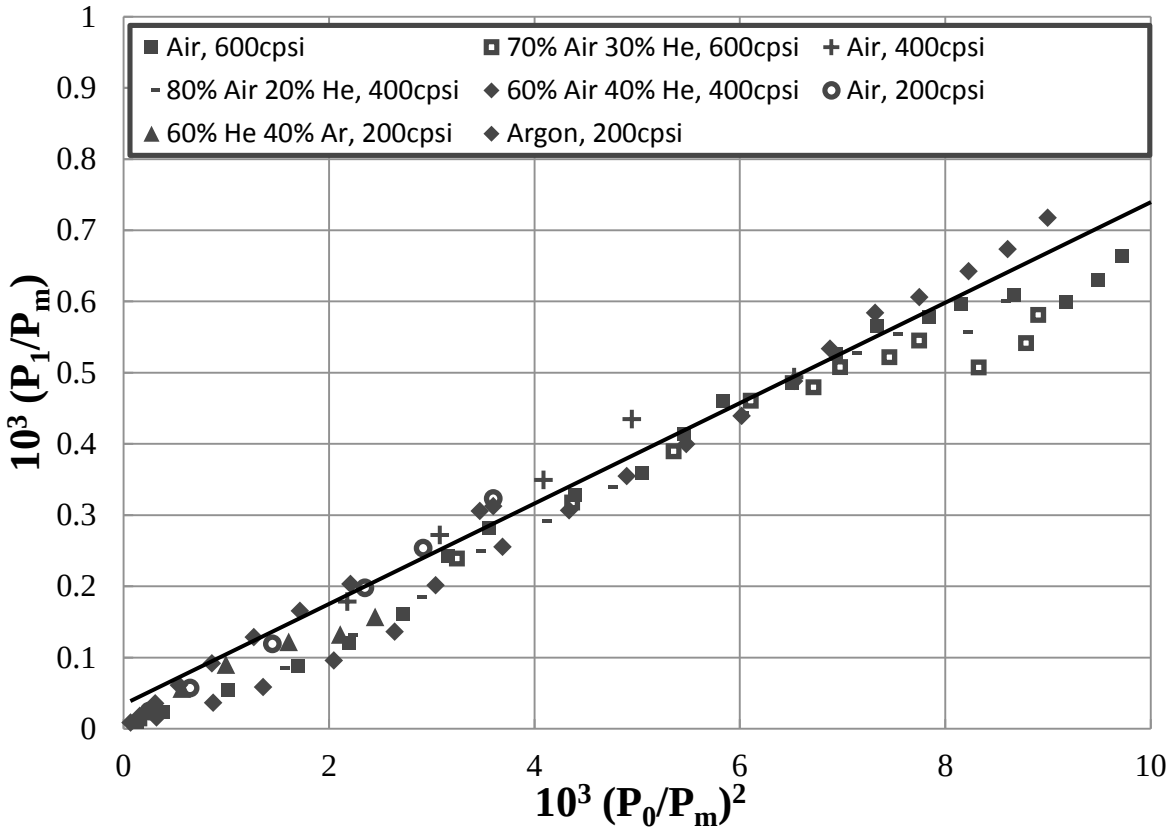

Figure 4.20: The linear behavior normalized first harmonic amplitude versus normalized squared fundamental amplitude at different gas compositions and different pore sizes.

Swift also suggests that the excess heat flow carried by P_1 is expected to be nearly proportional to P_1^2, and hence to P_0^4, so that the excess acoustic power absorbed from the fundamental must share this proportionality. The excess temperature difference needed should therefore be proportional to P_1^2, which is proportional to the input heat flow.

This dependence is visible in figure 4.21. It shows that, while DELTAEC calculations show that temperature difference increase is very low, the measurements showed a higher linear increase in temperature difference, indicating that the excess temperature difference is directly proportional to the input heat flow.

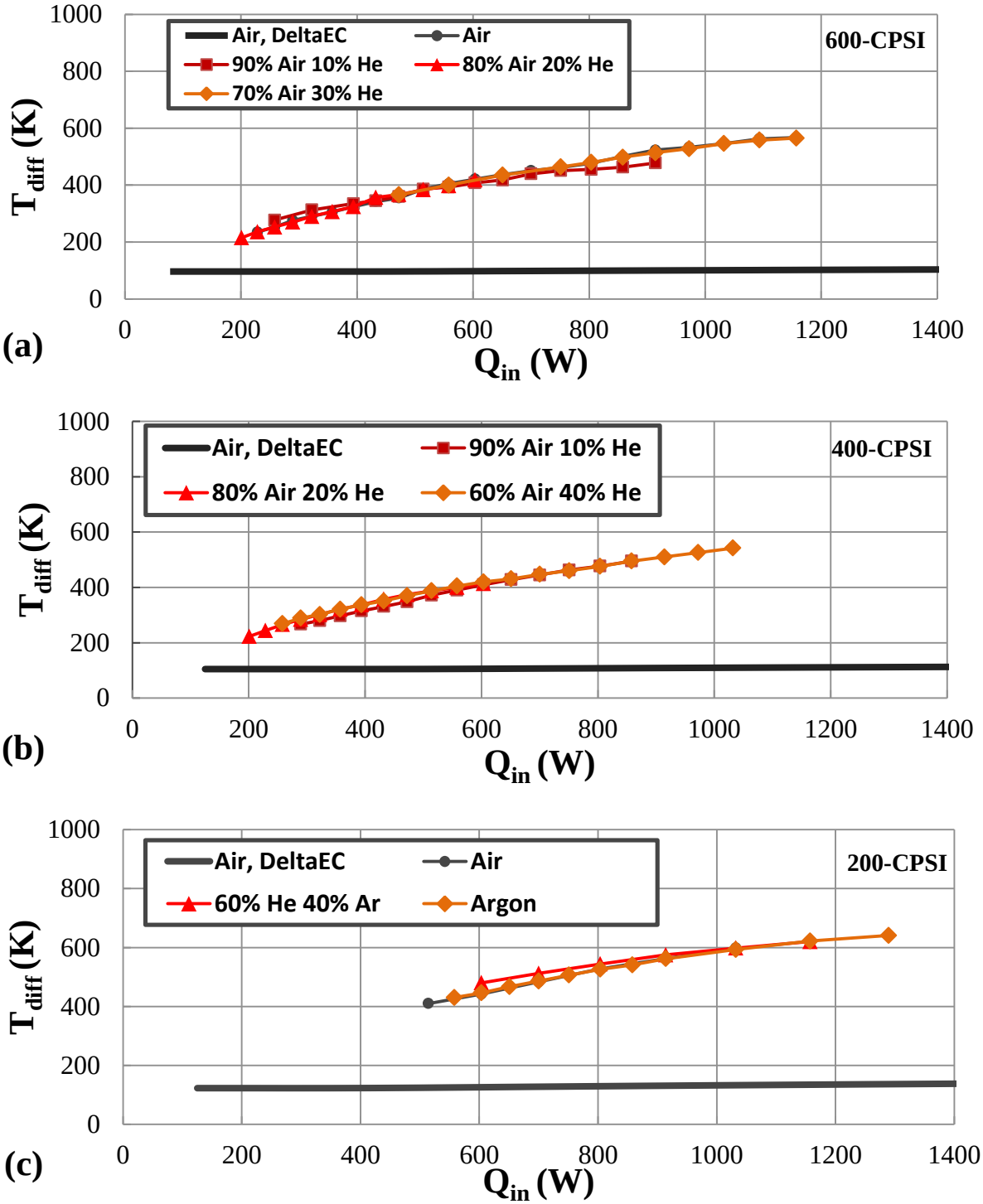

Figure 4.21: Temperature difference between the two sides of the stack versus the heat input for different gas compositions and different pore sizes. **a.** 600-CPSI, **b.** 400-CPSI and **c.** 200-CPSI compared to DELTAEC calculations for 100% air.

4.5 Harmonic suppression

Despite its high environmental and simplicity advantages, the built thermoacoustic engine presented in this work suffers high losses. One of the most obvious losses in the current engine is the existence of harmonics.

Harmonic distortion of the resulting acoustic wave in a thermoacoustic engine is regarded a loss. This is due to the fact that power generating devices from thermoacoustic engines, such as linear alternator, work at a single frequency. Moreover, devices that can use the resulting wave energy directly, such as in a thermoacoustically-driven thermoacoustic refrigerator, also need to receive a single frequency. The power carried by higher order harmonics is therefore lost as viscous heating in the air. Figure 4.22 shows that the power carried by the harmonic in the system reaches 38.8% of the power carried by the fundamental wave which is rather a significant loss.

Swift investigated the effect of adding inserts in the resonator on the first harmonic amplitude [24]. Placing an insert with lower flow area than the resonator at the velocity antinode of the first harmonic resulted in decreasing its ratio to the fundamental amplitude. However, Swift discussed neither the shape nor the blockage area or the thickness of these inserts.

The inserts are described in section 4.1.4. Every experiment is named as XYZ-N, where X is the open insert area ratio (gas area/total resonator area), Y is the shape code: either A which is a hollow ring, C which is multiple holes, or D which corresponds to DELTAEC calculations. Z is the thickness of the insert in cm and N is the distance in cm between the insert center and the hot-side blind flange. For example, the experiment 50C3-60 was done using a stack which contains multiple holes, a stack open area of half the area of the resonator area, a stack thickness of 3 cm, and the insert is placed 60 cm away from the blind flange.

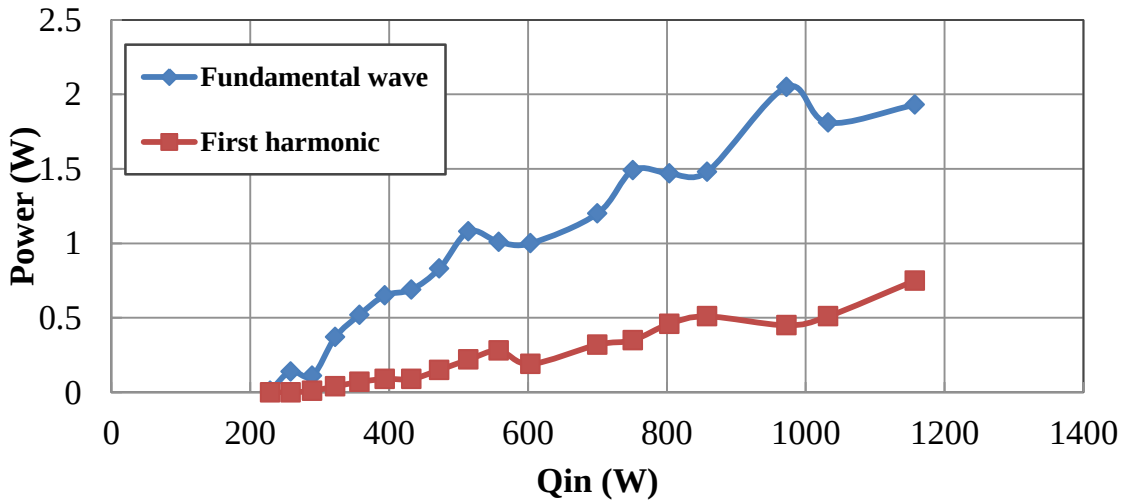

Figure 4.22: power carried by the fundamental wave and the first harmonic for the 400-CPSI stack operated with air as working fluid. Power measured using 2 microphones at 14.5cm and 59.5 cm from the hot-side blind flange.

4.5.1 Inserts effect on power and wave components

In this series of experiments, Inserts with various shapes and blockage areas are tested in the resonator. All experiments are done with a 400-CPSI stack with air as working fluid. The

stack center is placed at 5 cm away from the hot side flange. For every insert, the wave components are studied and the acoustic power output is calculated. Calculations were done using DELTAEC, modeling inserts as a duct which length is the stack thickness and has a smaller area. This duct was placed in various places in the model. The model results indicate the expected power, the expected frequency, and the fundamental dynamic pressure at the same measurement location. As DELTAEC works at a single frequency, it is not possible to obtain information about the harmonic content.

For every insert at a certain position, the voltage input to the heater is varied from 220V to 60V, which is equal to heat input ranging from 1680W to 125W. Figures 4.23 and 4.24 show some notable results of the experiments. The first graph shows the acoustic power output from the experiment sorted from higher to lower power output for different insert configurations. The other graphs sort the columns according to the same order.

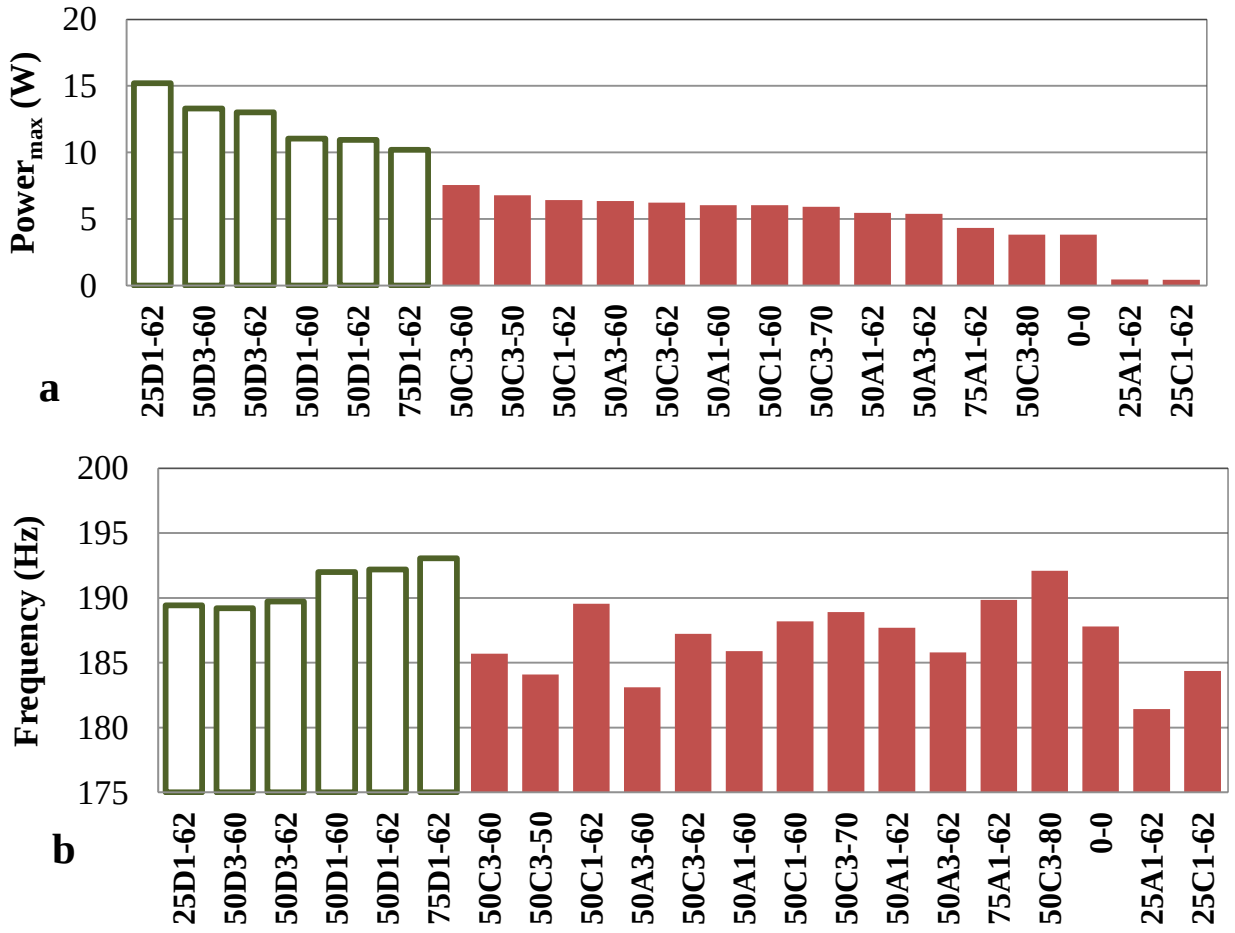

Figure 4.23: Power and frequency for multiple inserts with various shapes and positions. Solid columns are measurements, hollow columns are DELTAEC calculations.

The results show the complexity of the parameters that control the power output. The experiment named 0-0 is carried out with no insert placed in the resonator. It is seen that all inserts of 50% and 75% open area resulted in power increase than the case with no insert. DELTAEC predicted that inserts with 25% open area would result in higher power output. This is due to that fact that DELTAEC does not take the non-linear losses of vortices and flow restriction into account.

The increase in the acoustic power that occurs in DELTAEC model results shows that the insert does not only save the power lost in harmonics, but it also changes the acoustic impedance of the resonator. The effect of this change in impedance on frequency is clearly noticed in figure 4.23b. When frequency changes, the stack position in the wave changes and the power output changes accordingly. DELTAEC results show that acoustic power output is lower for the experiments with higher operating frequencies. This suggests that the change in frequency changes the relative position of the fixed stack with respect to the acoustic wave, resulting in a higher acoustic power output for the cases with lower frequencies. Measurements confirms that result as the experiment with the highest operating frequency, 50C3-80, produced low acoustic power output compared to the same experiments that used the 50C3 insert. Figure 5.24a shows the values of the fundamental pressure at the position of the first microphone, 14.5 cm away from the hot side flange. This value is related to the blockage that is present in the system due to the insert addition. For DELTAEC calculations, the fundamental pressure at this location did not change significantly, ranging only from 5369 Pa to 5319 Pa.

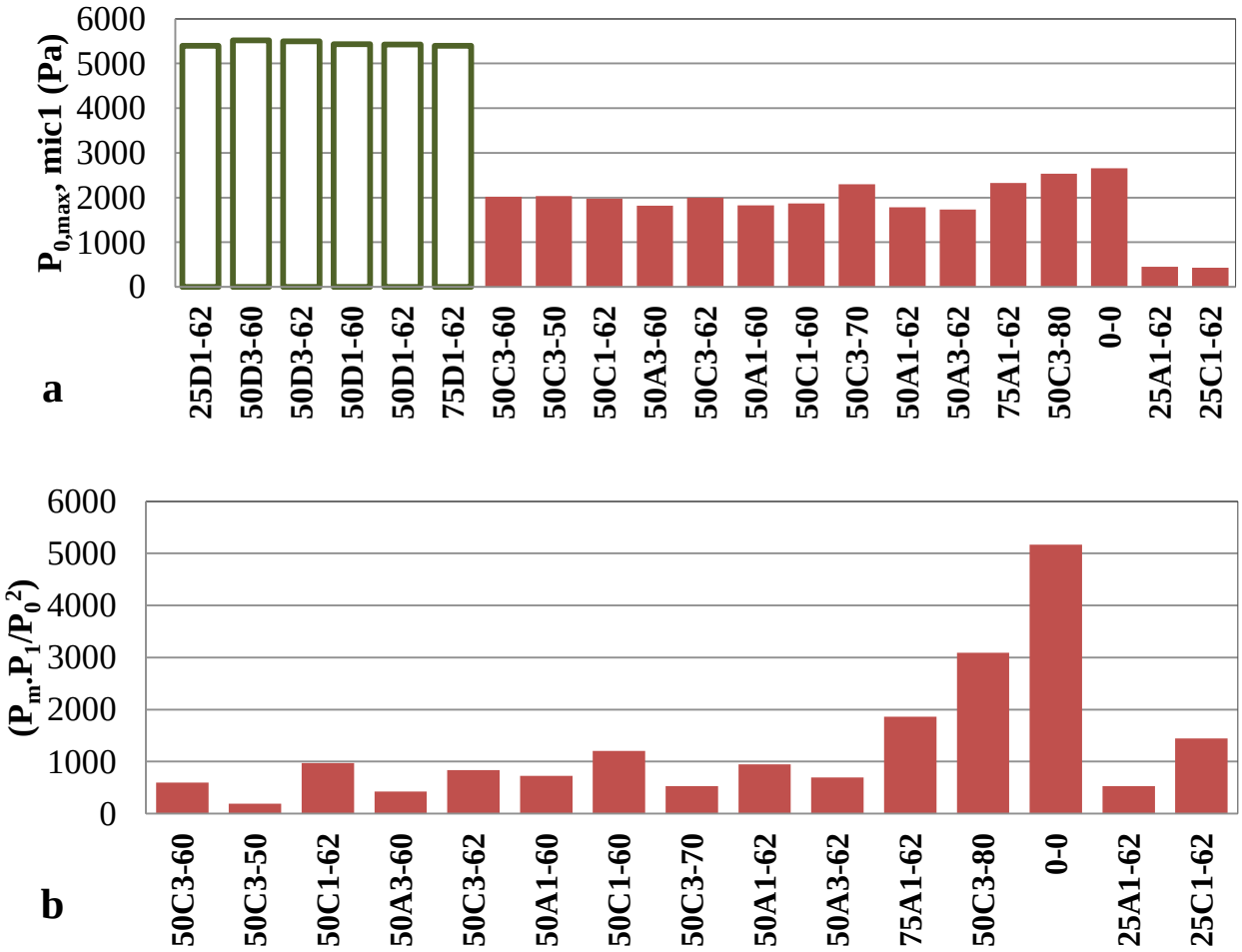

Figure 4.24: Fundamental amplitude, and normalized ratio ($P_m.P_1/P_0^2$) for multiple inserts with various shapes and positions. Solid columns are measurements, hollow columns are DELTAEC calculations.

The measurements show that all the inserts caused the fundamental pressure to decrease due to blockage, but the output acoustic power increased for some cases.

Results shown in figure 4.24b present the ratio of the amplitude of the first harmonic and the squared amplitude of the fundamental wave. Results show that it is maximum for the case of no insert in the resonator. Cases that produce higher power output have a very low harmonic content compared to the case with no insert. For example, the case that produced the highest output power, 50C3-60, had a value for the quantity (P_m*P_1/P_0^2) of only 10% of the no-insert case. The lowest harmonic content was 3.6% of the no insert case which was measured at the 50C3-50 case.

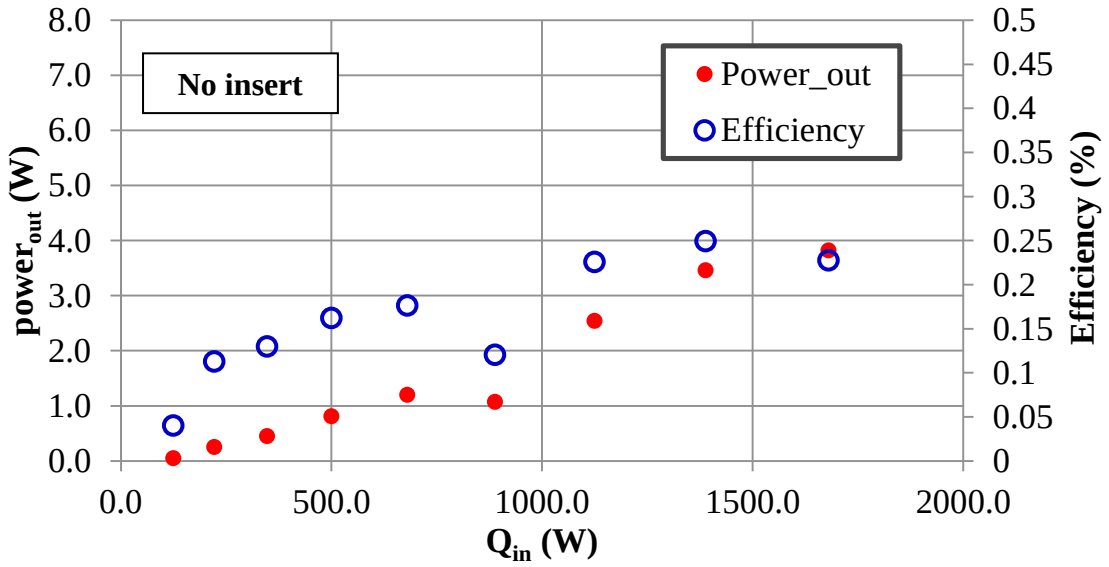

Figure 4.25: Power output and thermal to acoustic efficiency versus heat input to the system with no insert in the resonator.

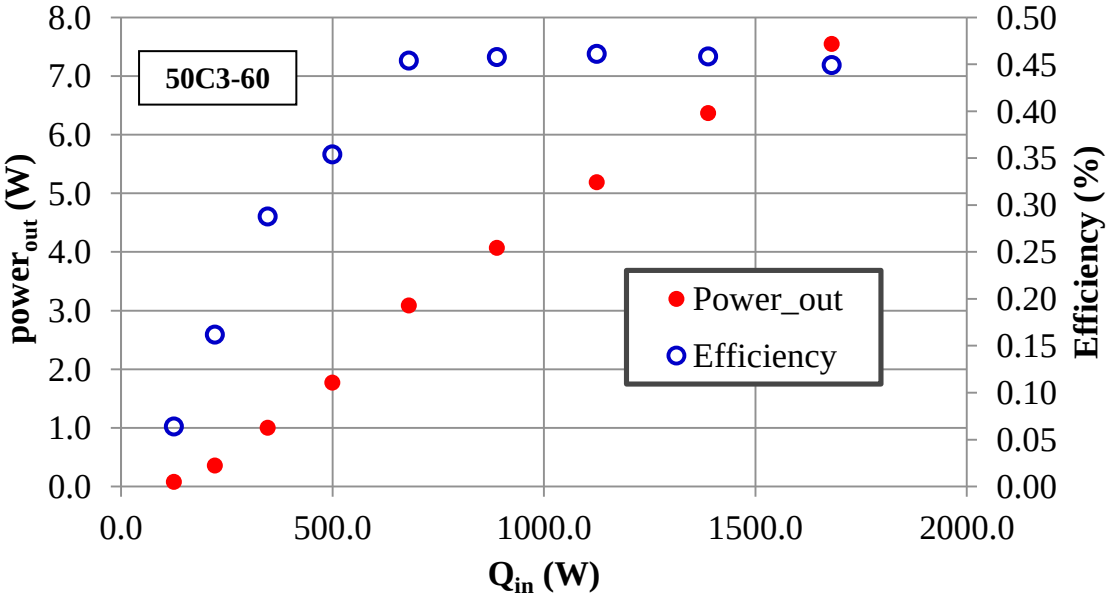

Figure 4.26: Power output and thermal to acoustic efficiency versus heat input to the system with 50C3 is placed in the resonator 60 cm away from the hot-side flange.

The position of the insert 50C3 is changed inside the resonator. At every position, the heater input is varied and the power and efficiency are calculated at every point. Figures 4.25 and 4.26 show the effect of varying the heat input to the system on efficiency and the acoustic

power output values for the case of no insert and the case with the insert 50C3 located at 60 cm from the hot-side flange. The results also include the wave components which indicate the fundamental and harmonic amplitudes. Power increases almost linearly with power input, while efficiency has a maximum value of about 0.25% for no insert, and 0.46% for 50C3-60. The relatively low efficiencies reported here are because the working gas is air at 1 bar. Gases with larger sonic speed at higher pressures, like helium at 20 bars are typical in devices of reasonable efficiencies, but related leakage problems arise.

4.5.2 Effect of insert position

The effect of the position, normalized with the wavelength, is shown in figure 4.27. DELTAEC calculations, green points in figure 4.27a, show that the power output of the system has a maximum value that occurs when the insert is located at about 0.32 of the wavelength calculated from the hot-side flange. Measurements confirm these results, taking the same trend but the powers are all scaled down about 40% due to non-linear losses that are not accounted for on DELTAEC.

The fundamental pressure amplitude at the highest measured input power, 1680W, is shown in figure 4.27b. Green dots show that fundamental pressure amplitude is not much affected by the position of the insert in DELTAEC calculations, while measurements showed that the pressure amplitude is less affected by blockage when the insert is closer to the cold side blind flange. This suggests that the insertion of the flange nearer to the velocity antinode where the velocity is meant to increase causes more vorticity and dissipates more energy.

Calculations of frequency using DELTAEC included in figure 5.17c, show that there is a point with minimum frequency. These point are the same points that gave the model's highest power output, confirming the previously suggestions that the acoustic impedance changes and makes the position of the stack closer to the optimum case in those positions in the linear modeling. Measurements did not take the same trend. Measured frequency increases as the distance from the hot-side flange increases.

Figure 4.27d shows the effect of the insert when placed at 62 cm from the hot-side flange on the axial distribution of the first harmonic amplitude. It shows that the axial distribution doesn't change a lot when the insert is introduced. The location of the velocity antinode for the first harmonic without the insert is at 62 cm from the hot-side flange. When the insert is introduced, the position was not affected by this change.

The use of the DELTAEC model showed that the increase in power is not related only to harmonic content reasons, but also occurs due to a change in the thermoacoustic characteristics of the system.

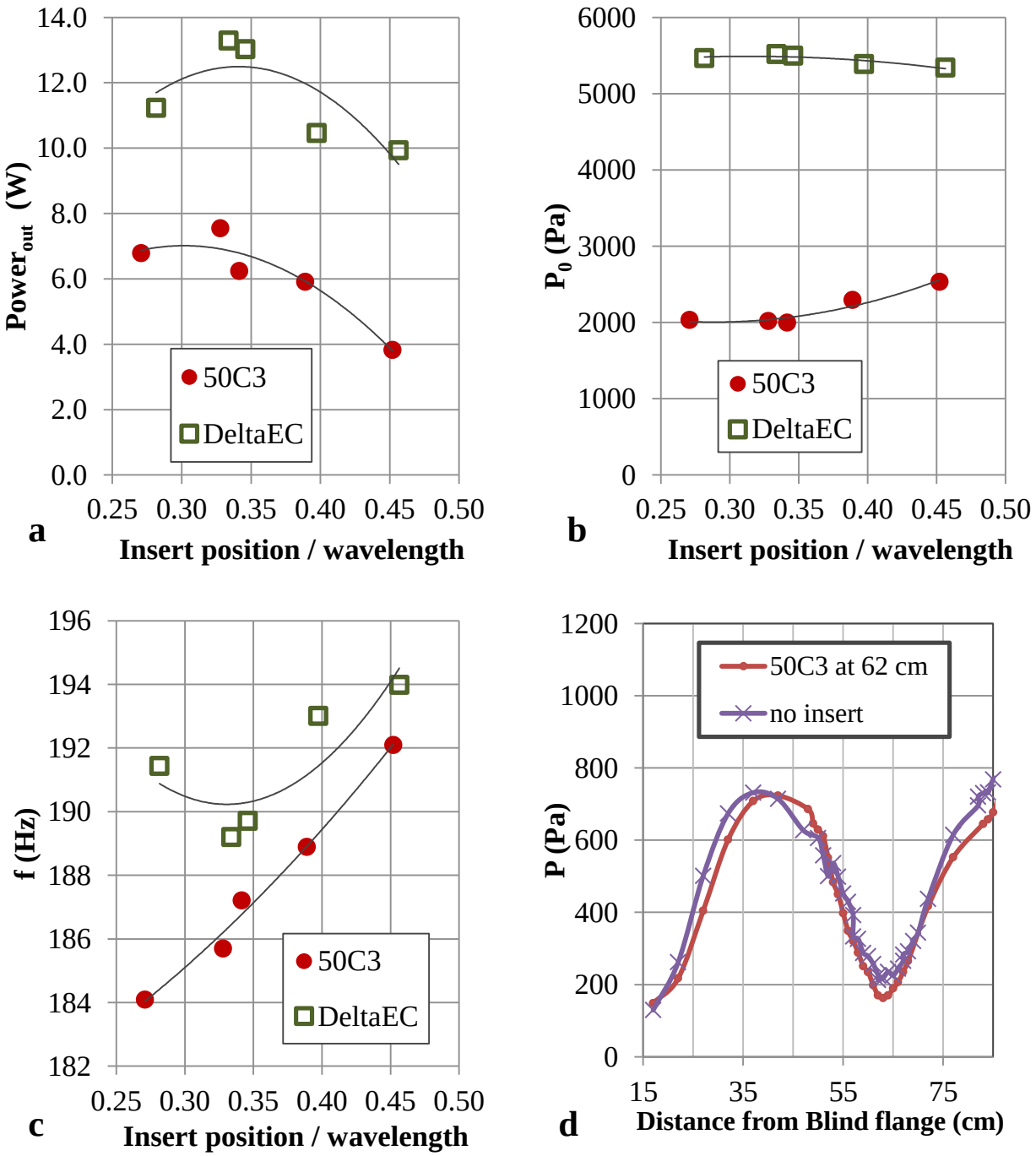

Figure 4.27: Effect of normalized position of insert on selected parameters with 400cpsi stack. **a)** Output power **b)** Fundamental pressure amplitude at 14.5 cm from hot-side blind flange **c)** Frequency **d)** First harmonic amplitude along the resonator with and without the insert. Position is the distance from hot-side flange.

5. Conclusions and Suggestions for Future Work

5.1 Introduction

The present study aims to experimentally investigate the performance characteristics of a thermoacoustic engine. A prototype of a standing-wave thermoacoustic engine was built in the labs of the department of physics at The American University in Cairo. The engine was operated using several gases and gas mixtures, stacks with different CPSI and different operating conditions. Full runs of different running time were performed and data of temperatures and dynamic pressure was collected to characterize the thermoacoustic engine transient performance and to analyze the hysteresis of the acoustic power output. The harmonic content of the wave is analyzed using a MATLAB code and related to the temperature difference between the stack sides.

The engine was also operated at different constant heat inputs to analyze the steady state performance and study the effect of gas mixture composition, stack CPSI, and heat input on the operating frequency, acoustic power output and fundamental pressure amplitude of the acoustic wave.

A numerical model of the engine is built using the DELTAEC software. The experimental data is used to validate the results of the model. The model predicted the dynamic pressure amplitude, volumetric velocity and the power flow inside the resonator. The code was also used to investigate the performance of the engine at steady state. The predictions of the code were significantly higher than the measurements.

The harmonic content of the output acoustic wave was analyzed at different heat input different for several gases and gas mixtures. The effect of adding a flow semi-blocking insert inside the resonator was investigated. Several inserts of different blockage areas and different holes pattern were placed around the velocity antinode of the first harmonic to suppress it. The effect of the insert on the losses related to the harmonic content is studied. The effect of the insert thickness, position, shape and blockage area on the engine acoustic power output, operating frequency, fundamental pressure amplitude, and suppression of the first harmonic pressure amplitude is presented.

5.2 Conclusions of the present work

In view of what has been presented the following conclusions are drawn:

The prototype of the thermoacoustic engine produced a half-wavelength standing wave. Measurements show that the acoustic power output increase linearly with the heat input for low heat input. Working with air at atmospheric pressure using a 600-CPSI stack gives low power density and therefore low efficiency. Higher acoustic power outputs can be obtained by using mixtures of air and helium. A mixture of 80% air and 20% helium gives the highest acoustic power and dynamic pressure at atmospheric pressure.

The numerical model of the engine gives accepted results for the resonance frequency. However, the model calculations of the pressure and power agree *only* in trend with the measured values. This may indicate that the model is not accurate for applications at atmospheric mean pressure.

The mean temperature of the working gas filling the resonator is the critical parameter for the hysteresis characteristics of the engine. At the same temperature difference, the dynamic pressure amplitude during start-up and shut-down differs significantly for a longer running time, lower helium content, lower starting temperature, or a stack of smaller pores.

Several inserts were used to suppress harmonics. All inserts of open area of 50% and 75% of the resonator area increased the acoustic power output, while inserts with open area of 25% of the resonator area caused high blockage and high losses and produced lower acoustic power output. The insert with several holes with open area of 50% of the resonator area gave the highest acoustic power output when placed at 0.32λ from the hot blind flange.

DELTAEC predicted that the thickness and the open area of the insert have a significant effect on the acoustic power output. This suggests that the change is not only related to the non-linear effect of the first harmonic which is not taken into account by DELTAEC, but also due to the change of the wave shape inside the resonator. Specific inserts cause the stack to be in a better position inside the resonator.

The position of the insert significantly affected the acoustic power output, the operating frequency, and the fundamental pressure amplitude. An optimum position is at 0.32 of the wavelength away from the hot-side blind flange.

5.3 Recommendations

More efforts are needed to reach a better understanding of the performance of thermoacoustic engines. Further analysis of the hysteresis paths is needed to explain the main factors that affect the phenomena. Harmonic content of the output acoustic wave need to be further analysed.

References

(1) N. Rott, *Thermoacoustics*, Adv. Appl. Mech., 20:135-175 (1980).

(2) K.T. Feldman, *Review of the literature on Rijke thermoacoustic phenomena*, J. Sound Vib. 7:83 (1968).

(3) N. Rott, *Damped and thermally driven acoustic oscillations in wide and narrow tubes*, Zeitschrift für Angewandte Mathematik und Physik. 20:230 (1969).

(4) G.W. Swift, *Thermoacoustic engines*, J. Acoust. Soc. Am. 84:1146 (1988).

(5) N. Rott, *Thermally driven acoustic oscillations, part II: Stability limit for helium*, Z. Angew. Math. Phys, 24:54 (1973)

(6) N. Rott, *Thermally driven acoustic oscillations, part III: Second-order heat flux*, Z. Angew. Math. Phys., 26:43 (1975).

(7) N. Rott, *Thermoacoustic heating at the closed end of an oscillating gas column*, Fluid Mech., 145:1(1984).

(8) M.E.H. Tijani, *Loudspeaker-driven thermo-acoustic refrigeration*, Ph.D. Thesis, Technische Universiteit Eindhoven, (2001)

(9) H. Babaei and K Siddiqui, *Design optimization of an automotive thermoacoustic air refrigeration system*, Acoustique Canadienne, 35:166-167 (2007).

(10) O. G. Symko, E. Abdel-Rahman, Y. S. Kwon, M. Emmi and R. Behunin, *Design and development of high-frequency thermoacoustic engines for thermal management of microelectronics*. Microelectron J. 35:185-191 (2004).

(11) M. Hatazawa , H. Sugita , T. Ogawa and Y. Seo, *Performance of a thermoacoustic sound wave generator driven with waste heat of automobile gasoline engine*. Trans. Jpn. Soc. Mech. Eng., 70:292-299 (2004).

(12) H. Babaei , K. Siddiqui and W. A. Chishty, *Sustainable thermoacoustic refrigeration system for gas turbine power plants*, 17th symposium of industrial application of gas turbines (IGAT); Banff, Canada (2007).

(13) L. Zoontjens, C. Howard, A. Zander and B. Cazzolate, *Feasibility study of an automotive thermoacoustic refrigerator*. Proceedings of acoustics, Busselton, Australia, (2005).

(14) R. L. Chen and S. L. Garrett, *Solar/heat-driven thermoacoustic engine*, J. Acoust. Soc. Am., 103(5):2841 (1998).

(15) J. A. Adeff and T. J. Hofler, *Design and construction of a solar powered thermoacoustically driven thermoacoustic refrigerator*, J. Acoust. Soc. Am., 107(6):L37-42 (2000).

(16) R. Chen, *Design, construction, and measurement of a larger Solar powered thermoacoustic cooler*, Pennsylvania State University (2001).

(17) C. Shen, Y. He , Y. Li, H. Ke, D. Zhang and Y. Liu, *Performance of solar powered thermoacoustic engine at different tilted angles*, Applied Thermal Engineering, 29:2745-2756 (2009).

(18) P. Merkli and H. Thomann, *Thermoacoustic effect in a resonance tube*, J. Fluid Mech., 70:161 (1975).

(19) G.W. Swift, *A unifying perspective for some engines and refrigerators*, Acoustical Society of America, Melville, (2002).

(20) N. M. Arafa, A. H. Ibrahim, K.Addas and Ehab Abdel-Rahman, *Design considerations for thermoacoustic engines for low onset temperature and efficient operation*, Forum Acusticum, Aalborg, Denmark (2011)

(21) J.R. Olson and G.W. Swift, *Similitude in thermoacoustics*, J. Acoust. Soc. Am., 95:1405-1412 (1994).

(22) T. Jin, B. Zhang, K. Tang, R. Bao and G. Chen, *Experimental observation on a small-scale thermoacoustic prime mover*. Journal of Zhejiang University, 8(2):205-209 (2007).

(23) G.W. Swift, *Analysis and performance of a large thermoacoustic engine*, J. Acoust. Soc. Am. 92:1551-1563 (1992).

(24) A. H. Ibrahim and E. Abdel-Rahman, *Innovative Solar-Energy-Driven Power Converter: Efficient Operation of Thermo-acoustic Engines*, The 2nd International Conference on Renewable Energy: Generation and Applications, AlAin, UAE, 4 - 7 March, (2012).

(25) J. R. Belcher, W. V. Slaton, R. Raspet, H. E. Bass and J. Lightfoot *Working gases in thermo acoustic engines*, J. Acoust. Soc. Am. 105 (5):2677-2684 (1999).

(26) W. C. Ward and G. W. Swift , *Design environment for low-amplitude thermoacoustic engines*, J. Acoust. Soc. Am., 95(6):3671-3672 (1994).

(27) G. W. Swift, and W. C. Ward, *Simple harmonic analysis of regenerators*, J. Thermophysics and Heat Transfer, 10:652-662 (1996).

(28) D. L. Gardner and G. W. Swift, *A cascade thermoacoustic engine*, J. Acoust. Soc. Am. 114(4):1905-1919 (2003).

(29) A. H. Ibrahim, N. M. Arafa and E. E. Khalil, *Geometrical optimization of thermoacoustic heat engines*. 49th AIAA Aerospace Sciences Meeting. AIAA 2011-129, Orlando, Florida (2011).

(30) N. M. Arafa, A. H. Ibrahim and E.E. Khalil, *Sensitivity analysis of a standing-wave thermoacoustic engine*, 9th Annual International Energy Conversion Engineering Conference, AIAA 2011, San Diego, California, (2011).

(31) H. Babaei and K. Siddiqui, *Design and optimization of thermoacoustic devices*, Energy Conversion and Management, 49:3585-3598 (2008).

(32) M. Wetzel, *Experimental investigation of a single plate thermoacoustic refrigerators*, Ph.D. thesis, Johns Hopkins University (1998).

(33) E. Besnoin, *Numerical study of thermoacoustic heat exchangers*, Ph.D. thesis, Johns Hopkins University (2001).

(34) L. Zoontjens, C.Q. Howard, A.C. Zander and B.S. Cazzolato, *Modeling and optimization of acoustic inertance segments for thermoacoustic devices*, Proceedings of Acoustics, 435-441 (2006).

(35) Y. Ueda, T. Biwa, U. Mizutani and T. Yazaki, *Experimental studies of a thermoacoustic Stirling prime mover and its application to a cooler*, J. Acoust. Soc. Am., 72 (3):1134-1141 (2003).

(36) M.E.H. Tijani, J.C.H. Zeegers and A.T.A.M. de Waele, *Design of thermoacoustic refrigerators*, Cryogenics 42:49-57 (2002).

(37) S. Backhaus and G.W. Swift, *A thermoacoustic stirling heat engine: detailed study*, J. Acoust. Soc. Am.,107:3148-3166 (2000).

(38) M.E. Poesse and S.L. Garrett, *Performance measurements on a thermoacoustic refrigerator driven at high amplitudes*, J. Acoust. Soc. Am., 107:2480-2486 (2000).

(39) J. Lighthill, *Acoustic streaming*, J. Sound and Vibration 61:391-418 (1978).

(40) W.L.M. Nyborg, *Physical Acoustics*, Vol. IIB, New York, (1965).

(41) M. Watanabe, A. Prosperetti and H. Yuan, *A simple model for linear and nonlinear processes in thermoacoustic prime movers, Part I: Model and linear theory*, J. Acoust. Soc. Am., 102(6):3484-3496 (1997).

(42) H. Yuan, S. Karpov and A. Prosperetti, *A simple model for linear and nonlinear processes in thermoacoustic prime movers, Part II: Nonlinear oscillations*, J. Acoust. Soc. Am., 102(6):3497-3506 (1997).

(43) S. Karpov, A. Prosperetti, *Nonlinear saturation of the thermoacoustic instability*, J. Acoust. Soc. Am., 107(6):3130-3147 (2000).

(44) M. F. Hamilton, Y. A. Ilinski and F. A. Zabolotskaya, *Nonlinear two-dimensional model for thermoacoustic engines*, J. Acoust. Soc. Am., 111(5): 2076-2086 (2002).

(45) B. L. Smith and G. W. Swift, *Measuring second-order time-average pressure*, J. Acoust. Soc. Am., 110:717-723 (2001).

(46) A.A. Atchley, H.E. Bass, and T. Hofler, *Frontiers of nonlinear acoustics*, Elsevier Science Publishers, London, 603-608 (1990).

(47) D.F. Gaitan and A. Atchley, Finite amplitude standing waves in harmonic and anharmonic tubes, *J. Acoust. Soc. Am.* 93:2489–2495 (1993).

(48) P.H.M.W Panhuis, *Mathematical aspects of thermoacoustics*. Eindhoven: TUE: Department of Mathematics and Computer Science (2009).

(49) P.C.H. Aben, P.R. Bloemen, and J.C.H. Zeegers, *2-D PIV measurements of oscillatory flow around parallel plates*, Experiments in Fluids (2008).

(50) P. Merkli and H. Thomann, *Transition to turbulence in oscillating pipe-flow*, J. of Fluid Mechanics, 68:567–575 (1975).

(51) D.L. Gardner, J.R. Olson, and G.W. Swift, *Turbulent losses in thermoacoustic resonators*, J. Acoust. Soc. Am., 98:2961 (1995).

(52) A. H. Ibrahim, A. Elbeltagy, M. Emam and E. Abdel-Rahman, *Development and analysis of non-linearity in the pressure waves resulting from thermoacoustic heat engines*, Acoustics 2012, Nantes, France, (2012).

(53) S. Backhaus and G. W. Swift, *A thermoacoustic Stirling heat engine*. *Nature*; 399:335–338 (1999).

(54) S. L. Garrett and S. Backhaus, *The power of sound,* American scientist, 88:516 (2000).

(55) T. Valdes-Solis, G. Marban and A.B. Fuertes, *Preparation of microporous carbon-ceramic cellular monoliths*, Microporous and Mesoporous Materials, 113-126 43(2001).

(56) T. Biwa, Y. Tashiro, H. Nomura, Y. Ueda, and T. Yazaki, *Experimental verification of two-sensor acoustic intensity measurements in lossy ducts*, J. Acoust. Soc. Am., 124(3):1584-1590 (2008).

(57) S. Backhaus, G. W. Swift, and R. S. Reid, *High-temperature self-circulating thermoacoustic heat exchanger*, Applied Physics Letters, 87 (2005).

(58) A. T. A. M. De Waele, *Basic treatment of onset conditions and transient effects in thermoacoustic Stirling engines*, Journal of Sound and Vibration, 325(4):974-988 (2009).

(59) A.H. Ibrahim, M. M. Emam, Hosny Omar, K. Addas and E. Abdel-Rahman, *Performance evaluation of thermoacoustic engine using different gases***,** Proceedings of ICSV19, Vilnius, Lithuania (2012).

Appendix A: Properties of working gas mixture

Table A : Thermal properties of air-He mixtures used in experiments							
Air Fraction	**Mixture Density**	**Kinematic Viscosity**	**Thermal Conductivity**	**Heat Capacity**	**Prandtl number**	**Gamma**	**Mole**
	Kg/m^3	m^2/s	$J.m^{-1}K^{-1}s^{-1}$	$J.Kg^{-1}K^{-1}$			Kg/Kmole
1.0	0.993	2.11E-05	0.030	1014	0.711	1.394	29
0.9	0.908	2.34E-05	0.036	1070	0.642	1.411	26.5
0.8	0.822	2.61E-05	0.042	1154	0.589	1.429	24
0.6	0.651	3.40E-05	0.058	1367	0.518	1.471	19
0.4	0.480	4.73E-05	0.081	1732	0.485	1.521	14
0.2	0.309	7.45E-05	0.115	2503	0.501	1.585	9
0.0	0.138	1.59E-04	0.170	5193	0.667	1.667	4

Appendix B: DELTAEC code

```
ENGINE 5 inch.out
!Created with DeltaEC version 6.3b11.12!under win32,
using Win 6.1.7601 (Service Pack 1) under Python DeltaEC.
!-------------------------------  0 -------------------------------
BEGIN      Global Variables
 1.0000E+05 a Mean P Pa
  202.50    b Freq   Hz       G
  325.00    c TBeg   K
 1.8005E+04 d |p|    Pa       G
    0.0000 e Ph(p)  deg
    0.0000 f |U|    m^3/s
    0.0000 g Ph(U)  deg
air          Gas type
!-------------------------------  1 -------------------------------
DUCT       Resonator
 1.2661E-02 a Area   m^2      Mstr       5362.4     A |p|    Pa
   0.39888 b Perim  m        1a          0.96877 B Ph(p)  deg
   0.3600  c Length m                    0.56247 C |U|    m^3/s
 5.0000E-02 d Srough                     -90.009   D Ph(U)  deg
                                 0.0000 E Htot   W
ideal          Solid type              -25.732   F Edot   W
!-------------------------------  2 -------------------------------
DUCT       Insert
 1.2661E-02 a Area   m^2      Mstr       3513.8     A |p|    Pa
   0.39888 b Perim  m        2a          1.5561  B Ph(p)  deg
 3.0000E-02 c Length m                    0.57782 C |U|    m^3/s
 5.0000E-04 d Srough                     -89.979   D Ph(U)  deg
                                 0.0000 E Htot   W
ideal          Solid type              -27.19    F Edot   W
!-------------------------------  3 -------------------------------
DUCT       Resonator
 1.2661E-02 a Area   m^2      Mstr       4040.9     A |p|    Pa
   0.39888 b Perim  m        3a          177.90    B Ph(p)  deg
   0.1200  c Length m                    0.57414 C |U|    m^3/s
 5.0000E-02 d Srough                     -89.806   D Ph(U)  deg
                                 0.0000 E Htot   W
ideal          Solid type              -46.521   F Edot   W
!-------------------------------  4 -------------------------------
SURFACE    MIC 2
    0.0000 a Area   m^2                 4040.9     A |p|    Pa
```

```
                                177.90    B Ph(p)  deg
                                 0.57414 C |U|    m^3/s
                                -89.806   D Ph(U)  deg
                                  0.0000 E Htot   W
ideal          Solid type              -46.521   F Edot   W
!--------------------------------  5 --------------------------------
DUCT       between mics
 1.2661E-02 a Area   m^2      Mstr       1.2785E+04 A |p|    Pa
   0.39888 b Perim  m        5a          179.32    B Ph(p)  deg
   0.1600  c Length m                    0.41453 C |U|    m^3/s
 5.0000E-02 d Srough                     -89.249   D Ph(U)  deg
                                  0.0000 E Htot   W
ideal          Solid type              -66.256   F Edot   W
!--------------------------------  6 --------------------------------
SURFACE    MIC 1
    0.0000 a Area   m^2                1.2785E+04 A |p|    Pa
                                179.32    B Ph(p)  deg
                                 0.41453 C |U|    m^3/s
                                -89.249   D Ph(U)  deg
                                  0.0000 E Htot   W
ideal          Solid type              -66.256   F Edot   W
!--------------------------------  7 --------------------------------
DUCT       before mic 1
 1.2661E-02 a Area   m^2      Mstr       1.7072E+04 A |p|    Pa
   0.39888 b Perim  m        7a          179.74    B Ph(p)  deg
   0.1300  c Length m                    0.1869  C |U|    m^3/s
 5.0000E-02 d Srough                     -87.631   D Ph(U)  deg
                                  0.0000 E Htot   W
ideal          Solid type              -73.283   F Edot   W
!--------------------------------  8 --------------------------------
HX         Ambient HX
 1.2661E-02 a Area   m^2                1.7320E+04 A |p|    Pa
   0.9000  b GasA/A                    179.61    B Ph(p)  deg
 1.0000E-02 c Length m                   0.16772 C |U|    m^3/s
sameas  10d d y0     m                 -86.799   D Ph(U)  deg
-1680.0     e HeatIn W                -1680.0     E Htot   W
 500.00    f SolidT K                 -91.106   F Edot   W
                                325.00    G GasT   K
copper         Solid type              274.05    H SolidT K
!--------------------------------  9 --------------------------------
RPN        ChangeMe
    0.0000 a G or T                  1680.0                 A ChngeMe
8e ~
```

```
!-------------------------------- 10 --------------------------------
STKRECT    Ceramic stack
 1.2661E-02 a Area   m^2              1.7936E+04 A |p|    Pa
   0.85866 b GasA/A         10def      178.62    B Ph(p)  deg
 3.0000E-02 c Length m                 0.1259  C |U|    m^3/s
 4.8000E-04 d aa     m        Mstr     -92.751   D Ph(U)  deg
 3.8000E-05 e Lplate m        Mstr     -1680.0     E Htot   W
sameas  10d f bb     m        Mstr      26.956   F Edot   W
                              325.00    G TBeg   K
celcor          Solid type            499.37    H TEnd   K
!-------------------------------- 11 --------------------------------
HX         Hot Hex
 1.2661E-02 a Area   m^2              1.8042E+04 A |p|    Pa
   0.9000  b GasA/A                  178.49    B Ph(p)  deg
 1.0000E-02 c Length m                 0.10471 C |U|    m^3/s
sameas  10d d y0     m                -91.621   D Ph(U)  deg
sameas   9A e HeatIn W                  0.0000 E Htot   W
  300.00    f SolidT K                1.8243  F Edot   W
                              499.37    G GasT   K
copper          Solid type            552.13    H SolidT K
!-------------------------------- 12 --------------------------------
DUCT       Change Me
sameas   7a a Area   m^2              1.8227E+04 A |p|    Pa
   0.39888 b Perim  m                178.49    B Ph(p)  deg
 5.0000E-02 c Length m                 3.2732E-12 C |U|    m^3/s
 5.0000E-04 d Srough                   69.359   D Ph(U)  deg
                                0.0000 E Htot   W
ideal           Solid type           -9.7738E-09 F Edot   W
!-------------------------------- 13 --------------------------------
HARDEND    target this to seal the end
    0.0000 a R(1/z)         =13G       1.8227E+04 A |p|    Pa
    0.0000 b I(1/z)         =13H       178.49    B Ph(p)  deg
    0.0000 c Htot   W                3.2732E-12 C |U|    m^3/s
                                69.359   D Ph(U)  deg
                                 0.0000 E Htot   W
                               -9.7738E-09 F Edot   W
                               -1.4524E-12 G R(1/z)
                               -4.1879E-12 H I(1/z)
!-------------------------------- 14 --------------------------------
RPN        Effeciency Calculations
    0.0000 a G or T                4.3621E-02              A etaI
                               0.34918                 B EtaC
                               0.12493                 C etaII
```

3.1913 D 2y/dk
174.37 E Tdiff
10H 10G - 10d 2 * dk / 7F ~ 11e / 10H 10G - 10H / / 10H 10G - 10H / 7F ~ 11e /
! The restart information below was generated by a previous run
! and will be used by DeltaEC the next time it opens this file.
guessz 0b 0d
xprecn 3.3414E-03 1.8656E-02
targs 13a 13b
mstr-slave 6 1 -2 2 -2 3 -2 5 -2 7 -2 10 -1
! Plot start, end, and step values. May be edited if you wish.
! Outer Loop: | Inner Loop

دراسات عملية حول أداء المحركات الحرارية الصوتية ذات الأمواج الموقوفة

إعداد

مهندس/ **محمود محمد إمام رجب**

رسالة مقدمة إلى كلية الهندسة، جامعة القاهرة
كجزء من متطلبات الحصول على درجة الماجستير
في هندسة القوى الميكانيكية

كليــة الهندســة ، جامعــة القاهــرة
الجيـزة ، جمهوريــة مصـر العربيــة
٢٠١٣

دراسات عملية حول أداء المحركات الحرارية الصوتية ذات الأمواج الموقوفة

إعداد

مهندس/ **محمود محمد إمام رجب**

رسالة مقدمة إلى كلية الهندسة، جامعة القاهرة
كجزء من متطلبات الحصول على درجة الماجستير
في هندسة القوى الميكانيكية

تحت إشـــراف

الأستاذ الدكتور/ محمود أحمد فؤاد
الأستاذ بقسم القوى الميكانيكية، كلية
الهندسة، جامعة القاهرة

الأستاذ الدكتور/ إيهاب عبدالرحمن
الأستاذ بقسم الفيزياء بكلية العلوم
والهندسة، الجامعة الأمريكية بالقاهرة

الدكتور/ عبدالماجد ابراهيم العيسوي
المدرس بقسم القوى الميكانيكية، كلية
الهندسة، جامعة القاهرة

كليـــة الهندســـة ، جامعـــة القاهـــرة
الجيـزة ، جمهوريـــة مصـر العربيـــة
٢٠١٣

دراسات عملية حول أداء المحركات الحرارية الصوتية ذات الأمواج الموقوفة

إعداد

مهندس/ **محمود محمد إمام رجب**

رسالة مقدمة إلى كلية الهندسة، جامعة القاهرة
كجزء من متطلبات الحصول على درجة الماجستير
في هندسة القوى الميكانيكية

يعتمد من لجنة الممتحنين:

الأستاذ الدكتور/ **محمود عبدالفتاح القاضي**	**عضو**
الأستاذ الدكتور/ **عصام الدين خليل حسن**	**عضو**
الأستاذ الدكتور/ **محمود أحمد فؤاد**	**مشرف ، و عضو اللجنة**

كليــة الهندســة ، جامعــة القاهــرة
الجيـزة ، جمهوريـة مصـر العربيــة
٢٠١٣

ملخص البحث

المحركات الحرارية الصوتية من النظم الحديثة لتحويل طاقة الحرارة إلى شغل مفيد على هيئة أمواج صوتية. يستهدف هذا العمل البحثي توضيح بعض الخصائص التي تظهر في أثناء التشغيل المستمر لمحرك حراري صوتي ذي موجة موقوفة بغازات مختلفة وتحت الضغط الجوي، في حالتي التشغيل المنتظم، ودورات التشغيل الكاملة؛ التي تشمل قيام المحرك وانتظام حالته ثم إيقافه. تظهر النتائج أن أداء المحرك يتأثر بطريقة كبيرة بنوعية الغاز المستخدم، ونفاذية المكوّن الفعال، وكمية الحرارة النافذة إلى المحرك. في التشغيل المنتظم، تظهر آثار هذه العوامل على الطاقة الصوتية الناتجة، وعلى الضغط الديناميكي التي تحمله الموجة الصوتية الموقوفة الناتجة، وعلى التشوه الهرموني الذي يظهر في الأمواج. ويظهر تأثير العوامل سابقة الذكر في أثناء دورات التشغيل الكاملة على تطور المحتوى الترددي للموجة مع تغير درجة الحرارة، وعلى ظاهرة التباينية Hysteresis التي تُظهر تغير مسارات الضغط في أثناء تزايد درجة الحرارة عنها أثناء تناقصها. يستهدف العمل أيضاً التحقق من فاعلية وضع عوائق خاصة في مسار الأمواج الصوتية الموقوفة لتحسين محتواها الهرموني وتقليل تشوهه لتقليل فقد الطاقة. وتدرس النتائج تأثير مكان وشكل ومساحة العوائق على الأداء. تظهر النتائج فاعلية كبيرة لهذه الطريقة التي ضاعفت الطاقة الصوتية الناتجة في بعض الحالات رغم تقليل نسبة الضغط الديناميكي الناتجة، إلا أن النتائج توضح أن هذا التحسن قد لا يكون نتاجاً خالصاً لتحسن الخصائص الهرمونية للموجة، وإنما قد تكون العوائق تسببت في تغييرات في التردد والمكان النسبي للمكون المنتج للطاقةStack في مسار الموجة الموقوفة.